INTERNATIONAL SPACE SCIENCE INSTITUTE - BEIJING
国际空间科学研究所 - 北京

太空 | TAIKONG

ISSI-BJ Magazine

No. 19 May 2020

SCIENCE OBJECTIVES AND OBSERVATION SYSTEM FOR THE INTERNATIONAL MERIDIAN CIRCLE

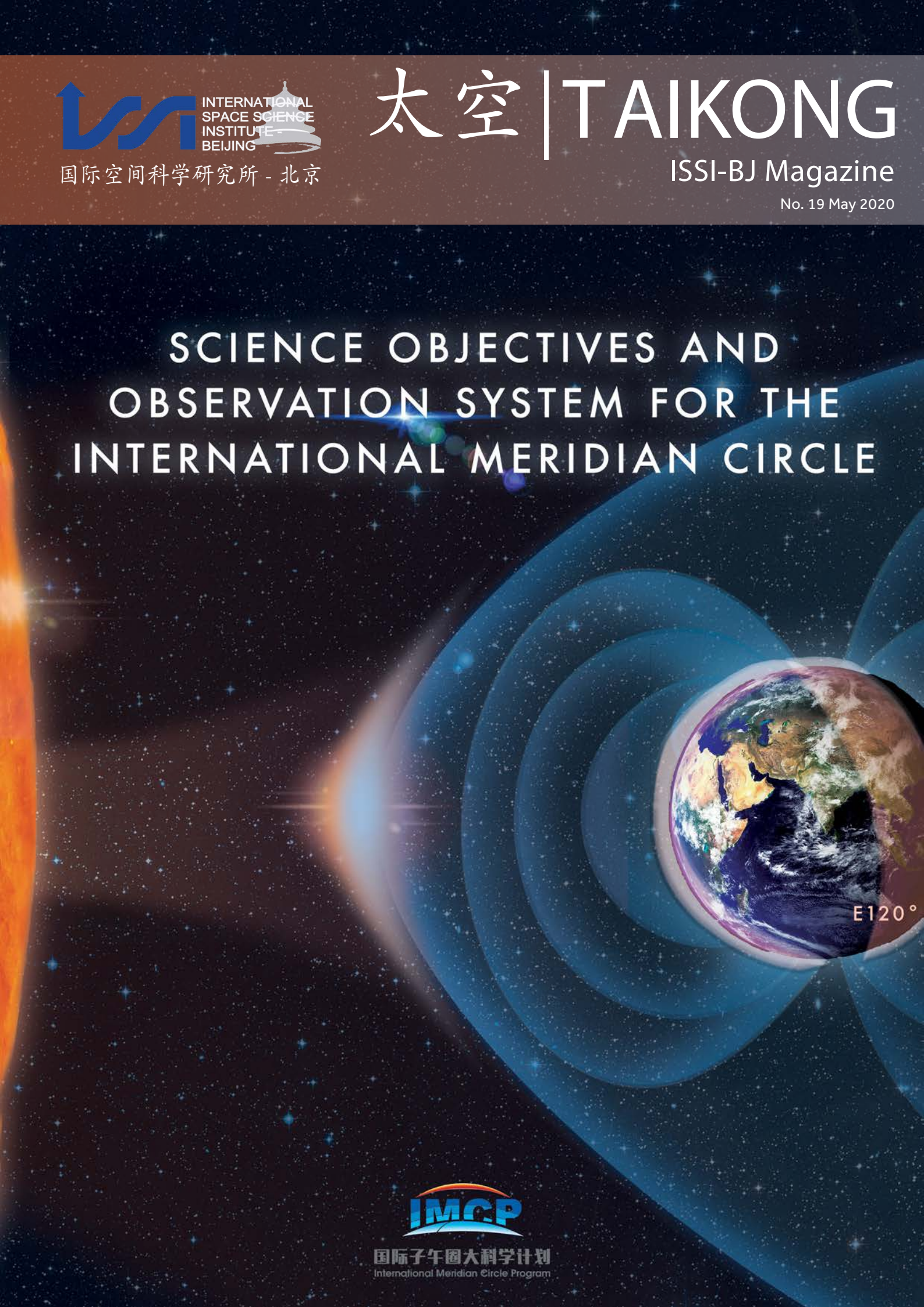

IMCP

国际子午圈大科学计划

International Meridian Circle Program

IMPRINT

太空 | TAIKONG
ISSI-BJ Magazine
License: CC BY-NC-ND 4.0

INTERNATIONAL SPACE SCIENCE INSTITUTE - BEIJING

Address: No.1 Nanertiao,
Zhongguancun,
Haidian District,
Beijing, China
Postcode: 100190
Phone: +86-10-62582811
Website: www.issibj.ac.cn

Authors

See the list on the back cover

Editor

Laura Baldis,
International Space Science Institute - Beijing, China

FRONT COVER

SAME Satellites
Image Credit: Innovation Academy for Microsatellite of CAS (IAMCAS), China

FOREWORD

There is little doubt that today's political and business leaders, as well as society at large, must face seriously the reality of global climate change and, in a broader perspective, define appropriate actions to protect our fragile high-technology society against the broad spectrum of natural and anthropogenic hazards which threatens it. There is an equal need for the scientific community to offer an adequate response to this major scientific challenge and strive together at the international level to offer the science-based information needed for society to take meaningful actions. The fact that our science sometimes still fails to give consistent, robust, and first-principle predictions of the occurrence and prediction of these hazards is obviously related to the enormous complexity of the Earth System and to the long timescales on which these predictions are to be made. It is essential in this context to recognize our own shortcomings, i.e. that we have not yet fully studied the Earth System as an interconnected whole. Future progress in this direction requires true multidisciplinary research, across a spectrum much wider than what a scientist is accustomed to today. This Forum addresses an important gap in the current global description of the Earth system: electrical, electromagnetic, and magnetized plasma interactions in the Earth System and the important roles they undoubtedly play in how this system works and how it can be monitored.

This is not to say that these interactions have not received their due attention. They have. The vigorous and robust research in Space Weather, which is centered on these interactions, is one of the highlights of Earth System Science in our still-young century. It is the interplay and interaction of the Space Weather System with the theatre of Global Change, namely the troposphere, oceans, land, and different life forms occupying the surface of Earth, which we believe have attracted insufficient attention: these interactions are likely actors in the underlying mechanisms controlling natural hazards and Global Change in the same way as Global Change and natural hazards originating from weather, lithospheric, and oceanic processes and geomagnetic field variations impact Space Weather. Establishing a quantitative estimate of these effects and of the associated energy transfer mechanisms, in both directions, will be a major scientific breakthrough with profound implications.

The central objective of the Forum on "Science Objectives and Observation System for the International Meridian Circle", whose scientific debates are summarized in this issue of Taikong Magazine, was to address this important

gap in the current description of the Earth System and to offer directions to cover the climate/weather system and space weather in a unified scientific perspective. Jointly organized by the International Meridian Circle Project at NSSC, CAS and the International Space Science Institute - Beijing (ISSI-BJ), this forum was successfully held in the premises of ISSI-BJ on September 23-25, 2019. It was convened by William Liu (NSSC, CAS, China), Michel Blanc (NSSC, CAS, China and IRAP, France), Eric Donovan (University of Calgary, Canada), John Foster (MIT Haystack Observatory, USA), Mark Lester (Leicester University, UK), Mioara Mandea (CNES, France) and Maurizio Falanga (ISSI-BJ, China), with the participation of 34 scientific experts from 13 countries. Our primary goal was to take stock of our research legacy and arsenals in the Space Weather discipline and apply them to the detection and possible prediction of major natural and anthropogenic hazards. This can be done by means of the deployment of a global natural screen on which these hazards can be projected and detected: our Ionosphere, Middle and Upper Atmosphere (IMUA). The international team of participants undertook rigorous and enlightening discussions on future steps to meet this major scientific challenge by joining forces across the five continents. We hope that the summary of this forum will serve as a trigger for a soon-to-come broader international discussion in view of the deployment of the global ground-based observation system of the IMUA we are proposing. With the additional support of new space assets and state-of-the-art computation and modeling capabilities, we trust this IMCP observation system will provide an unprecedented global monitoring of natural hazards and serve the emergence of a new understanding of our home planet.

We wish to thank the conveners and organizers of the Forum, as well as the ISSI-BJ staff, Lijuan En and Laura Baldis, for actively and cheerfully supporting the organization of the Forum. We would also like to thank all the participants who actively contributed to the Forum and to the editing of this report with dedication, enthusiasm, and scientific rigor. Our special thanks also go to Prof. Mioara Mandea and Prof. Alain Hauchecorne for their precious contributions to this report.

.

Maurizio Falanga,

Executive Director

ISSI-BJ, China

William Liu,

NSSC, CAS, China

Michel Blanc,

NSSC, CAS, China

IRAP, France

1. INTRODUCTION

Our Spaceship Earth sails the Solar System in a sea of plasmas, interfacing with it via a critical boundary layer through which a broad diversity of energy transfer processes takes place at time scales from a fraction of a second to millennia: our Earth's Ionosphere, Upper, and Middle Atmosphere, which will here be named the IMUA for short. Understanding the role that transfer processes through and to the IMUA play in the global changes driven by natural and anthropogenic forcing affecting our planet is a major scientific challenge for the scientific community of the XXIst century. It is this challenge, and the grand vision of a more comprehensive, better integrated and truly interdisciplinary description of our Earth System, which the International Meridian Circle Program (IMCP) has undertaken to meet.

The International Meridian Circle Program (IMCP) is an active proposal to the Chinese Ministry of Science and Technology for the international scientific community to address this major scientific challenge. Building on the already funded Chinese Meridian Project, its ambition is to deploy and operate for the first time a global, internationally coordinated observing system which will give us the capacity of monitoring at all relevant spatial and temporal scales the diversity of energy transfer processes affecting the IMUA, may they be driven from above (interplanetary space) or from below (solid and fluid Earth). The main purpose of this report is to describe the successive scientific and logical steps leading to the design of such an observation system.

Section 2 first establishes the "science case" for the IMCP. We summarize there how the different types of natural and anthropogenic hazards, from solar and interplanetary disturbances (disturbances "from above") to Earthquakes, tropospheric weather disturbances, greenhouse gases emissions and long-term geomagnetic field variations (disturbances "from below") affect the IMUA and produce imprints on it that can be used to monitor them. On the basis of this analysis, we conclude by defining the "ideal" spatial and temporal coverage required for the IMCP observation system: a pair of two great meridian circles in quadrature covering all geographic and geomagnetic latitudes and capturing the land-oceans contrast.

Starting from this scientific requirement, section 3 describes how the two great meridians should be equipped with a set of instruments that will provide a continuous survey of key parameters of the IMUA. We first describe the categories of instruments that are needed as global networks. We then focus on the design of the meridional chain of instruments running along the "primary" great circle (120° E and 60° W longitudes) which will link Eastern Siberia, Eastern Asia, Oceania, and the Americas with one single and coherent observation system. This primary instrument chain can largely be extrapolated from the instrument suite of the Chinese Meridian Project (CMP), which we will describe first. We then study, with the precious contributions of the European and African experts present at the forum, the potential

for the deployment of a second meridian circle along the 30 E and 150 W longitudes, in quadrature with the first one, which will cover Europe, Africa and the Pacific. This second circle will significantly improve the spatial coverage of the IMCP while bringing new capabilities and new players into the project.

Section 4 offers a preliminary exploration of the most advanced modelling, Big Data, and Artificial Intelligence tools, available today as never before, that the IMCP project will need to mobilize to reach its unique goal of unraveling the complexity and diversity of signatures of the different sources of hazards affecting the IMUA. It shows that a very close link between data, models, and AI interpretation tools will be needed in the definition of the IMCP scientific analysis strategy to maximize its scientific return.

We conclude by drawing some perspectives for the future steps in the design and worldwide deployment and operation of the IMCP with emphasis on the unique strength that a well-designed, balanced and global international cooperation will empower into the project. The need for a space-based complement to the IMCP ground-based observation system, only briefly touched on in this report, is critical and important enough that its preliminary design will justify a full new dedicated forum.

2. SCIENCE CASE

2.1. Scientific Scope, Objectives, and Overarching Science Goals of the IMCP

Our Earth's geospace is coupled to its space environment via a critical layer through which a broad diversity of energy transfer processes takes place at different time scales from a fraction of a second to millennia, i.e. our Earth's Ionosphere and Middle-Upper Atmosphere (IMUA). This thin layer which surrounds our planet between approximately 80 and 500 kilometers is a critical interface between "fluid Earth" (shown in blue in the bottom panel of Figure 1) and "plasma Earth" (pink domain in Figure 1).

Indeed, the neutral and ionized components of our atmosphere overlap within this thin layer, with important consequences on the flow of mass, momentum, and energy in geospace: while the dynamics of "fluid Earth" is governed by neutral gas hydrodynamics, the one of "plasma Earth" is governed by the electrodynamics of magnetized plasmas, of which MHD is a simplified scheme. In the overlapping region, i.e. IMUA, the two dynamical regimes co-exist and interact, making this layer a unique coupling domain for dynamical processes and a major sink region for energy transfer processes in geospace.

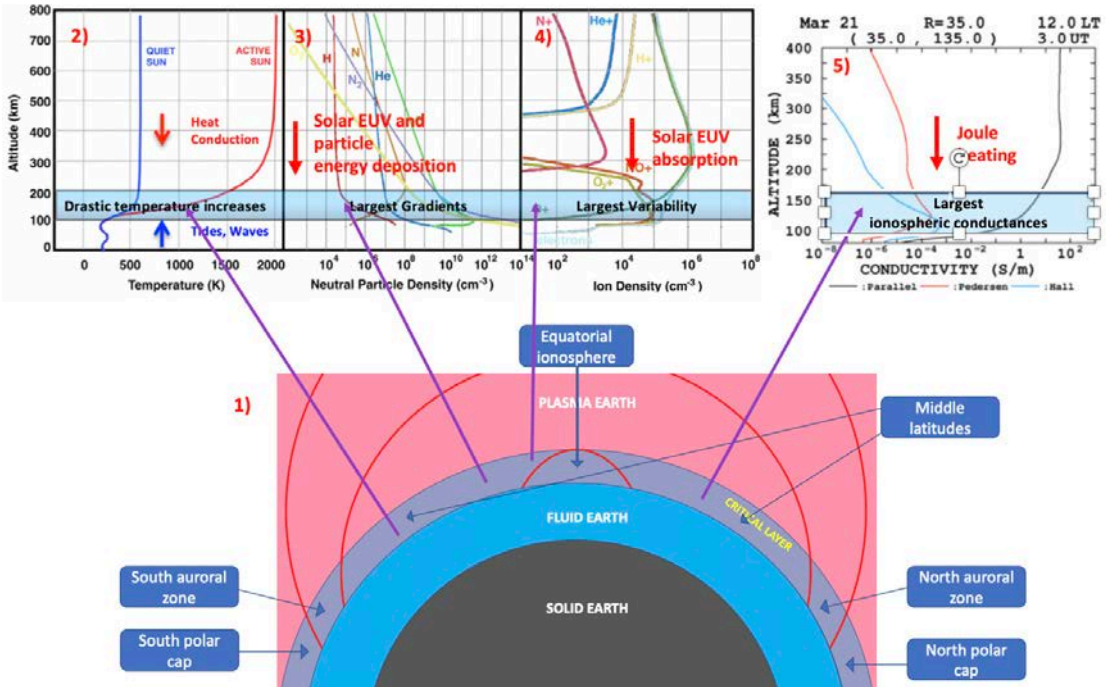

Figure 1: *Distinguishing three "phase domains" in our geospace (1), e.g. Solid Earth (black), Fluid Earth (blue) and Plasma Earth (pink) shows that fluid Earth and Plasma Earth overlap over a thin shell extending approximately from 50 to 500 km surrounding our planet, which we call the Ionosphere-Middle-Upper-Atmosphere (IMUA), a critical transport layer within which hydrodynamics and electrodynamics are coupled. The unique transport properties of the IMUA make it an efficient "screen" on which to project and detect disturbances coming from above (the coupled Sun-Earth system) and from below (fluid and solid Earth) in our geospace: the IMUA is a region of heat conduction from above related to the strong upward exospheric temperature gradient (2), energy deposition by solar EUV and X-ray radiation and by precipitating particles (3,4) and maximum Joule heating by ionospheric electric currents (5).*

This domain receives and absorbs energy both from above, via the sun-Earth energy coupling chain which drives space weather events through solar and interplanetary activity, magnetospheric activity, and finally their coupling to the ionosphere and upper-middle atmosphere. It also receives and absorbs energy from the "Fluid Earth" domain: propagating atmospheric waves generated by solar heating and weather systems; thunderstorms, which drive a global electric circuit connecting the lower atmosphere and the upper atmosphere and closing into the ionospheric conductor, as described for instance by Rycroft et al.

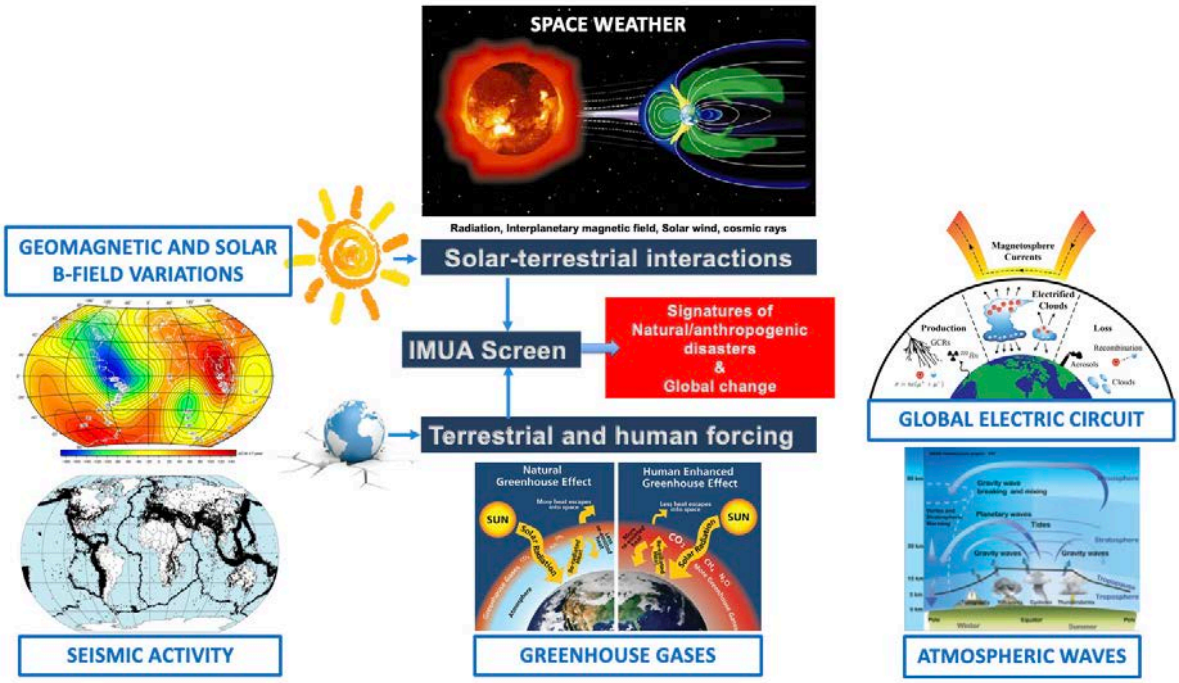

Figure 2: *A summary of the different types of disturbances of the Sun-Earth system propagating from above (classical space weather), from the coupled Earth system (terrestrial and solar magnetic field long-term variations and global electric circuit) and from below (seismic activity, injection of greenhouse gases into the atmosphere, atmospheric waves produced by solar heating and weather systems) which can be detected on the IMUA screen.*

(2000); injection of greenhouse gases into the atmosphere and their effects on climate change. Finally, the IMUA is also affected by disturbances generated within the "Solid Earth" (shown in black in Figure 1): seismic and volcanic activity, secular changes of the geomagnetic field produced by the geo-dynamo. These different sources of hazards are illustrated in Figure 2.

One can identify five main mechanisms by which energy released by these different types of disturbances is transferred to and deposited into the IMUA:

1. Irradiation (Electromagnetic or particle): energy deposition from the electromagnetic (EM) radiation of the Sun and background sky into the atmosphere at different altitudes (our main energy source); precipitation of energetic particles (cosmic rays, radiation belts, auroral particles); possible EM emissions of lithospheric

activity and earthquakes; EM and particle emissions of thunderstorms;

2. electrodynamic coupling of: solar and heliospheric activity and disturbances to the magnetosphere and ionosphere, across and along magnetic field lines (the dominant mode for the transfer of space weather disturbances to our upper atmosphere); thunderstorms, feeding the global atmospheric electric circuit which closes into the ionospheric conductor within the IMUA;
3. emission, propagation, and dissipation of atmospheric waves: acoustic-gravity waves, planetary waves, tides;
4. atmospheric circulation changes: perturbations of general circulation (horizontal advection); convection cells, which couple horizontal and vertical motions at different locations and scales; and
5. release into the atmosphere of gas and aerosol produced by volcanic activity and anthropogenic emissions (including greenhouse gases).

2.1.1. Overarching Science Goal of the IMCP

By the action of these different processes, energy deposited into the IMUA is the result of dynamical perturbations developing above and below it. Given a well-designed science plan for their interpretation, they can be used as tracers of these perturbations of geospace, turning the IMUA into a giant, planetary-scale spherical screen on which one can detect, study, and characterize them. The overarching science goal of the proposed International Meridian Circle Project (IMCP) can then be summarized as the need to monitor, understand, predict, and mitigate the hazards and major perturbations threatening our human environment by means of the deployment, coordinated operation, and scientific use of a global observing system that shall provide a continuous monitoring of the Ionosphere and Middle-Upper Atmosphere (IMUA) covering the different temporal scales of these perturbations.

2.1.2. Detailed Scientific Objectives

To reach its overarching goal, the IMCP will deploy a global-scale, ground-based observation system to be complemented by a space segment tailored to its specific needs, which can be used to study the different types of disturbances and hazards illustrated in Figure 2 (clockwise from the top), with corresponding time scales indicated between brackets:

A. Solar Activity and heliosphere/solar wind/magnetosphere/ionosphere disturbances (minutes to decades);

B. disturbances of the troposphere/stratosphere weather system acting through atmospheric waves and atmospheric electricity (hours to years);

C. disturbances and long-term evolution of the climate system (months to decades);

D. lithospheric activity and earthquakes (seconds to years); and

E. secular variations of the geomagnetic field, including reversals (decades to centuries and more) and their long-term interactions with the interplanetary magnetic field.

Three scientific questions will be addressed for each observed source of threat thanks to the increased observation capacity provided by the IMCP observation system:

I. What are their coupling mechanisms to the IMUA?

II. What is their impact on our space environment?

III. How can we use their effects on the IMUA to improve the characterization and prediction of these threats?

This section presents a summary of these different sources of hazards, from A to E. For each one, their main observational characteristics and underlying mechanisms will be presented, and the temporal scales and spatial coverage needed to observe them will be identified.

2.2. Solar Activity and Heliospheric Processes (Hazard A)

The interplanetary processes that affect Earth's space environment (illustrated in Figure 3) are linked to the solar origin of interplanetary (IP) magnetic structures. The fast solar wind originating from coronal holes results in corotating interaction regions (CIRs) when it interacts with slower wind ahead. A CIR consists of a region of compressed plasma and enhanced magnetic field intensity moving with speeds intermediated between the slow wind ahead and fast wind behind. Coronal mass ejections (CMEs) originate from closed magnetic field regions on the Sun such as active regions and filament regions. CMEs and CIRs affect Earth's space environment in two ways: by accelerating particles to high energies and by causing geomagnetic storms. CIRs produce about 15% of all major geomagnetic storms, the rest being due to CMEs. The strength of a geomagnetic storm (e.g. as measured by the Dst index) from an IP structure with a southward magnetic field component Bz (nT) and a speed V (km/s) is empirically given by the relation: Dst (nT) = -0.01V|Bz| - 32 (Gopalswamy, 2010).

Several interplanetary processes affect V and Bz and hence the geoeffectiveness of these structures. For both CIRs and CMEs, the minimum requirement for a storm to occur is a southward Bz. Once this is met, the storm strength depends on the product V.|Bz|. The speed of an interplanetary CME (ICME) impinging on Earth depends on the initial speed of the CME (Vi) measured in the coronagraph field of view and on how Vi changes as the CME propagates through interplanetary medium. The main effect of this propagation on Vi is due to the solar wind drag which decelerates fast CMEs and accelerates slow CMEs. CMEs can also be deflected away and toward the Sun-Earth line by other large-scale structures (coronal holes, other large CMEs), thus modifying the Earthward component of V. CMEs can also rotate, affecting the orientation of the field lines that determine the magnitude of Bz. Finally, if the ICME is driving a shock, the compressed sheath located between the shock and the ICME flux rope can also be geoeffective if the compressed heliospheric magnetic field in the sheath has a southward Bz. At the Sun, Vi depends on the free energy available in the source region. The free energy is stored in the stressed magnetic field lines of the corona and released during an eruption. The kinetic energy (and hence Vi) of the CME is closely related to the amount of magnetic flux that participates in the eruption. This is known as the total reconnected (RC) flux. The Bz part of the Dst formula also depends on the RC flux, which is approximately the poloidal flux of the flux rope formed during the eruption. The poloidal flux gives all the components of the flux rope magnetic field, including the Bz

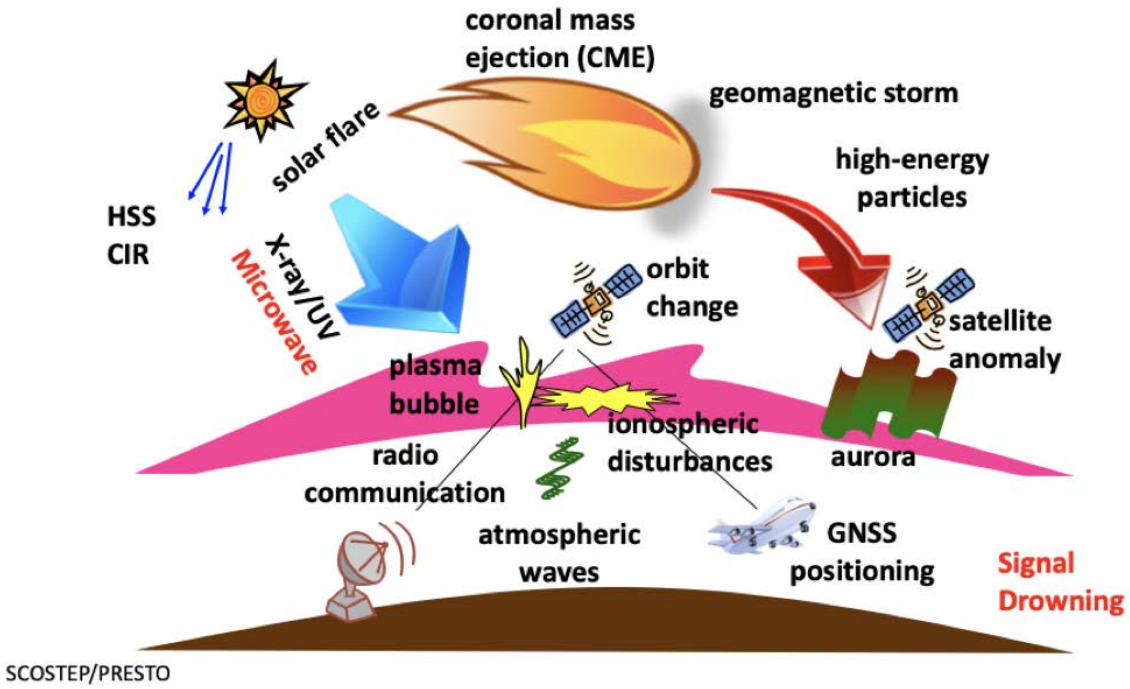

Figure 3: *A cartoon illustrating the diversity of sources of space weather events and disturbances (top) and of their effects on human systems*

component needed to determine Dst. Thus, the reconnection process during the eruption at the Sun is fundamental in determining both the V and Bz parts of the Dst formula.

In the case of CIRs, the compression region between fast and slow winds often displays a southward Bz due to Alfven waves propagating in the solar wind. In the compression region, the wave can be amplified and Bz can be significantly enhanced. The V-part is determined by the speeds of the fast and slow winds that form the CIR.

While the geo-effectiveness of a CME depends on its internal structure and the sheath, the production of a solar energetic particle (SEP) event depends on the shock-driving capability of the CME. The typical speed of SEP-associated CMEs is ~1500 km/s, which is more than the local Alfven speed. CME-driven shocks are very efficient in accelerating particles by a process known as diffusive shock acceleration. The acceleration efficiency depends on the ambient Alfven speed, seed particles, and shock geometry. Typically, about 10% of the CME kinetic energy is converted into the energy of SEPs (e.g., Mewaldt et al. 2005). Shocks can form very close to the Sun. CMEs rapidly accelerating to high speeds are generally associated with large and energetic SEP events that have a hard spectrum. These events typically occur in active regions because they are sites of high magnetic energy storage. Shocks also form at large distances from the Sun (beyond 3 solar radii), in which case CMEs are slowly accelerating and result in a soft-spectrum SEP event. The harder the spectrum, the more important is the impact of SEP events on humans and technology in space. CME-driven shocks also accelerate electrons that can be detected in space as electron events. The shock-accelerated electrons also produce type II radio bursts via a plasma emission process. These radio bursts can track CME-driven shocks beyond the coronagraph field of view and often all the way to an observing spacecraft near Earth.

CIRs also accelerate particles, but generally beyond 2 AU from the Sun and the energy and intensity are much smaller than those of CME-related SEP events.

2.3. Magnetospheric Processes (Hazard A cont'd)

The short review of Magnetospheric Processes presented in this sub-section focuses particularly on the energetics and dissipation processes of the magnetospheric system.

The diversity of time scales involved in the response of the magnetosphere to the solar/interplanetary drivers associated with solar activity ranges from a few minutes (during solar flares) up to a few days (during geomagnetic storms and substorms). This is also the range

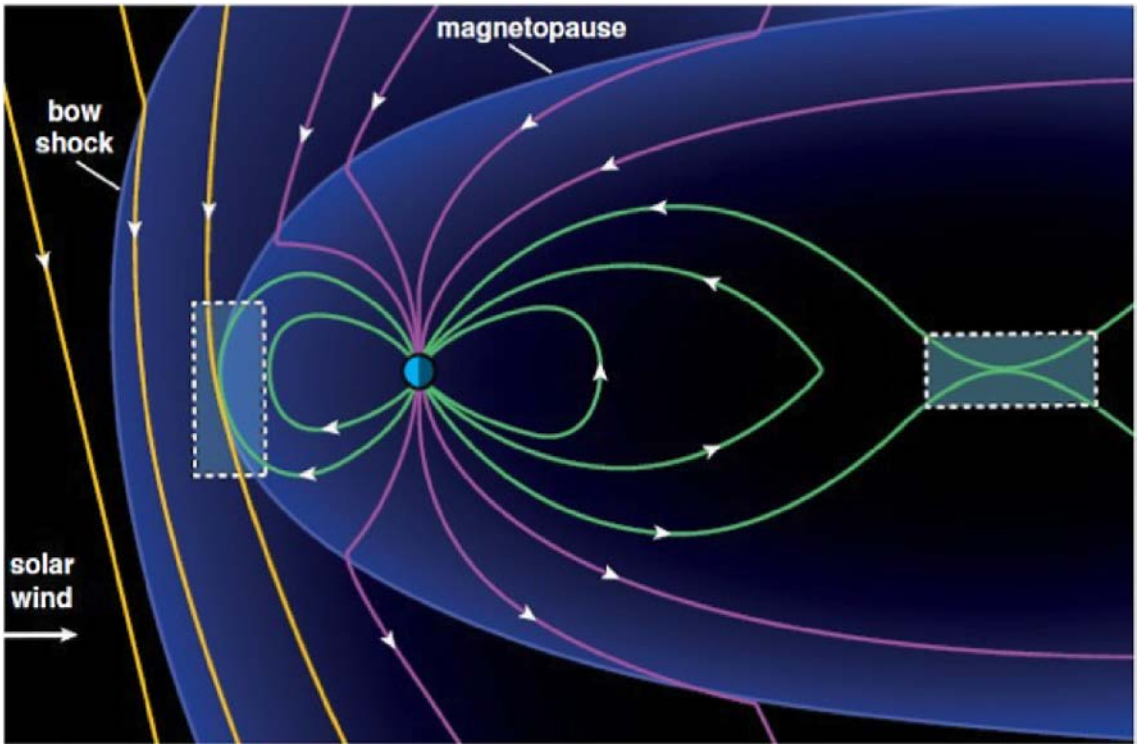

Figure 4: *Illustration of the two main regions of magnetic reconnection in the Earth magnetosphere (magnetopheric "nose" on the dayside and tail plasmasheet center) by means of which energy coming from the solar wind is channelled into the inner magnetosphere and IMUA after temporary storage in the tail magnetic field configuration.*

of time scales of interest for studying space weather variability. A modulation of this basic time-scale variability has also been studied in the context of seasonal and solar-cycle time scales.

The main physical process responsible for transmitting momentum and energy from the solar wind to the magnetosphere is magnetic reconnection, which is active in two specific regions of the magnetosphere on the dayside and on the nightside, as illustrated in Figure 4. Based on several decades of intensive studies of these reconnection regions through in-situ observations and large-scale modeling, one can make estimates of the total energy that enters the magnetosphere as a function of the plasma and magnetic field parameters of the interplanetary drivers. Such estimates give values of about (1 to 5) x 10^{12} watts for the power input to the magnetosphere, which represents about 2% to 5% of the total kinetic power of the solar wind impinging on the magnetosphere. When compared with the total solar electromagnetic power arriving to

Earth, the latter is about three to four orders of magnitude smaller.

The power transmitted by the solar wind to the magnetosphere by magnetic reconnection is temporarily stored into the magnetic configuration of the magnetospheric tail before being quickly released and dissipated into geomagnetic substorms and storms, with intensities that depend on the value of the initial transmitted power from the solar wind. The power dissipated in storms and substorms, mainly via current systems, growth of the circum-magnetosphere ring current, and particle precipitation in the ionosphere/atmosphere, can have values of about 10^{11} to 10^{12} watts.

Of special concern for the technological consequences of space weather impacts is the arrival to the magnetosphere of very intense solar/interplanetary disturbances: they can cause the occurrence of superstorms and extremely intense substorms, with related power values reaching an order of magnitude larger or more than those mentioned above.

Thus, to improve the present capabilities of space weather variability forecasting, it is of primary importance that the Meridian Circle Program helps the international space agencies to define new near-Earth satellite missions which could improve such capabilities, using new techniques and missions that could involve several satellites measuring simultaneously at different and complementary spatial scales, such as the SMILE and SAME missions that are presently being developed and managed by NSSC/CAS.

2.4. Magnetosphere-Ionosphere-Thermosphere (MIT) Coupling (Hazard A cont'd)

The transmission of the dynamical state of the solar wind and magnetosphere to the other components of geospace works through what is referred to as Magnetosphere-Ionosphere-Thermosphere (MIT) coupling. Downward coupling by means of transmission of solar-wind and magnetospheric electric fields to the ionosphere and closure of field-aligned currents along magnetic field lines, momentum input from magnetospheric convection, storms, and substorms, and charged particle precipitation into the upper atmosphere link processes in the IMUA layer to the magnetospheric and solar wind drivers reviewed in sections 2.2 and 2.3, as shown in the cartoon of Figure 5 (from Sarris et al., 2019). At the same time, atmospheric waves (tidal waves, atmospheric gravity waves, planetary waves etc.) propagating upward from the lower and middle atmosphere (see section 2.5) also transfer momentum and energy to the IMUA. These drivers from above and from below both interact with the internal dynamic

and energetic processes of the IMUA: control of ionospheric conductivities by solar illumination and precipitating particles; generation of a quiet-time horizontal ionospheric current system by tides locally generated or propagating from below. This horizontal ionospheric current system, whose average quiet-time circulation is represented by the so-called "Sq current system", closes in part along the equatorial electrojet, a major dynamical feature of the equatorial ionosphere within which the effective conductivities and the total current flow are spectacularly enhanced by the near-horizontal geometry of magnetic field lines (Figure 5). In return, changes in thermospheric structure and winds and in the ionospheric current system couple back upward and downwards, thus contributing to modify the global state of geospace.

We give here several examples of particularly important magnetosphere-ionosphere-thermosphere coupling processes and stress their significance and effects across geospace.

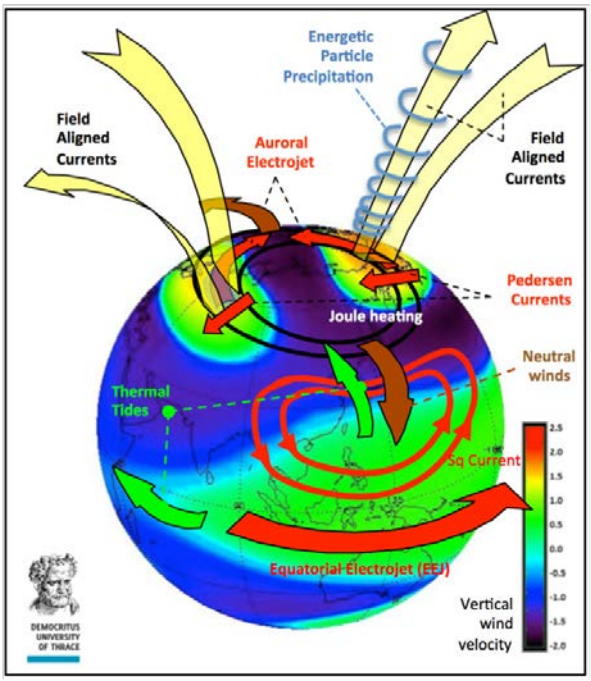

Figure 5: *A simplified representation of the main MIT coupling processes acting on the IMUA. In order to retrieve and interpret the signatures of disturbances from above and from below to be detected on the IMUA screen, one must also solidly understand the planetary-scale energy redistribution processes operating horizontally within the IMUA itself under the effect of the energy deposition associated to these disturbances. Figure from T. Sarris et al. (2019).*

2.4.1. Penetration of magnetosphere-driven Electric Fields to middle and equatorial latitudes

During storm conditions, electric fields of solar wind origin can penetrate the inner magnetosphere to low latitudes. Eastward penetrating electric fields produce a strong E x B uplift at the equator that redistributes ionospheric plasma to higher latitudes. At the equator, a severe total electron content (TEC) depletion can form at longitudes near the South American magnetic anomaly in Brazil. Gravity pulls ions downward along the magnetic field

to higher latitude and off-equatorial peaks in ionospheric density result. This downwelling plasma increases TEC at low/middle latitudes, creating an enhanced and spread Equatorial Anomaly. Figure 6 shows an example of TEC enhancement produced by this mechanism, observed through three successive passes of the CHAMP satellite (see note 2 in section 3.2).

Significant space weather effects are related to this MIT coupling process, including ionospheric scintillations and sharp TEC spatial gradients. Unstable plasma within the Earth's ionosphere results in irregularities in refractive index. Scintillations occur when radio waves pass through a turbulent ionosphere, reducing signal quality. Scintillations disrupt signals, with important consequences for communications/ navigation systems.

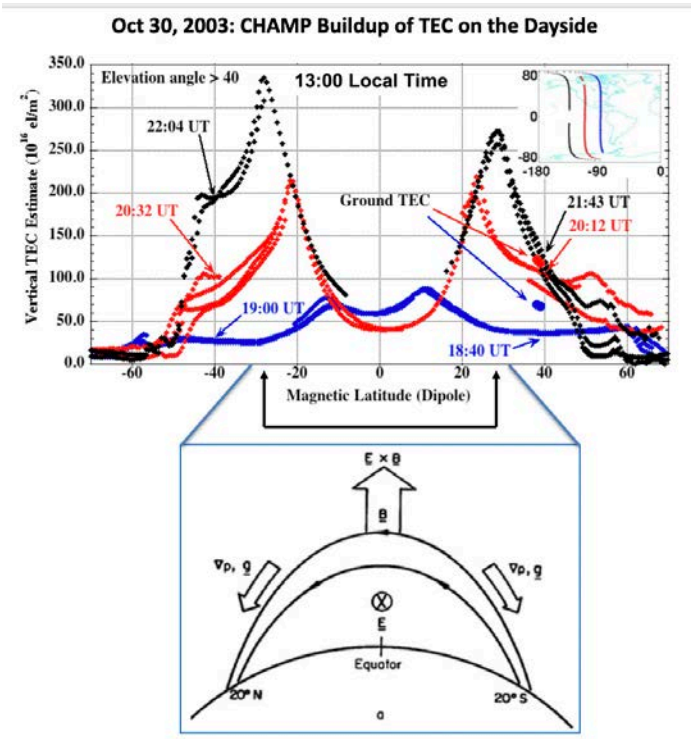

Figure 6: *An example of an ionospheric Total Electron Content (TEC) perturbation produced on the equatorial ionospheric anomaly by the penetration of an eastward electric field from higher latitudes. Under the effect of the enhanced electric field and upward drift applied to equatorial magnetic flux tubes, plasma is depleted at the equator and diffuses along magnetic field lines away from the equator (equatorial fountain effect), enhancing the TEC at latitudes of 15 to 40 degrees, as shown by CHAMP TEC data in the south-atlantic anomaly region on three successive passes (blue, red and black).*

2.4.2. Storm-Enhanced Density (SED)

Significant perturbations of the middle latitude ionosphere results from magnetospheric electric field effects during geomagnetic storms. Large-scale dayside increases in ionospheric density and total electron content (TEC) are observed at low, middle, and auroral latitudes as disturbance electric fields and neutral winds uplift F region plasma into a region of reduced recombination. Advection carries nightside plasma across the sunset terminator and draws out plumes of storm-enhanced density (SED plumes) that stretch from the dusk sector to the noontime cusp ionosphere. GPS TEC maps have enabled researchers to determine that SED, initially identified as a disturbance MIT coupling phenomenon on the basis of incoherent scatter radar observations, occurs globally, is associated with large TEC gradients and is a magnetically conjugate phenomenon. Observations of the SED plume at different altitudes indicate that it is a continuous phenomenon extending between the ionosphere and the apex of the magnetic field line. The erosion of the outer plasmasphere and the extension of the plasmasphere drainage plume to the dayside boundary of the magnetosphere are related directly to the characteristics of the SED plume at ionospheric heights. The SED plume cannot be considered in isolation from other disturbance effects since it is only one manifestation of the more widespread interconnected geospace system response to solar wind forcing.

2.4.3. Sub-Auroral Polarization Stream (SAPS)

A strong electric field forms in the low-conductivity region between the inner edge of the plasma sheet precipitation region and the plasmapause during disturbed conditions: under such conditions the disturbed ring current drives magnetic field-aligned currents into the sub-auroral ionosphere. Pedersen current closure sets up a strong poleward-directed electric field across the low conductance ionospheric density trough. The associated E x B plasma drift results in a strong westward (sunward-directed) ionospheric flow channel, the sub-auroral polarization stream (SAPS).

The SAPS flow channel leads to sunward plasma redistribution within the SED Plume. Combined ground and space-based observations have shown that the features observed at ionospheric altitudes map directly to features and processes in the magnetosphere. To first order, cold plasma redistribution proceeds such that plasma parcels at ionospheric heights and at the apex of a magnetic field line move together in the E x B direction maintaining their magnetic field alignment. In this way, ground-based observations of ionospheric characteristics and dynamics provide a remote determination of the occurrence, timing, and

spatial structure of magnetospheric processes that are important drivers of space weather effects across the coupled system. Statistical studies have indicated the persistence and predictability of the polarization stream. SED is observed on field lines where SAPS overlaps the outer plasmasphere, forming plasmasphere erosion plumes at high altitudes and SED plumes in the ionosphere.

The MIT coupling that leads to the pronounced characteristics of SED and SAPS in the disturbed ionosphere goes far beyond the downward extension of magnetospheric forcing into the lower regions of the ionosphere and atmosphere. The feedback of ionospheric conductivity onto the magnetospheric field-aligned current system results in the SAPS electric field. This electric field transports ionospheric and plasmaspheric material to the dayside cusp and magnetopause, where reconnection redistributes this dense cold plasma through the tail lobes, across the polar caps and into the magnetotail. Injected into the inner magnetosphere during subsequent substorm dipolarizations, these ionospheric ions play a significant role in ring current formation, particle precipitation, and modulate wave-particle interactions and radiation belt energization.

These few examples illustrate the complex nature of the geospace coupled system. These MIT coupling processes and their effects are repeatable but vary in intensity from event to event and are both local-time and longitude dependent. Continuous global observations of multiple parameters are needed to better understand and predict the closely coupled aspects of Earth's space weather system.

2.5. Troposphere/Middle Atmosphere Weather System (Hazard B)

The troposphere/middle atmosphere (stratosphere + mesosphere) weather system is a major source of waves and other types of emissions that can propagate to the IMUA, disturb it and be detected there: (i) atmospheric waves over a broad range of temporal and spatial scales, from infrasound to planetary waves, (ii) electromagnetic emissions, (iii) upward-propagating energetic charged particles. The sources and variability of these phenomena are closely connected to the geographical and seasonal distributions of the weather system itself. Figure 7 displays a global map of the average distribution of surface winds for January (panel A) and June (panel B) and the corresponding structure of the air mass motions in a meridian plane from pole to pole. These maps reveal two major characteristics of the mean distribution of wind patterns in the troposphere:

First, it is mainly organized in latitude bands of alternatively easterly and westerly winds as one moves from equator to pole. This dominant

zonal flow is related in the meridional plane to an alternating pattern of convective cells, the Hadley cells on either side of the equator, then the Fennel cells at midlatitudes and finally the two polar cells (panel C). The net average effect of these meridional circulation cells is to redistribute towards the poles the excess of solar heating received in the lower latitude regions and to redistribute the angular momentum carried by zonal winds between adjacent latitude bands.

Second, it shows a very strong wind speed contrast between lands (where they are slower) and oceans (where they reach their maximum values). This contrast is mainly due to the friction effect of land topography on air flow and to the strong temperature contrasts existing between land and ocean surfaces.

The middle atmosphere is divided in two regions defined by their vertical gradient of temperature (see Figure 10, right hand side curve). The stratosphere, characterized by a positive gradient, extends from 10-17 km to 48

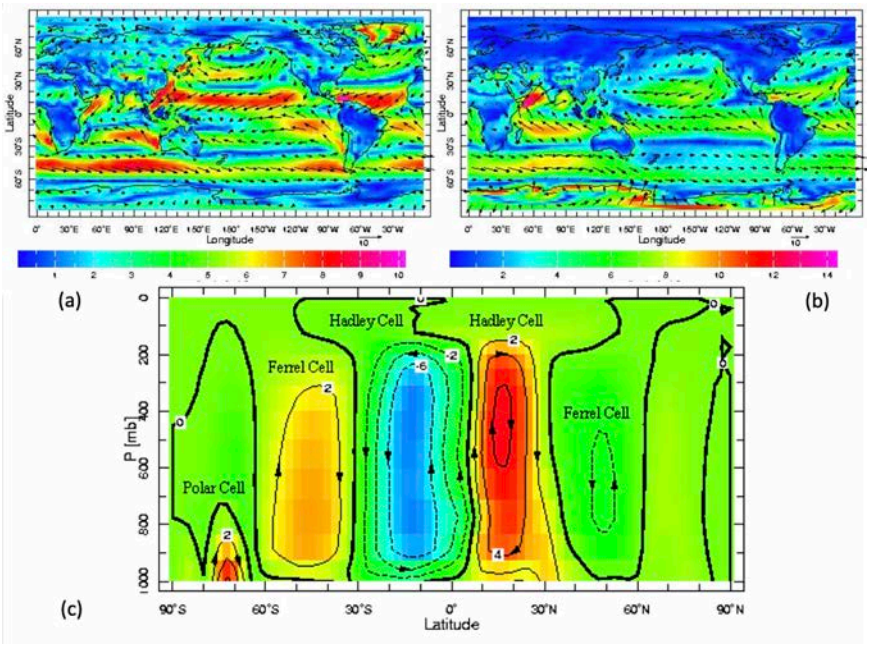

Figure 7: *An illustration of the mean latitudinal structure of tropospheric circulation: at the top, mean zonal wind at ground level for January (a) and June (b), showing that the circulation is dominantly zonal, with a strong intensity contrast between continents and oceans; at the bottom (c), mean mass air circulation in the troposphere, showing the different meridional cells which transport angular momentum and redistribute heat received from the sun predominantly at low latitudes towards higher geographic latitudes.*

km. This is the region where the ozone layer is formed. The mesosphere, characterized by a negative temperature gradient, extends from 48 to 90 km. This is a very dynamically active region. In the stratosphere, the main meridional-vertical dynamical feature is the Brewer Dobson circulation (Shepherd 2000; Hauchecorne et al., 2018), displaying an ascending branch in the equatorial region, a meridional transport from the equator to the poles and a descending branch in the polar regions. In the mesosphere, circulation is mainly from the summer pole to the winter pole, with an ascent (descent) of air and an adiabatic cooling (warming) at the summer (winter) pole.

Together with general circulation and weather systems, thunderstorms, and associated lightning strokes are another major source of upward-propagating disturbances. The global annual cumulative distribution of these flashes, shown in Figure 8, has been studied and established by Christian et al. (2003) on the basis of five years of observations by the Optical Transient Detector (OTD), an imaging instrument carried on a 70° inclination low Earth orbit by the Microlab-1 satellite launched in April 1995. This map shows that the world-wide maximum of lightning flash activity is reached in western and central Africa over the Congo basin, constituting a thunderstorm "hot spot" over the territories of Rwanda and the Democratic Republic of Congo. It also shows a spectacular contrast between lands and oceans: thunderstorm flashes are in the average ten times more frequent over lands. Thunderstorms are concentrated there over the two major equatorial fluvial basins (Congo and Amazon) and on the eastern coasts of the American and Asian continents, where they are triggered by the flow of cold continental air over warmer ocean water. Just like weather in general, the geographic distribution of

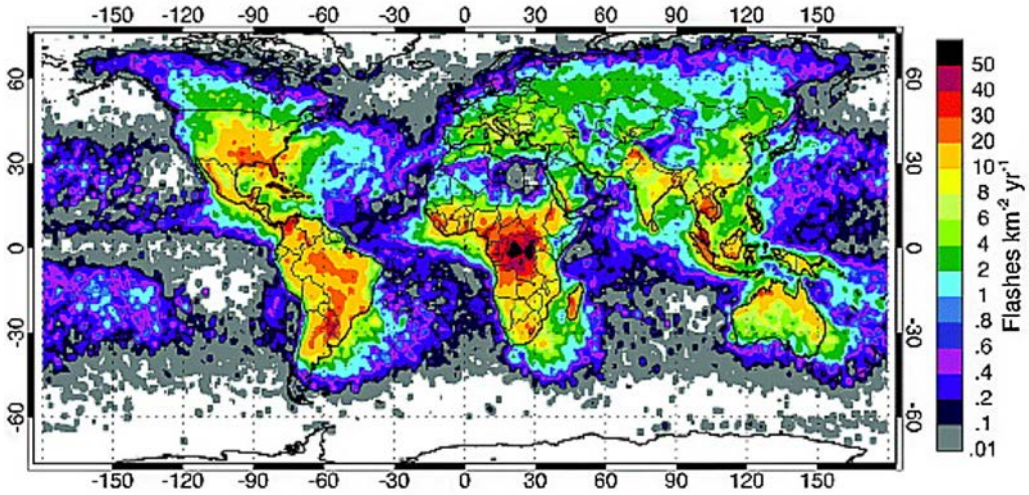

Figure 8: *Annualized global distribution of lightning strokes over the globe, expressed in units of number of flashes per square km and per year, showing a pronounced maximum over equatorial Africa in the Congo basin over Rwanda and the Democratic Republic of Congo, maximizing over the Rwandan city of Kamembe, and a strong land-oceans contrast. From Christian et al. (2003).*

thunderstorms is dominated by strong latitude variations and land-to-oceans contrasts.

The modes and schematic latitudinal distributions of upward propagating disturbances produced by weather phenomena are illustrated in Figure 9. Its panel A displays in a meridian plane the main sources of waves and weather events in the troposphere and the host of atmospheric waves they produce. The efficiency of atmospheric waves in transferring energy and momentum vertically between the different atmosphere layers is a consequence of the exponential decrease of atmospheric density with increasing altitude: conservation of wave kinetic energy density imposes that their relative amplitude increases exponentially with upward propagation, until it reaches a critical value where the wave breaks and deposits energy and momentum into the mean flow. Let us describe the different wave modes involved in order of decreasing spatial scales (or periods).

Rossby planetary waves (PW) are a consequence of the equator-to-pole gradient

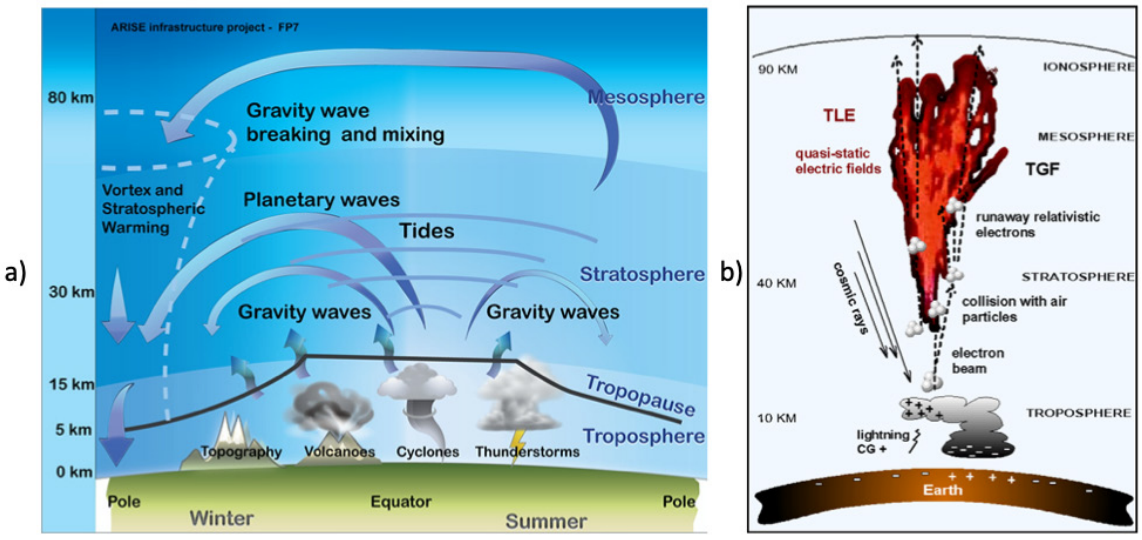

Figure 9: *A schematic of the atmospheric dynamic processes encountered in the Earth's lower and middle atmosphere which lead to different types of wave emissions responsible for transfer of energy and momentum between atmospheric layers and between latitude regions: a) planetary waves, tides, gravity waves and infrasound waves (not shown in the figure) generated by topography, weather evens and volcanoes transfer momentum and deposit energy by reflection, absorption and/or breaking (from E. Blanc et al. (2018), ARISE FP7 Infrastructure project of the European Union); b) Thunderstorm clouds are responsible for the generation of different types of emissions into the IMUA: Transient Luminous Events (TLE), Transient Gamma Ray Flashes (TGFs) possibly triggered by upward-accelerated electron beams, ELF radio emissions penetrating into the ionosphere and interacting with radiation belts (not shown) (from Blanc E. et al., 2007)*

of potential vorticity and are produced by flows over orography and by temperature contrasts between land and ocean. They also contribute very significantly to the vertical redistribution of momentum and energy, and for this reason play an important role in the variability of atmospheric circulation in the IMUA (see the review articles by Salby, 1984, and Hauchecorne et al., 2010). The stratosphere acts as filter for the upward propagation of PWs. In summer, the stratospheric circulation is from east to west and PW propagation is blocked. In winter, stratospheric circulation is from west to east and PWs propagate upwards with an increasing amplitude until they break. This process can lead to a sudden stratospheric warming (SSW), an event characterized by an increase of temperature of several tens of degrees in one or two weeks in the polar region, a destruction of the polar vortex and a reversal of the zonal wind. The forcing of the IMUA by the lower atmosphere is strongly modified during a SSW. For instance Goncharenko et al. (2018) showed that the electron density in the nighttime ionosphere was dramatically reduced for several days by the effects of the January 2013 SSW.

Atmospheric tides are generated by the solar diurnal excitation of the atmosphere via absorption of solar radiation mainly by ozone in the stratosphere and secondarily by water vapor in the troposphere. They appear as quasi-periodic global oscillations of the atmosphere at the diurnal period and its harmonics. Though of very low amplitude in their source region, they experience a spectacular amplification with upward propagation and reach horizontal wind amplitudes of tens of m/s in the mesosphere, where they can be detected by MF radars (Kishore et al., 2002) and lidars (Kechkut et al., 1996) and penetrate into the lower thermosphere where they can be measured by incoherent scatter radars (Blanc M. et al., 1977; Blanc M. and Amayenc, 1979; Richmond et al., 1980). Adding their effect to the locally generated thermospheric tides, these tidal winds generate ionospheric currents and electric fields in the lower ionosphere by dynamo action which are the main source of the regular Sq daily variations of the geomagnetic field at ground level (see sections 2.8 and 3.2).

Gravity waves (GW), propagating at frequencies above the Brunt-Väisälä frequency, are the most important example of interactions between waves and the mean flow. They are generated by flows over topography, thunderstorm-related convection, cold fronts, and jet imbalance. They contribute to the redistribution of momentum and energy between latitude regions, mainly from summer to winter (Figure 9, panel A) and from the lower atmosphere to the middle atmosphere and lower thermosphere where they break and deposit energy. At the ionosphere level they can be detected as Travelling Ionospheric Disturbances (TIDs). Their sources and contributions to middle atmosphere dynamics and variability have been reviewed by Fritts and Alexander (2003).

At shorter scales, infrasound waves are continuously produced by sources like ocean swells and volcanoes, winds over topography, and thunderstorms. It has been suggested that they can propagate up into the lower thermosphere and contribute to its energy

budget. With the development of the International Monitoring System (IMS) which uses a network of micro-barographs as a tool for the verification of the Comprehensive Nuclear-test-ban treaty, is has been progressively realized that the upward propagation of infrasound waves is very sensitive to winds in the stratosphere (Le Pichon et al., 2008) and can be potentially used in return to measure these winds (see citations in Blanc E. et al., 2015; 2018).

A nice example of the use of the IMS to study atmospheric dynamics can be found in Blanc E. et al. (2014). These authors, analyzing ten years of IMS observations of the emission of gravity waves by thunderstorms over Ivory Coast, Western Africa, unambiguously showed the relationship of GW emissions to the location of thunderstorm cells and the interaction of the emitted waves with the mean wind. They also established that thunderstorms far dominate orography and other sources in GW emission over this region.

Gravity waves, however, are not the only type of upward-propagating disturbances generated by thunderstorms. Until the end of the XXth century, it was believed that the major visible manifestation of thunderstorms was their lightning strokes and associated flashes, corresponding to intracloud or cloud-to-ground electric discharges. But from the end of the XXth century, observations from mountain tops and from space progressively revealed that thunderstorms do not only produce intracloud and cloud-to-ground electric discharges: they also generate a host of other emissions that propagate into the ionosphere, as illustrated in panel B) of Figure 9 (from Blanc E. et al., 2007): Transient Luminous Events (TLE's), Transient Gamma-ray flashes (TGFs), upward acceleration of energetic electron beams, VLF radio emissions etc.. The role of space observations in the characterization of these phenomena has been crucial, as illustrated for instance by the study of TLE's by Blanc E. et al. (2010), so much that a new space mission dedicated to their observations and to be launched in 2020, TARANIS, has been developed by the French space agency, CNES (Blanc E. et al, 2007).

In summary, a ground-based observation system like the IMCP designed to capture the variety of emissions of waves, particles, electric discharges, and electromagnetic emissions produced by tropospheric and middle atmospheric weather systems will need to include families of sensors that can detect and characterize these various phenomena. Their geographical distribution will have to be tailored to capture the two main sources of atmospheric dynamics variability we identified: latitudinal variations and land-to-ocean contrasts. As the example of thunderstorm-related emissions illustrates, this observation system will need to be complemented by space observations.

2.6. Long-Term Evolution of the Climate System (Hazard C)

CO^2 concentrations due to climate change increase at least up to the lower thermosphere at approximately the same rate as near the surface, as confirmed by satellite measurements (e.g. Rezac et al., 2018). The increasing concentration of CO^2 cools the upper atmosphere instead of heating it, because the very low density of the upper atmosphere is not sufficient to trap the outgoing longwave radiation and cooling due to IR radiation by CO^2 dominates. While CO^2 is the most important driver of global change and long-term trends in the upper atmosphere, there are other trend drivers: secular changes of the Earth's magnetic field (very regional effect), long-term changes of geomagnetic and solar activity, stratospheric ozone decline and recovery, water vapor (mesosphere), and atmospheric waves (planetary, tidal, and gravity waves), whose impact is largely unknown and varies with time and region. Therefore, trends need not be stable in space and time. The most recent review of progress in trend studies is that by Laštovička (2017).

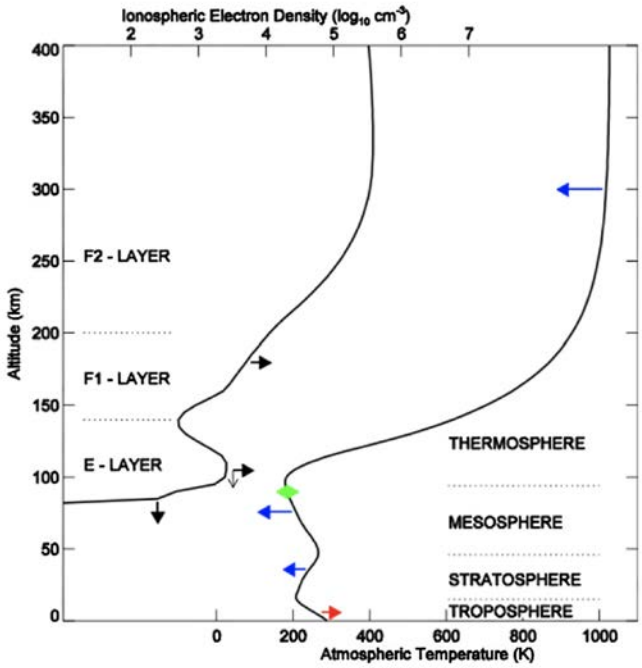

Figure 10: *Summary of the consistent mesospheric, thermospheric and ionospheric trends which form the global pattern/scenario of evolutions associated with mid-term climate change in the upper atmosphere, translated in terms of temperature and electron density. This scenario, directly derived from observations, is supported by model simulations.*

Since the publication of the first scenario of global change in the upper atmosphere (Laštovička et al., 2008), it has been continuously broadened and improved by follow-up studies. The resulting observational scenario (Figure 10) is supported by model calculations and confirms that long-term trends are primarily caused by the increasing concentration of CO^2.

Trends in mesospheric temperatures are significantly affected by long-term changes of stratospheric ozone concentration, which account for up to one third of observed temperature changes (Lübken et al., 2013). Ozone also produces negative trends in the neutral atmospheric density up to the lower thermosphere, where they produce decreases on the order of -2%/decade at 400 km (Emmert, 2015). Such density decreases can increase the orbital lifetime of low-orbiting satellites but also of dangerous space debris. Ionospheric parameters also display long-term trends (Laštovička, 2017 and references herein). In some regions they are also significantly affected by the secular change of the Earth main magnetic field (e.g. Cnossen et al., 2016).

2.7. Lithospheric Activity and Earthquakes: Effects on the IMUA (Hazard D)

Earthquakes are the result of plate tectonic motions. The major seismic belts and active volcanoes in the world are mainly distributed in the boundary areas of plates (Figure 11, upper panel) with a high concentration along the "fire belt" surrounding the Pacific Ocean, which happens to be nearly tangent to the 120°E and 60°W meridians near its maximum eastern and western extensions. As a result of the collision of Indian, Pacific, and Philippine plates, seismicity in China is particularly strong and widely distributed. Almost all provinces have experienced strong earthquakes with M>6. About 20 active volcanoes have been discovered until now in China, mainly distributed in the northeastern provinces. Although volcanic activity is much lower than seismic activity, the associated hazard is larger.

Seismic activity originates from mantle convection which drives plate motions. It may produce effects in near-Earth space, including the IMUA, by means of Lithosphere-Atmosphere-Ionosphere-Coupling (LAIC) mechanisms. Although it seems well-established that a significant fraction of earthquakes generates ionosphere anomalies prior to their occurrence (Hayakawa et al., 2010; Liu et al., 2009; Liu et al., 2000; Zhao et al., 2008), the generation mechanisms of seismo-ionospheric disturbances are still poorly understood. The possible coupling mechanisms between seismic activity and the upper atmosphere include:

- electric field mechanisms (Pre-earthquake): vertical electric field emerging from the seismogenic zone and extending into the upper atmosphere (e.g., Freund, 2011;

Freund et al., 2009; Freund et al., 2004; Kuo et al., 2011; Kuo et al., 2014; Sorokin et al., 2001; Zhou et al., 2017);

- electromagnetic wave mechanisms (pre-earthquake): electromagnetic waves emerging from the seismogenic zone (Freund et al., 2006; Gao et al., 2016; Hayakawa et al., 2000; Molchanov & Hayakawa, 1995; Nemec et al., 2008; Simpson & Taflove, 2005); and

- acoustic gravity wave mechanism (co-seismic): AGWs emerging from the seismogenic zone and propagating towards the upper atmosphere (Hao et al., 2012; Liu et al., 2006).

Making progress in understanding these mechanisms and identifying the most important ones requires three-dimensional "steric" observations of earthquake effects ideally covering different altitudes from the seismogenic zone up into the IMUA (described in section 3.2) combined with theoretical and modeling studies (some of which are described in section 4.6). This progress in our scientific understanding of pre-earthquake processes is a prerequisite to the development of a predicting capability on Earthquakes occurrence. Comprehensive reviews of the observational, theoretical and modeling aspects of this major scientific and societal challenge can be found in the AGU book edited by Ouzounov et al. (2018) and in Pulinets and Ouzounov (2018).

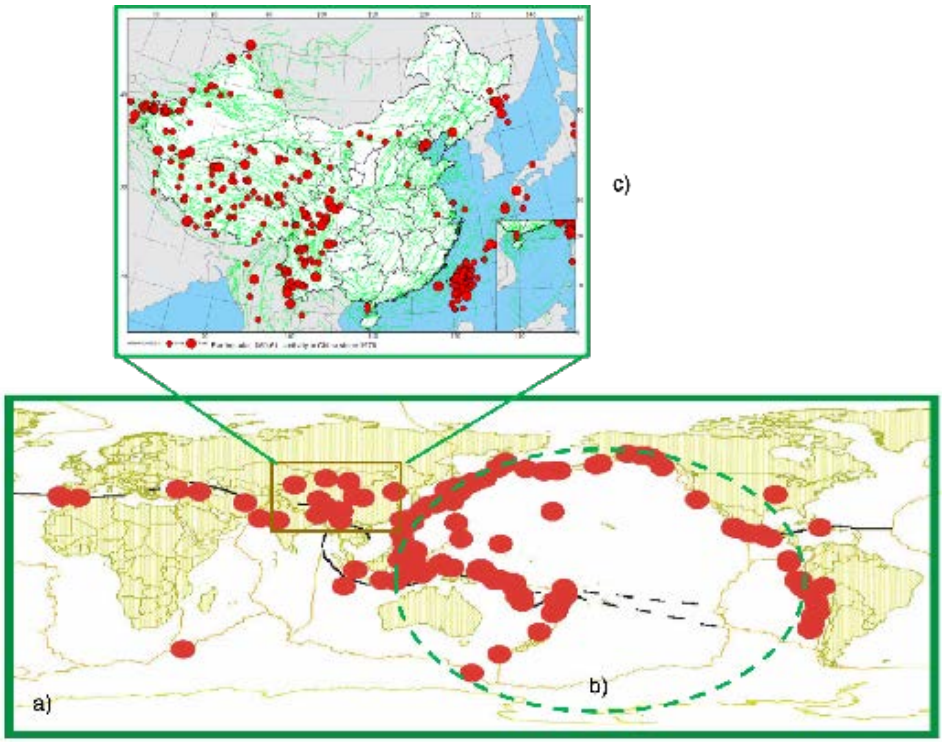

Figure 11: *Distribution of seismic activity over the world (a) and in China (c). Seismicity is mainly driven by tectonic plate collisions and has a particularly strong occurrence rate along the "fire belt" (b) encircling the Pacific Ocean. The upper panel shows the distribution of major earthquakes in China since 1970 for two magnitude levels : 7< M < 8.5 (large red circles) and 6 < M < 6.9 (small red circles). Credits: Map of major earthquakes in China, Institute of Crustal Dynamics (ICD), China Earthquake Administration (CEA).*

2.8. Geomagnetic Field Processes and their Long-Term Evolution (Hazard E)

Solar activity and heliospheric processes are the main sources of external perturbations to the Earth's environment. Their geo-effectiveness entirely relies on the processes taking place when they interact with the Earth's magnetic field and atmosphere. Thus, before going further, we will give a brief description of the geomagnetic field, its different sources, and their specific temporal variations.

2.8.1. Sources of the Geomagnetic Field

The Earth's magnetic field is a dynamic system and varies on a wide range of timescales from microseconds to hundreds of millions of years. The internal sources of the geomagnetic field include those originating in the core and lithosphere of the Earth (see Figure 12). The core field (e.g. Hulot et al. 2015 or the recent IAGA book edited by Mandea et al., 2019) is dominated by fields generated from a self-sustaining dynamo in the Earth's fluid outer core. This dynamo creates around 95% of the magnetic field strength at the Earth's surface. The measured magnetic field averages a strength on the order of 50,000 nT, varying, however, between some 20,000 and some nearly 70,000 nT. The strongest scalar magnetic fields originating from the Earth's core are found in the Earth's polar regions. The area just off shore of Antarctica, in the ocean between Australia and the Antarctic, possesses the largest scalar magnetic fields, averaging more than 66,000 nT. The core field varies on timescales of months to millennia, even millions of years when reversal processes are considered. The variations on decadal to millennial timescales are known as the secular variation.

Another internal source is the quasi-stable lithospheric field (Purucker and Whaler 2015) which is generated in rocks containing minerals carrying the magnetization and situated below the Curie temperature, generally in the upper 530 km below the Earth's surface. Globally, its contribution is much smaller and on the order of 20 nT, but it can locally be much larger. It has a bimodal character, lineated above the ocean lithosphere and weaker than the fields associated with continental lithospheres, which are characterized by much more varied directions. At the surface of the Earth, this weakness is dominantly a function of the difference in thickness of the oceanic vs continental crust (7 vs 35 km, respectively). Two kinds of magnetization can exist within cool lithospheric rocks, permanent (remanent) magnetization, and induced magnetization. The direction and intensity of permanent magnetization is dependent on the origin and history of a rock. Induced magnetization

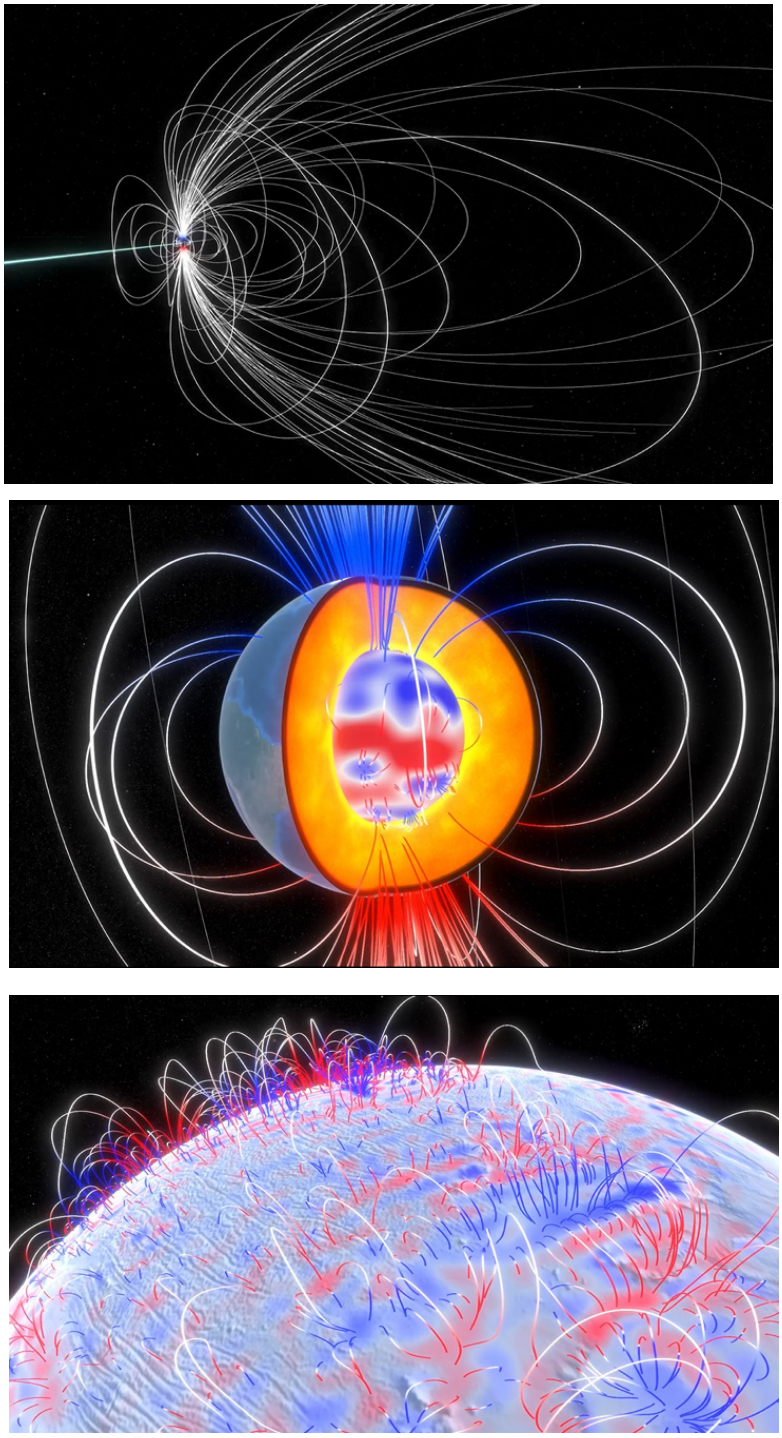

Figure 12: *The different sources of the geomagnetic field. a) The magnetosphere shielding our planet against the solar wind; b) Contour lines of the dominating core field intensity at Earth's surface and downward continued (radial field component) to the core-mantle boundary (CMB). The South Atlantic weak field anomaly is seen as a minimum in the intensity at the surface, caused by a large patch or reverse (blue) magnetic flux at the CMB; c) The lithospheric field caused by magnetized rocks, revealing the striped normal and reverse magnetic field pattern (after Mandea, 2018).*

is proportional in magnitude, and generally parallel to the ambient core field. Another first-order observation about the strength of the lithospheric field is that the field, while variable in detail, varies in magnitude from the magnetic poles to the equator by a factor of two, a reflection of a strong contribution from induced magnetization. The lithospheric field changes on time-scales of millions of years except at sources such as active volcanic regions or along mid-ocean ridges.

The geomagnetic field external sources are generated by solar-terrestrial interactions and include those originating in the ionosphere, those which couple the magnetosphere and ionosphere, and those associated with more distant regions of the magnetosphere, in particular the ring current, the magnetotail, and the magnetopause. These fields are produced by electric current systems in the ionosphere and magnetosphere. Strong electric currents are also generated and flow down to the ionosphere in the auroral zones where intense east-west currents, named the auroral electrojets, are produced. The magnetic disturbances observed at high latitudes are due to the magnetic fields of these auroral electrojets.

2.8.2. Geomagnetic Field Temporal Variations

The geomagnetic field is in a permanent state of change. The longer variations, over time-scales of months to decades, mostly reflect changes in the Earth's core, and the very long ones, from centuries to millions of years, reveal different aspects of core processes and space climate. The shortest time scales are linked to processes arising in the ionosphere and magnetosphere and their coupling, and cover the scope of space weather. We list in the following paragraphs the main characteristics of the core magnetic field temporal variations.

2.8.2.1. Inversions and Excursions

A dramatic change in the core field is the reversal of its polarity or sometimes an important decrease of its intensity which does not reach the reversed, anti-parallel, directional state. The ocean floors and lake sediments are one of the only, albeit imperfect, records of these geomagnetic events (Merrill et al. 1996; Valet 2003). The occurrence of reversals is not constant through time. The last geomagnetic reversal, known as the Brunhes-Matuyama reversal, occurred about 780,000 years ago. Recent estimates indicate that the actual directional shift between the two opposite polarities lasted less than 1 Kyr (Valet et al.

2012). Recently, when investigating this event, Sagnotti et al. (2014) proposed the idea that this polarity reversal occurred over an even shorter time.

Another significant change in the Earth's magnetic field is produced during geomagnetic excursions. Unlike reversals, however, an excursion does not permanently change the large-scale orientation of the field. These events represent a decrease in the field intensity up to 20% of its normal value and usually last a few thousand to a few tens of thousands of years. The field remains largely dipolar, but wanders away from the rotational axis (Valet et al. 2012). One of the first investigated excursions is the Laschamp event, dated at around 41 kyr ago, which occurred during the last ice age (Korte et al. 2019).

2.8.2.2. Secular Variation

The secular variation, defined as the first temporal derivative of the core field, carries information about the dynamics of the core. One of the characteristics of secular variation is the geomagnetic jerks, which are sharp changes in its trend (Mandea et al. 2010). The temporal evolution of secular variations generally appears as a series of nearly straight lines separated by abrupt and short changes of slope — the geomagnetic jerks — which separate two successive straight lines. In spite of many attempts, the physical origin of geomagnetic jerks is not yet fully established. Aubert and Finlay (2019) reviewed them and proposed numerical models of the geomagnetic field favoring the occurrence of geomagnetic jerks.

A better characterization and understanding of these events can provide a way to discriminate internal (core) or external (space-weather) signatures with similar time-scales.

2.8.2.3. Dipole Moment Decay

Magnetic field measurements can be used to compute the dipole component of the field and its dominant axial part, parallel to the Earth's rotation axis. Since magnetic field intensity measurements exist, the dipole moment has decreased by nearly 6% per century. Figure 13 (top panel) shows the temporal variation of the axial component of the dipole field, as computed from the IGRF-12 field model, throughout the XXth century. The observed average rate of decrease is of some 16 nT.yr-1. In some epochs, the field had very different rate fluctuations. For example, around 1980 it diminished twice as fast as nowadays. If

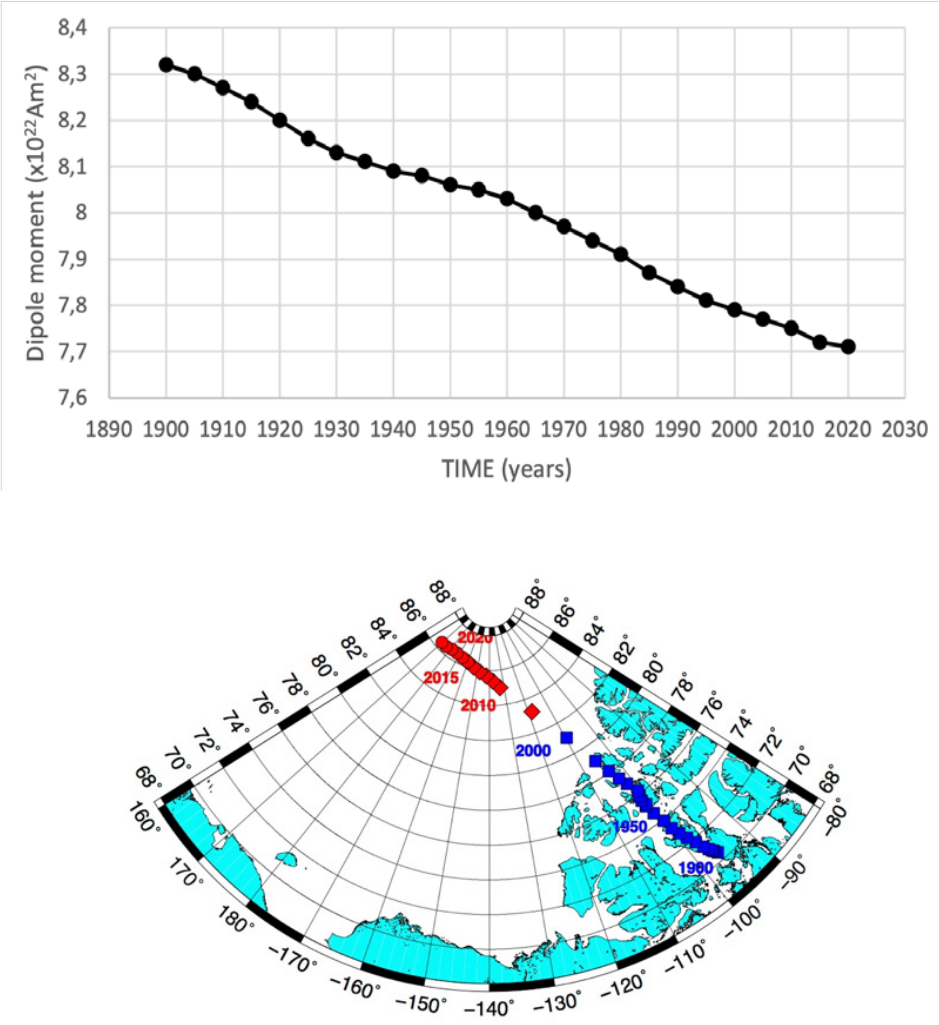

Figure 13: *(Top panel) Geomagnetic dipole moment variation since 1900 as computed from the IGRF-12 model. (Bottom panel) North magnetic poles positions as obtained from IGRF-12 model (blue diamonds - values at 5 yr interval, red diamonds - values at 1-year interval). The values for 2015-2020 are based on a predictive secular variation.*

the same rate of decay is extrapolated in time, the axial dipole would reach zero values in less than 2000 yrs. However, the current value of the dipole moment is not as low as the mean moment in the Holocene.

2.8.2.4. Magnetic Poles Drifts

The positions of the north and south magnetic poles gradually change with time, as illustrated in Figure 13 (bottom) for the north pole. Considering the gufm model (Jackson et al. 2000) and more recent models such as IGRF-12 (Thebault et al. 2015), the locations and velocities of the two magnetic poles can be computed. Such computations indicate that over more than 400 years both magnetic poles have changed their positions, however with very different rates of change for each pole. During the first half of the XXth century, the north and south magnetic poles velocities are comparable, around some 10 km.yr-1. Since 1970 (the time of a well-documented geomagnetic jerk), the north magnetic pole has moved from Canada towards Siberia, with velocities reaching some 60 km.yr-1 (Newitt et al. 2002; Olsen and Mandea 2007) and the south pole towards Australia, with a much lower velocity of around 5 km.yr-1. Figure 13 (bottom panel) shows the positions of the north geomagnetic pole as obtained from the IGRF-12 model. Its drift speed has recently entered a deceleration phase, decreasing from about 53 km.yr1 in 2015 to 43 km.yr1 in 2020. The latter value, however, relies on the predictive secular variation.

The location of the north magnetic pole appears to be governed by two large-scale patches of magnetic field, one beneath Canada and one beneath Siberia, and could be linked to a high-speed jet of liquid iron beneath Canada (Livermore et al. 2016). The fast acceleration/deceleration of the north magnetic pole drift has a large impact on space weather, since the locations of all dynamic polar processes are affected by this drift.

2.8.2.5. South Atlantic Anomaly

Another striking characteristics of the geomagnetic field is named the South Atlantic Anomaly (SAA), a region where the particle flux is unusually high and the total field intensity unusually low (Figure 14), reaching a minimum value around 20,000 nT for the epoch 2020. Comparing MAGSAT and CHAMP satellite measurements and considering only Swarm measurements, it was possible to estimate the changes in the core field intensity over the last decades, which are on the order of 1% per year. The SAA behavior seems to be connected to the general decrease of the dipole moment and to the significant increase of the non-dipolar field in this region. The weakness of the field intensity is caused by an increasing patch of magnetic flux opposite to the dipole direction at the core-mantle boundary. This observed behavior is well reproduced by numerical modeling.

Understanding the evolution of the SAA is important for space weather: this regional weakening in field intensity allows energetic particles and cosmic rays to penetrate much deeper into the magnetosphere than in other regions, resulting in significant space weather effects.

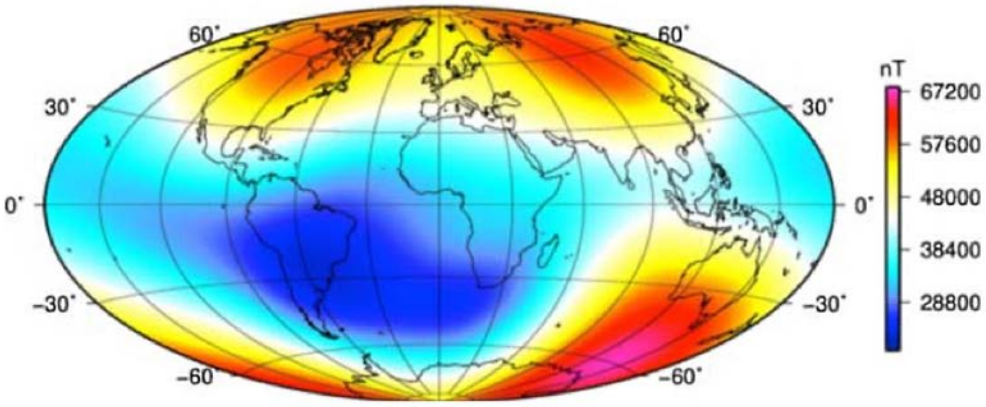

Figure 14: *The total field intensity at the Earth's surface. The South Atlantic Anomaly is the region with the lowest magnetic field values.*

2.9. Summary

This section briefly reviewed the different categories of disturbances associated to natural or anthropogenic hazards which can be detected by their imprint on the IMUA "screen", illustrated in Figure 2. To observe these imprints, the IMCP observation system must be able to capture the space and time variability of these sources. We will now review and synthesize the temporal and spatial coverage characteristics required to achieve this goal.

2.9.1. Temporal Coverage Requirements on the IMCP Observation System

Figure 15 summarizes the characteristic time constants associated with the different types of disturbances and hazards we reviewed in this section, using the same color coding for the three phase envelopes of geospace: solid, fluid, and plasma Earth. The relevant time scales extend from fractions of seconds for LAIC mechanisms transmitting effects of Earthquake-related activity to the IMUA, to decades for climate change and long-term changes in the solar and terrestrial magnetic fields, and to 10^8 year timescales for changes associated with plate tectonics which will remain outside the temporal filter of the IMCP observation system. In summary, it clearly appears that:

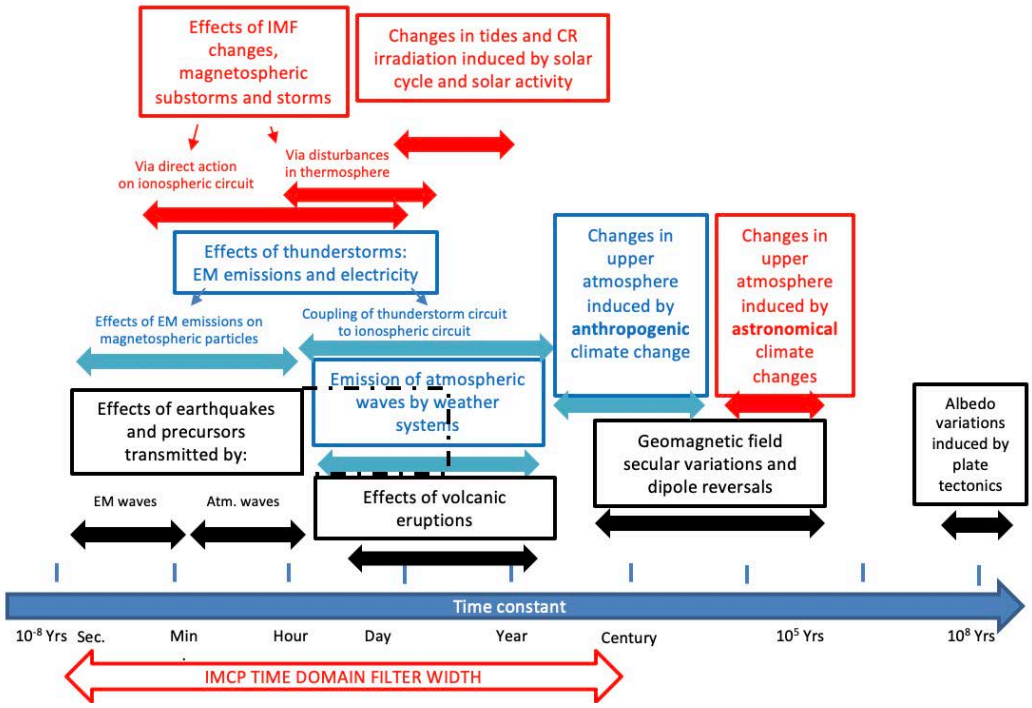

Figure 15: *A representation of the time scales of the different types of disturbances affecting the IMUA, from "plasma Earth" (red), "fluid Earth" (blue) and "solid Earth" (black). The red arrow at the bottom shows the time domain that needs to be covered by the IMCP observation system to capture most of these phenomena: seconds to decades. The implication is that this system must be established and operated in a coordinated and consistent way for several decades.*

1. on the short time scale limit, a fraction of the IMCP instruments need to cover very short, order-of-seconds variations; and

2. on the long time scale limit, one, or better several decades must be covered by the IMCP observation system. This implies that this system shall be deployed and operated consistently, and its data analyzed and delivered to its community of users over such a time scale. This is a strong requirement for the international organization which will manage it and for the institutions which will contribute to it.

2.9.1. Spatial/Geographic Coverage Requirements on the IMCP Observation System: Rationale for two Great Meridian Circles in Quadrature

In order to determine the "ideal" geographic distribution of a global observation system of the IMUA, one must start from a study of the geographical distribution of the sources and expected effects of the five categories of hazards we identified in section 2.1. This is what the different Mercator maps of the Earth grouped in Figure 16 show: from top to bottom, a comparative map of geomagnetic and geographic latitudes (relevant for hazard A), a map of the most seismically active zones of the globe (hazard B), a map of the average tropospheric circulation showing the zonal band and land-ocean contrasts, relevant for weather-related hazards (C) and climate change (D) and finally a map of the world distribution of lightning stroke impacts (C), on which we have overlaid the traces of the 120°E - 60°W Great Circle (red full lines) and of the 30°E – 150°W Great Circle (red dash-dotted lines).

Inspection of the different maps of Figure 16 inspires the following comments:

1. all categories of hazards are well organized in latitude (mainly geographic for weather and climate, mainly geomagnetic for the entries of energy due to space weather), except for seismicity and volcanism. This dominant latitude dependence goes along with a significant longitude dependence for weather and climate, mainly due to the land-ocean contrast. Thus the minimum possible coverage of the IMCP observation system is a full latitudinal coverage, either geographic (hazards B and C) or geomagnetic (A and E). The 120°E – 60°W Great Circle, spanning through east Asia, west Australia, and the Americas, happens to pass very close to the two geomagnetic poles and offers a maximum coverage of lands for the deployment of the instruments: it nearly perfectly combines by all practical means geographic and geographic latitude coverage;

2. to capture the land-ocean contrast, it appears ideal to combine it with a second

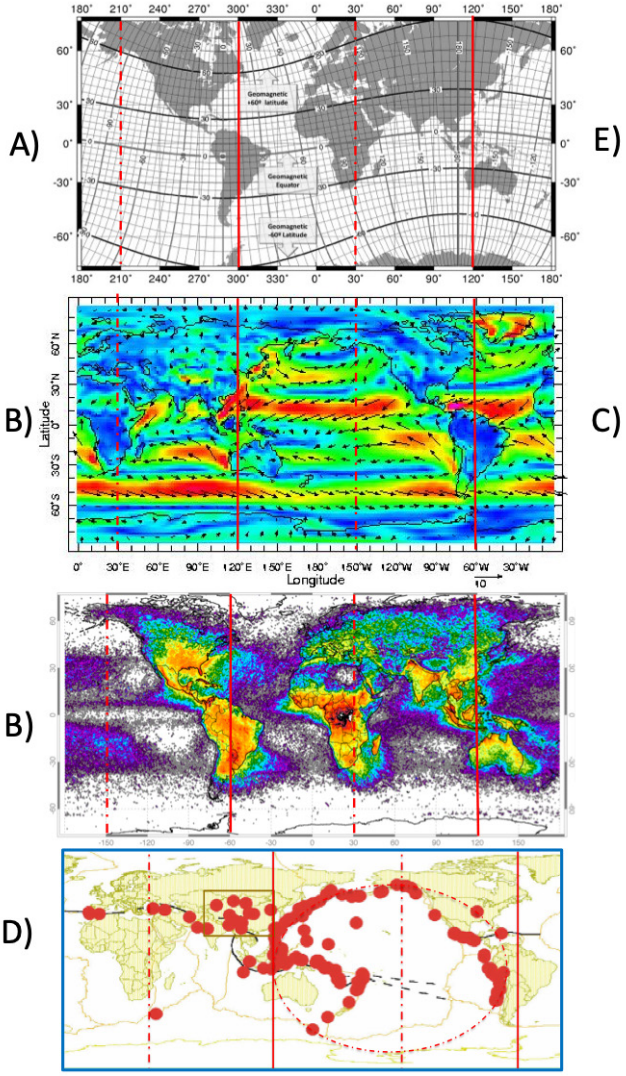

Figure 16: *Summary of the unique properties of an IMCP observation system deployed along two Great Circles in quadrature, the main 120°E-60°W meridian over east Asia, west Australia and the Americas (full red vertical bars) and a second Great Circle 30°E-150°W over central Europe, Africa, Alaska, Hawaii, Polynesia and the Pacific. The geographic and geomagnetic coverage offered by these two circles is near optimum for a scientific investigation of each of the five categories of hazards described in this section, which will be monitored and studied by the IMCP: A) the Sun-Earth coupling chain and space weather; B) lower atmosphere weather, thunderstorms and the global atmospheric electric circuit; C) climate change effects in the upper atmosphere; D) seismic activity; E) long-term evolution of the geomagnetic field . See text.*

Great Circle in quadrature: the 30°E – 150°W meridian happens to cover central Europe and Africa on one side, and to run across the Pacific from Alaska close to the Hawaiian archipelago and to French Polynesia on the other side;

3. the map of thunderstorm activity (bottom panel) strongly reinforces the case for this second Great Circle: while the first Great Circle does a fair job of covering active thunderstorm regions in south America and east Asia, the second one passes over the region of worldwide maximum lightning occurrence in central Africa, and over a remarkably quiet zone around its antipodal point in the middle of the Pacific. It will make it possible to compare the signatures of thunderstorms on the IMUA between two totally different levels of lightning activity; and

4. finally, concerning seismic and volcanic hazards (B), the first Great Circle, given its finite extension in longitude, will cover remarkably well the easternmost and westernmost segments of the circum-Pacific fire belt (Figure 11). As a complement, the second Great Circle will mainly monitor regions of low activity and of intra-plate (hot-spot related) activity, particularly near the Hawaiian archipelago.

In conclusion, the analysis of the material presented at the forum and summarized in Figures 15 and 16 shows that the 120°E – 60°W Great Meridian Circle, complemented by a second Great Meridian Circle meridian at the 30°E – 150°W longitudes, is the optimal possible choice for the deployment of the observation system of the IMCP. Section 3 presents and discusses the possible instrumental components, existing or to be developed, of this "ideal" IMCP observation system.

3. THE IMCP OBSERVATION SYSTEM

The realization of the scientific objectives of the IMCP presented in the previous section requires a continuous acquisition of observations of multiple parameters at a global scale to better understand and predict how the solar output, the interplanetary space, and the different layers of geospace drive disturbances that can be detected by monitoring the IMUA. In addressing this need, the IMCP needs to establish a baseline long-duration observing system consisting of networks of stations or facilities housing multiple instruments. These networks will form the core of the desired observing system and will provide the continuity of observations that is needed. Shorter-duration and regional instrument clusters will also contribute to this objective.

During the ISSI-BJ/IMCP Forum, an international group of participants provided descriptions of the instruments, their capabilities, and existing networks of immediate relevance to IMCP goals. This section provides a summary of their presentations.

3.1. The Chinese Meridian Project

The Chinese Meridian Project (CMP) is a ground-based space environment monitoring facility funded by China's National Development and Reform Commission as part of a series of major scientific infrastructures. It is a joint effort of more than ten institutions and universities in China, led by the National Space Science Center (NSSC) of the Chinese Academy of Sciences. The project was scheduled to be organized in two major steps. The first phase of the project has been put into operation since 2012. The organization of the second phase started in 2019 and will be completed in 2023.

The CMP is a very important component of the design of the IMCP, in the sense that it is a template of its future structure for the following two reasons:

1. after completion of phase II, it will be able to monitor all the chain of energy transfer from the solar output to the space environment above the Earth polar regions and above a representative fraction of the Chinese territory; and

2. it combines in its set-up a series of network instruments using the full diversity of techniques (optical, radio, magnetic, etc.), providing a basic horizontal coverage of the IMUA, mainly deployed during phase I, with a few key "heavy" instruments capable of monitoring in detail the vertical structure or a few columns of the atmosphere above selected experimental sites (lidars and incoherent scatter radars).

The first phase of the project, with the full name of East-sphere Space Environment Ground-based Comprehensive Monitoring Chain, consists of chains of 15 ground-based observatories located roughly along 120°E longitude and 30°N latitude. One chain of observatories, extending along the 120°E longitude circle, starts from Mohe, the northernmost city of China, and runs south roughly through Beijing, Wuhan, Guangzhou, and the island of Hainan (with instruments at Hikou, Fuke, and Sanya) and extends to China's Zhongshan station in Antarctica. Distances between neighboring stations are roughly 4°-5° of latitude or about 500 km apart, except the Zhongshan station in Antarctica. Another chain of stations was constructed roughly following 30°N, spanning from Lhasa to Shanghai. Each observatory is equipped with multiple instruments to comprehensively measure key parameters of the baseline and time-varying geomagnetic field as well as of the middle and upper atmosphere and ionosphere. Parameters of the solar wind are also tentatively measured.

Instruments of the first phase of the Chinese Meridian Project mainly include magnetometers, traditional and digital ionosondes, digisondes, incoherent scatter radars, high-frequency backscatter radars, mesosphere-stratosphere-troposphere radars, meteor radars, lidar, Fabry-Perot interferometers (FPI), and aurora spectrographs. Overall, the instruments can be grouped into four categories, named geomagnetic (geoelectric) field, radio wave, optical, and sounding rocket.

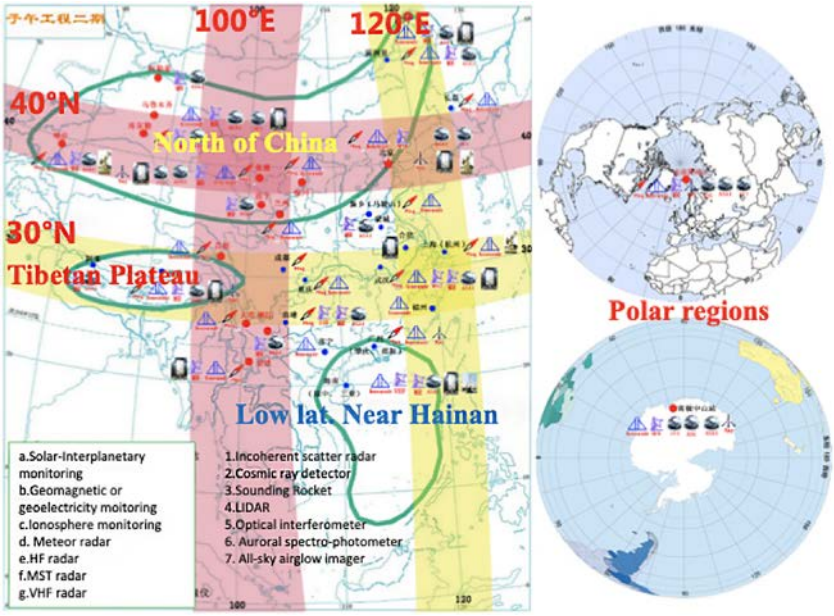

Figure 17: *Distribution of observatories that will be part of the Chinese Meridian Project at completion of the second phase of the project. The map shows the four focus regions of the second phase: polar regions, north of China, Tibetan plateau and low latitude region near Hainan island.*

Altogether, 87 instruments have been built and installed.

Besides, the space environment monitoring system provided by these instruments, a Data and Communication System and a Research and Forecasting System have also been built and are located in Beijing. The Data and Communications System is responsible for collecting, transferring, processing, storing, and distributing data in quasi real time. All data is made public via the website data.meridianproject.ac.cn. The Research and Forecasting System coordinates observations, develops relevant data analysis and space weather forecasting tools, and promotes international collaborations.

In 2018, the Chinese government approved an even more ambitious program to make a grand upgrade to the Chinese Meridian Project by deploying the instruments shown in Figure 17. This was to be the second phase of the project. This enhanced and more powerful observation system will deploy another 16 comprehensive stations with two main goals: to better cover China's territory and to build a stereo monitoring capability covering all space spheres of the solar terrestrial system, namely the solar surface, interplanetary space, magnetosphere, ionosphere, middle-upper

atmosphere. Complementing the existing two monitoring chains deployed in the first phase, other two chains will be established along 100°E longitude and 40°N latitude respectively, together forming a two-cross network configuration. In this design, four focus observation regions were selected to receive more emphasis. They are the polar regions where solar wind particles precipitate directly into the ionosphere and atmosphere, the north of China whereby disturbances from high latitude regions propagate towards the middle and low latitude regions, the Tibetan plateau region where unique geographic conditions give rise to a particularly complex atmosphere environment, and the low latitude region near Hainan island closest to the equatorial ionospheric anomaly, where ionosphere disturbances and anomalies occur very frequently.

Upon completion of its construction, the Chinese Meridian Project will run nearly 300 instruments deployed at 31 different stations.

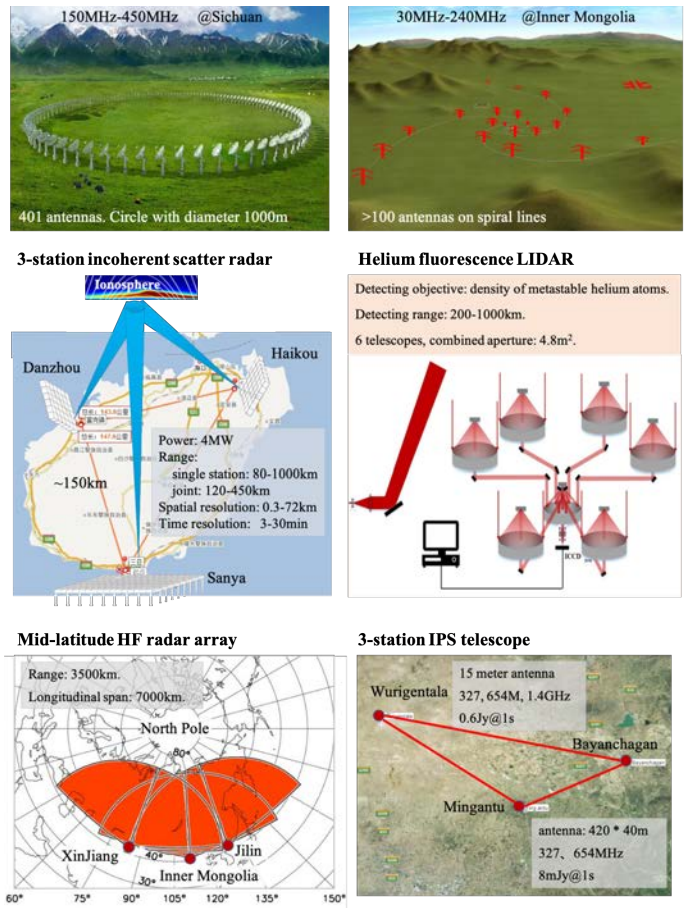

Figure 18: *Some innovative instruments of phase two of the Chinese Meridian Project*

Its instruments include regular ones often deployed in networks, such as magnetometers, FPIs, Lidars, Digisondes. In addition, many innovative and powerful instruments will be developed as part of the second phase, such as radio heliographs with a very wide combined frequency band, three-station interplanetary scintillation telescope (IPS) for interplanetary monitoring, three-station phased incoherent radar to make 3-D measurement of the low-latitude ionosphere, a high frequency radar array for middle to high latitude ionosphere observation, and a synthetic aperture helium lidar to measure atmosphere density up to 1000 km.

3.2. Global Observation Networks

3.2.1. Solar and Interplanetary Observations

The Sun is a unique star that can be observed across almost the entire electromagnetic spectrum, with cross-scales, high resolution, and high sensitivity in all physical parameters, from multiple view-points and close-approaching positions. Based on these observations significant achievements have been made in our understanding of solar surface phenomena, the Sun's internal structure and dynamics, solar magnetism and solar activity, and the propagation of the solar output through interplanetary space.

In China, the main solar physics observations include the following: the Huairou Solar Observing Station at National Astronomical Observatories, Chinese Academy of Sciences (NAOC), that measures and studies the solar magnetic and velocity fields at various altitudes of the solar atmosphere with (1) a 35-cm Solar Magnetic Field Telescope, (2) a 60-cm Solar Three-Channel Telescope and (3) Monitor System of Solar Activity consisting of a 10 cm full-disk vector magnetograph that measures the full-disk vector magnetic field at Fe I 5324.19 Å and a 20-cm Full-disk Hα telescope that obtains full-disk Hα monochromatic images; the Mingantu Spectral Radioheliograph (MUSER) with two arrays of 40 4.5-meters antennas covering 0.4-2.0 GHz and 602 m antennas covering 2.0-15 GHz with high time, frequency and space resolution for solar radio imaging-spectroscopic observations are operated at Mingantu Observing Station of NAOC. The solar radio spectrometers in dm-cm wavelengths are also operated in HSOS/NAOC. The Fuxian Solar Observatory (FSO) is operated by Yunnan Observatories, CAS, with the 1-meter New Vacuum Solar Telescope (NVST) for high resolution imaging and spectral observations of the Sun. A 70-700MHz spectrometer with a 11-meter dish and high time and spectral resolution is operated as well. The Optical and Near-infrared Solar Eruption Tracer (ONSET) of

Nanjing University with a three-tube telescope working in Ha, continuum and the near infrared He I 10830 Å is also operated at FSO. At Purple Mountain Observatory (PMO), CAS, the Multi-wavelength Solar Spectral telescope monitors three spectral lines: Ha, Ca II, and He I 10830 Å. There are several radio spectrometers operated by Shandong University at metric wavelength, among other instruments. Several solar monitoring telescopes are operated by the China Meteorological Administration in east and west China.

Phase II of the Meridian Project will include a Solar and Interplanetary Subsystem as a new component of the project. It will include (a) Metric and decametric arrays with a dish array in Tibetan Plateau (operated by NSSC) and a dipole array in Mingantu Observing Station; (b) an IPS telescope with three sites and two frequencies including a major site at Mingantu Observing Station; (c) a magnetograph at PMO; (d) a coronagraph at Yunnan Observatories, and (e) a μ-telescope operated by NSSC.

Big Bear Solar Observatory (BBSO) in California of New Jersey Institute of Technology now operates the largest aperture ground-based solar telescope in the world — the 1.6-meter Goode Solar Telescope (GST). GST is the highest-resolution operating solar telescope built in the U.S. in a generation. Benefitting from the long periods of excellent local seeing at Big Bear Lake, the GST, equipped with high-order adaptive optics, routinely collects diffraction-limited spatial resolution (~ 0.1") photometric, spectroscopic and/or polarimetric data, with a high cadence (<40 s), across the spectrum from 0.4 - 5.0 μm. Since the beginning of its regular operation in 2010, it has provided the community with open access to observations of the photosphere, chromosphere and up to the base of the corona with unprecedented resolution, shedding new light on the fundamental nature of solar activity and the sources of space weather. BBSO is the home of several synoptic programs – Full-disk Ha Global Network, GONG, SOLIS. BBSO expects to join the IMCP.

3.2.2. Neutron Monitors

Neutron monitors are particle detectors operating at the Earth surface. They observe particles resulting from the interaction of primary cosmic rays — mostly protons — with the Earth's atmosphere. If the primary has an energy of about 450 MeV, these reactions create a cascade of hadrons down to sea level. In most neutron monitors these hadrons interact with lead, producing secondary neutrons that are eventually detected via nuclear reactions in counter tubes. A more detailed description of neutron monitors and additional references are given in the open-access article of Bütikofer (2018).

Neutron monitors, which were conceived during the International Geophysical Year, remain state-of the art instrumentation to detect primary cosmic rays in the energy range from about 450 MeV to a few tens of GeV. The

primary particles are the permanent galactic cosmic rays and the sporadic contributions from the relativistic part of solar energetic particle events. The solar events are called ground-level events. The worldwide network of more than 50 neutron monitors allows one to derive the energy spectra, due to the filtering function of the geomagnetic field. For solar energetic particles the network also allows one to determine the anisotropy imposed by propagation along the heliospheric magnetic field.

Neutron monitors continue to be used for scientific research and are of increasing utility in space weather applications, for instance for the monitoring of radiation doses at aircraft altitudes. This made different groups realize that a common and easy access to their data will be mandatory for future utilization. The NMDB project of a neutron monitor database was developed and realized in 2008-09 with support from the European Union's 7th Framework Programme. After its establishment, the database, hosted and operated by the University of Kiel (Germany), succeeded to integrate a majority of the neutron monitors worldwide. Their data are available mostly with one-minute time resolution via the web site www.nmdb.eu , with more than 30 stations

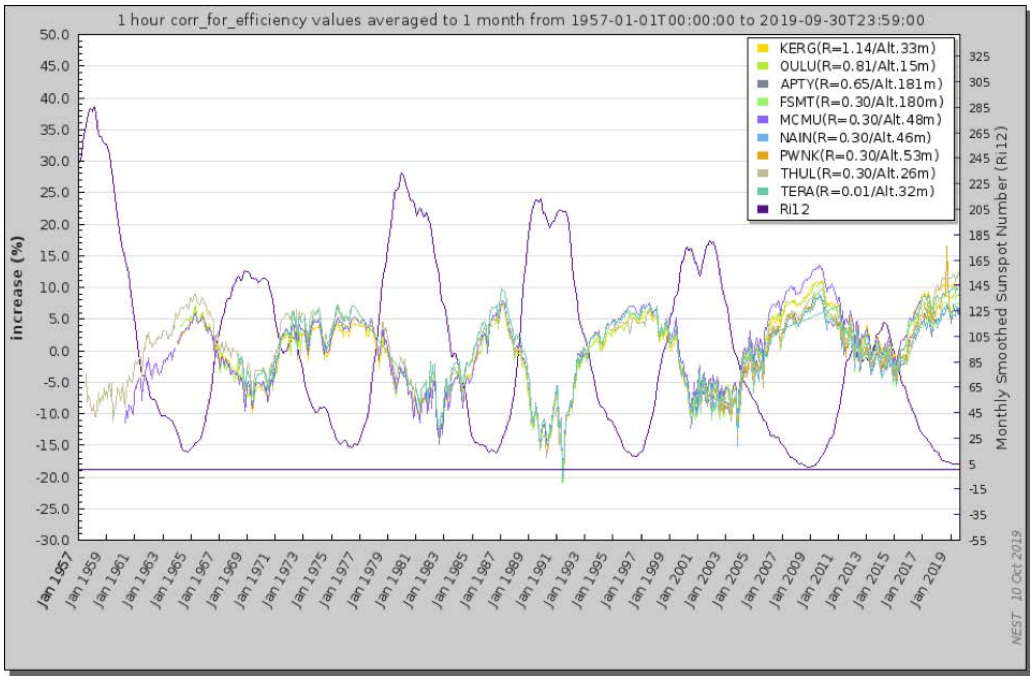

Figure 19: *Long-term evolution of neutron monitor count rates at sea level at a series of stations (color curves) from 1957 to 2019, compared with the monthly average sunspot number. The anticorrelation between cosmic ray fluxes and solar cycle appears bery clearly.*

providing them in near real time. Besides new data, the database also holds historical data, which in the case of some instruments date back to 1957.

A potentially interesting contribution of neutron monitors to the IMCP is their ability to characterize one of the mechanisms of energy input from outer space and its long-term variation. The impact of cosmic rays on the atmosphere leaves traces such as the production of radioactive nuclides, which can be used to reconstruct solar activity in the past. The impact varies on scales of the 11-year solar activity cycle and beyond: Figure 19 shows the long-term evolution of neutron monitor count rates (multi-colored curves) at sea level, using monitors with cutoff energies between 450 and 1500 MeV. It is well known that the cosmic ray flux is anti-correlated with solar activity during the 11-year cycle, as traced here by the smoothed monthly sunspot number (violet curve). This behavior reflects the obstacle that the heliospheric magnetic field opposes to the entry of galactic cosmic rays into the inner heliosphere. The obstacle evolves on multi-decadal time scales: the heliospheric magnetic field has been decreasing, and the galactic cosmic ray flux incident on the Earth's atmosphere increasing since the early XXIst century. The minimum cosmic ray fluxes during solar maxima were substantially higher in 2001-03 and 2013-15 than earlier. The data pool of the international neutron monitor network allows us to trace this evolution.

3.2.3. The Geomagnetic Environment

The geomagnetic environment of the Earth is the regime of magnetic currents deforming the magnetic field of the terrestrial dipole, in response to solar wind forcing (see section 2.8). This system of currents basically separates the magnetic field lines originating from inside and outside the magnetosphere, thus sculpting the comet-like magnetospheric cavity: solar wind magnetic field lines are compressed upstream and pulled out downstream into the magnetotail by strong magnetopause and magnetotail plasma sheet currents.

The magnetopause forms a well-defined obstacle to the solar wind. It is threaded by surface currents — the so-called Chapman-Ferraro currents — which result from the pressure balance between the impinging solar wind plasma and the Earth's magnetic field.

Other currents within the magnetosphere are driven by the relative motion of electrons and ions, caused inside the magnetospheric cavity mainly by combinations of convection, neutral wind drag, magnetic field gradients or electric fields. They are:

1. the cross-tail plasma sheet current maintaining the elongated magnetic tail;

2. the ring currents, carried by hot plasma and energetic particle drift motions in

the gradients and curvature of the closed dipole field;

3. magnetic field aligned currents, coupling the tail current and some of the magnetopause and ring currents to the highly conducting upper atmosphere;

4. the so called auroral electrojets resulting from the closure of these field-aligned currents inside the ionospheric conductor. They flow mostly at high latitudes but can expand to sub-auroral and middle latitude during large magnetic storms;

5. the so-called solar quiet (SQ) current system, driven by thermospheric neutral winds over the dayside ionosphere. They are caused and modulated by solar irradiation which generates significant levels of ionospheric conductivities. This current system appears however to be far from quiet during extreme space weather events; and

6. the equatorial electrojet, a drastic enhancement of horizontal east-west ionospheric currents along the dayside equator caused by the special horizontal magnetic field geometry prevailing there.

In the framework of the studies of space weather impacts on man-made infrastructures, one has come to pay special attention to fast and sometimes violent dynamic changes in any of these magnetospheric and ionospheric current systems, which may induce large electric fields in the terrestrial crust through rapid magnetic field changes at space and ground level (as readily seen by magnetometers), causing detrimental and sometimes destructive currents (so called Geomagnetically Induced Currents - GICs) in any conducting man-made infrastructure around the globe, e.g. powerlines, pipelines, communication lines, and railway systems. Of course the potential for damage by such currents ultimately depends on the crust's 3-D conductivity structure and network geometry and extent at any given location.

All the current systems described above can exhibit so-called "freak-events" of large and sudden dB/dt, mostly in response to and driven by violent space weather, and can cause varying types and degrees of disturbances in technological systems anywhere around the world. The auroral electrojets at high and sub-auroral latitudes exhibit violent enhancements in terms of substorms and spikes, the physical mechanisms of which are not yet fully understood, which clearly originate from solar wind space weather drivers. The sharp magnetic spike occurring at the beginning of most major magnetic storms, the so-called sudden storm commencement SSC, is the magnetic signal of a sudden and rapid enhancement of Chapman Ferraro currents, when a major CME plasma bubble hits the dayside magnetopause. These SSCs generate immediate and rapid electric field spikes all over the world which can cause potential space weather issues at latitudes usually not affected by the auroral currents systems. Likewise the equatorial electrojet and even the global dayside Solar Quiet current systems can respond rapidly to violent enhancements of the dayside ionospheric conductivities, as induced for example by extreme radiation enhancements caused by so

called solar Flares. Such Flare events can lead to so-called geomagnetic "crochets" all over the dayside part of the world.

Further studying the individual physical processes involved in such current systems and their potential interconnection — or at least the relative dependence of such currents on related solar wind drivers and dynamics — requires a denser and higher cadence observing system for magnetic fields, both in space and on the ground, than is currently available. At present, both the USA (NSF funded projects) and Europe (ESA funded MAGSWEDAN project) expand their magnetic observation capabilities to sub-auroral latitudes in order to better understand magnetic spikes in storms and other GIC-producing disturbances. However, these new observational systems and networks need to be coupled to other lower latitude systems, in order to better establish the global picture of disturbances that is needed.

As orbital constraints and land-mass distribution prevent the deployment of an equally dense global network of magnetometers everywhere, the new IMCP initiative will allow us to populate at least the three most important and readily accessible meridian regions with sufficient instrumentation both on ground (where one should strive for the same characteristics and same temporal resolution of magnetometer data everywhere along these meridians) and in space (where one should utilize high-inclination LE-orbiting multiple satellites equipped with high resolution magnetometers of the type of the ESA SWARM mission).

3.2.3.1. Observation Systems for the Geomagnetic Environment: Ground-based

In 1832, Gauss demonstrated the ability to measure the absolute intensity of the geomagnetic field, and the first magnetic observatories were installed. Magnetic observatories require a full description of the geomagnetic field and currently two types of measurements are needed: vector and scalar. The vector measurements are generally made with fluxgate magnetometers, which are subject to an instrument drift. To minimize this drift different approaches are used to calibrate their measurements. A scalar magnetometer is typically installed at each magnetic observatory to measure the field intensity. However, such a device provides no information about its direction. To obtain a complementary information about the direction of the geomagnetic field by measuring its declination and inclination, magnetic stations commonly use a fluxgate probe mounted onto the telescope of a theodolite (DI-flux). Modern magnetic observatories use similar instrumentation to produce similar data products (for a full description, see the INTERMAGNET website and documentation: http://www.intermagnet.org/). Most of magnetic observatories record one-second values. Averaged one-minute values of the

vector components and of scalar intensity are computed thereafter. From the one-minute data, hourly, daily, monthly, and annual mean values are produced.

3.2.3.2. Observation Systems for the Geomagnetic Environment: Space-based

High accuracy and precision measurements of the near-Earth geomagnetic field from space began with NASA's MAGSAT satellite which flew for six months from 1979 to 1980. This was followed in the first decade of the XXIst century by the Ørsted , CHAMP, and SAC-C magnetic field satellites.

Swarm, the three-satellite ESA constellation, is the most current and most advanced geomagnetic observatory in space. Its three satellites were launched on November 22, 2013, with a four-year nominal mission, after a three-month commissioning phase. In November 2017, the mission was granted a four-year extension to 2021. One of the novelties of the mission is not only the constellation concept, but also the new absolute scalar magnetometer: an optically pumped Helium magnetometer which provides absolute scalar measurements of the magnetic field with high accuracy and stability for the calibration of the vector field magnetometer (Leger et al. 2009). The mission was designed to derive the first global representation of the geomagnetic field variations on times scales from an hour to several years, addressing the crucial problem of source separation.

The three Swarm satellites are identical. The final constellation of the mission was achieved on April 17, 2014. Swarm A and C form the lower pair of satellites flying side-by-side (1.4 degrees of separation in longitude) at an altitude of 462 km (initial altitude) and at an 87.35 inclination angle, whereas Swarm B flies at a higher orbit of 511 km (initial altitude) and at an 87.75 inclination angle. The natural orbit evolution has led to a constellation in which spacecraft B is perpendicular to the lower A/C pair (2018) and later on spacecraft B is counter-rotating to the lower A/C pair every 47 minutes (2021).

3.2.4. Polar Ionospheric Phenomena

The polar region is one of the most dynamical regions on Earth. Its magnetic field lines are highly convergent, nearly vertical, and open to interplanetary space. In this region, energy, mass, and momentum from the solar wind can directly enter into the polar upper atmosphere,

and various dynamical processes generated by solar wind-magnetosphere coupling can be directly mapped to the polar ionosphere. This results in various features specific to the polar ionosphere, such as auroral activity, storm-enhanced density (SED)/tongue of ionization (TOI) (Foster et al., 2005, 2007), polar cap patches (e.g. Lockwood and Carlson, 1992; Carlson, 1994; Crowley, 1996, Carlson, 2012, Zhang et al., 2013), sun-aligned arcs (e.g. Frank et al., 1982; Fear et al., 2014), etc. In the polar cap region, polar cap patches appear often during southward interplanetary magnetic field (IMF) conditions and polar cap aurora, such as sun-aligned arcs/transpolar arcs, during northward IMF conditions (e.g. Carlson, 1994).

These phenomena are often associated with density gradients resulting in variable disturbances to High Frequency (HF) radio communications, over-the-horizon radar location errors, and disruption and errors in satellite navigation and communication (e.g. Moen et al., 2017; Wang et al., 2016). They are also directly subject to space weather disturbances linked to magnetosphere-ionosphere-thermosphere (MIT) coupling processes (e.g. Zhang et al., 2015, 2016). However, their formation and evolution under disturbed space weather conditions are poorly understood, and there is currently no forecasting tool to predict them. Improving our knowledge of these phenomena, partly via modeling efforts, is the key to making progress toward improved space weather forecasts and correction of global navigation satellite system (GNSS) signals in real-time in the polar cap regions.

Monitoring these phenomena requires large-scale, continuous, and global observations of polar regions by coordinated measurements of multiple instruments from both the space and the ground. With the fast development in the coverage of polar regions by multiple instruments during recent years, such as GNSS ground-based receivers, incoherent scatter radars (ISRs), Super Dual Auroral Radar Network (SuperDARN), and networks of all sky imagers as well as space-based measurements, a wealth of data on the global distributions of plasma and flows and the associated scintillations are now available. This already offers an excellent opportunity to study polar ionosphere phenomena and to understand in detail MIT coupling processes within a global perspective. But there are still many remaining data gaps and low temporal and spatial resolutions in the polar regions, especially in the Antarctic.

Six Chinese stations are deployed in the polar regions, four or which being in the Antarctic (Zhongshan, Great Wall, Taishan, and Kunlun) and two in the Arctic (Yellow River and China-Iceland auroral observatory), complemented by one new station under construction and the icebreaking research vessel Xue Long 1 and 2. China has established world-class observation systems with multiple devices in space physics and space weather both at Chinese Zhongshan Station in the Antarctic and at Yellow River Station in the Arctic, which are one pair of conjugate stations and have already obtained continuous observation data over more than one solar cycle (Liu et al., 2005). Great wall station and China-Iceland auroral observatory are also conjugate with the Millstone hill ISR

radar site and Japanese Syowa station in the Antarctic, thus offering excellent opportunities to monitor polar ionosphere phenomena from multiple conjugate sites.

Building on the Chinese meridian project (see 3.1) and Chinese observation systems in the polar regions, the IMCP is expected to extend the current observation systems to fill the coverage gaps with ground- and space-based observations, organize global campaigns of multiple instrument observations, stimulate data sharing and develop more powerful models to cover the global Solar Wind-Magnetosphere-Ionosphere-Thermosphere system. The IMCP can also establish a world-class international collaboration and scientific exchange platform, and promote a culture of talent.

3.2.5. Optical Observations of Ionosphere

The IMCP seeks to field core instrument on three meridians to provide both local time and latitude coverage of the IMUA. The IMCP instrument arrays should include comprehensive 3-D Ionosphere-Thermosphere (IT) imaging across a large (not global) region targeting composition, winds, convection, currents, and precipitation sampled with nested baselines and resolutions. These observatories provide deep coverage of the plasma, chemistry, composition, thermodynamics, and related features of the IMUA. Their observations will be processed to deduce electric and magnetic fields, ionospheric currents, velocity, temperatures, and conductance.

Optical and imaging instrumentation arrayed along the meridional strings should include FPIs, Airglow Imagers (simple & complex), Auroral Imagers (simple & complex), Riometers (Imaging), Imaging Spectrographs, and Lidars. UV and X-ray imaging from space would provide important complementary views.

3.2.6. Radio Observations of the Ionosphere

IMCP sciences focus on the geospace environment, especially the IMUA used as a screen to monitor natural and anthropogenic threats to our ecosphere. Studying variations in the plasma Earth is thus central to the IMCP mission. The technology of ionospheric radio sounding was born to make the revolutionary discovery of the ionosphere as an upper atmospheric region of charged particles (plasma). Electrons and their spatial and temporal variations are fundamental factors to influence radio propagation. Ionospheric

radio sounding relies on radio propagation properties in the ionosphere, including refraction, reflection, diffraction, absorption, scattering, and polarization, which are strongly radio-frequency dependent.

1. Ionosondes are capable of accurately measuring the most important ionospheric parameter, foF2 (the critical frequency of the F2-layer), in addition to the whole bottomside electron density profile. This most classic ionospheric sounding technique has led to an accumulation of ionospheric observations long enough to allow for the study of global changes driven by anthropogenic changes or secular geomagnetic field changes. Ionosondes are widely distributed around the world with well above 200+ sites;

2. incoherent scatter radars (ISRs) are the most powerful ground-based instrument, measuring multiple ionospheric state parameters including electron density, electron and ion temperatures, and ion velocity over a large altitude range (up to normally 500-600 km and sometimes 2000 km), some of which can provide important horizontal coverage. Currently a dozen of operating ISRs (Figure 20) operate at locations of fundamental geophysical significance for the study of magnetosphere-ionosphere-thermosphere coupling, as well as for the vertical coupling between upper and lower atmospheric layers. Next generation ISRs in China and Europe are under construction and will soon become available to serve IMCP science;

3. GNSS (Global Navigation Satellite System) total electron content (TEC) measurements provide an always-on continuous monitoring of the ionosphere with unprecedented spatial fidelity and versatile temporal coverage over the globe. The most sophisticated GNSS TEC systems make use of 6000+ receivers globally (Figure 21) or thousands of receivers regionally to study geospace disturbances as well as effects of perturbations generated from below (the low atmosphere and the lithosphere);

4. SuperDARN (Super Dual Auroral Radar Network) type HF (High Frequency) radar systems provide measurements of large-scale plasma drifts at high and middle latitudes of the ionosphere. These drifts are the key to understanding magnetospheric forcing and ionosphere-thermosphere responses. Therefore, the technique is essential for space weather sciences. Figure 22 provides the field-of-view of the SuperDARN systems for both hemispheres. While the high latitude has been reasonably well covered, the midlatitude is poorly covered in the Southern Hemisphere, and well covered in Northern Hemisphere, with gaps in Western Russia. The SuperDARN community has started planning an equatorial expansion of its observation system;

5. other radars with working frequencies ranging from MF (Medium Frequency) to HF and VHF (Very High Frequency) measure structures and dynamics in specific atmospheric regions, e.g. VHF radio waves scattered by equatorial irregularities

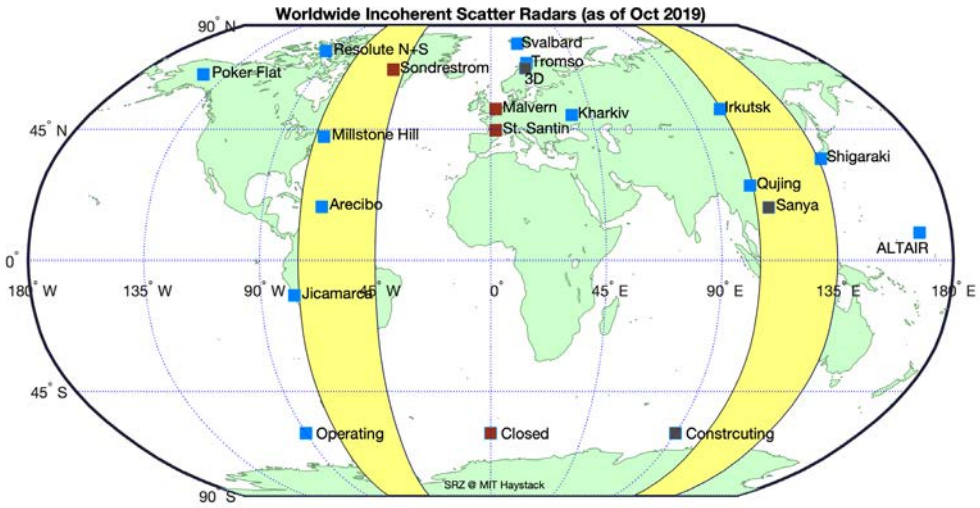

Figure 20: *A map of the world-wide network of incoherent scatter radars (as of October 2019). (Figure credit: S.-R. Zhang).*

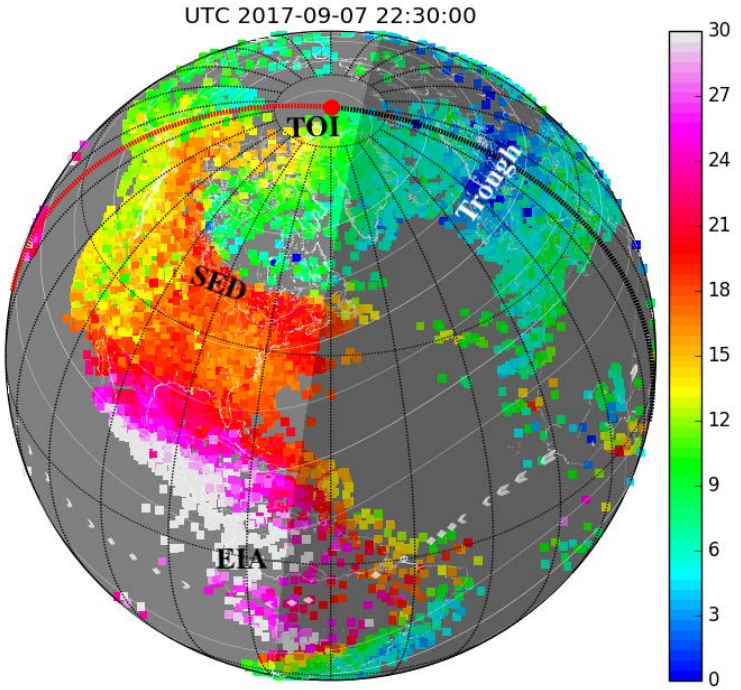

Figure 21: *A sample of measurements of the total electron content (TEC) storm-time geospace disturbances observed on September 7, 2017, based on the MIT GNSS TEC data processing system. (Figure after Zhang et al., 2019).*

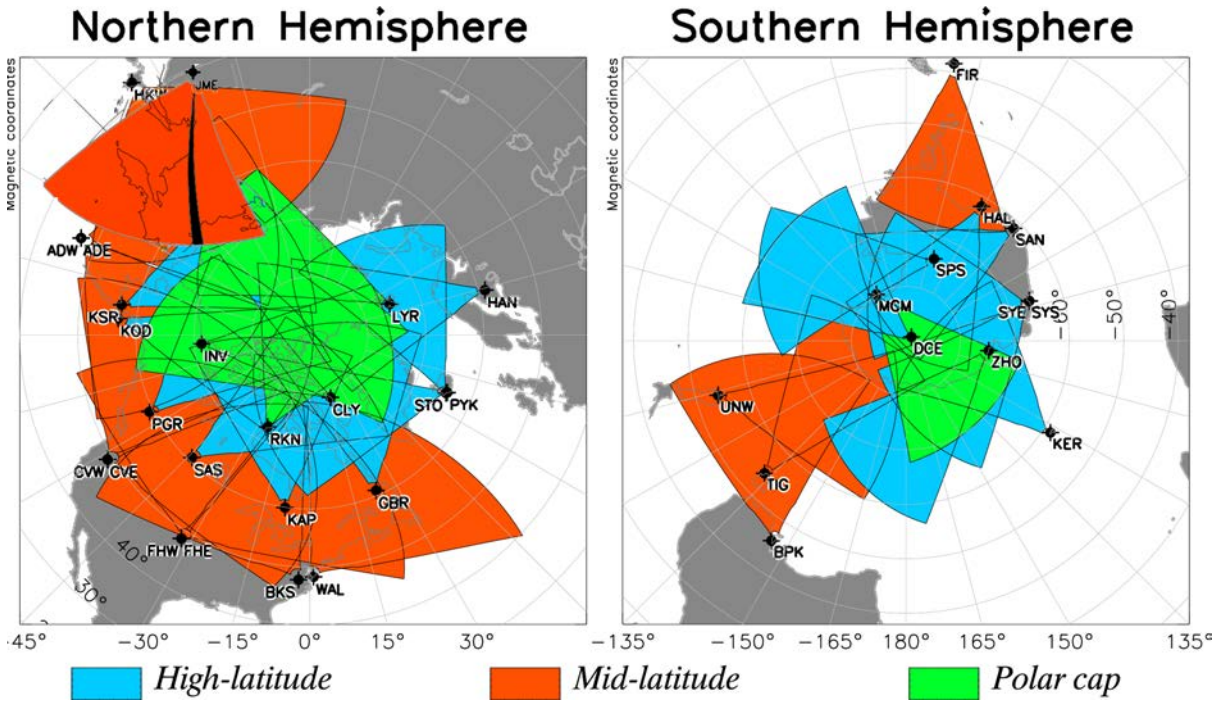

Figure 22: *The field-of-view of SuperDARN systems in the Northern and Southern Hemispheres as of 2019. Figure created by S.-R. Zhang using SuperDARN tools (http://vt.superdarn.org/) and information provided by Jiaojiao Zhang.*

for the ionospheric instability study, HF meteor radar echoes from meteor trails for the mesospheric dynamics study, MF/HF partial refection echoes for MLT (mesosphere and lower thermosphere) dynamics measurements, etc.; and

6. radio occultation (RO) techniques onboard LEO (Low Earth Orbit) satellites enable 3-D ionospheric electron density monitoring where and when these satellites are available. In a few years, with more and more CubeSats and LEO satellites becoming available for ionospheric RO measurements, truly global ionospheric imaging will soon become a reality.

In conclusion, a variety of radio sounding techniques are available to measure ionospheric plasma density, temperatures, drifts, irregularities, and disturbances in different regions of the plasma earth. These measurements can address directly the IMCP sciences.

3.2.7. Atmospheric Electricity

Atmospheric electricity phenomena involving disastrous thunderstorm and lightning activity in the troposphere, transient luminous events (TLEs) in the middle atmosphere, terrestrial gamma-ray flashes (TGFs) and disturbances of the global electrical circuit (GEC) (see section 2.5 and Figure 9), are of significant importance in understanding the evolution of the Earth and space environment, the exploitation of near space and the sustainable development of human beings. Electrification, charge accumulation, and severe discharge during thunderstorms and lightning may affect the ionospheric characteristics including electric potential and charge density. The large-scale extension (tens to hundreds of kilometers) of TLEs gives rise to a strong coupling between troposphere, stratosphere, middle atmosphere, and even magnetosphere. TGFs with high energy threaten aerospace activities. To date, comprehensive long-term and large-scale monitoring of global atmospheric electricity is lacking, and many issues involving atmospheric electricity are unsolved. To make progress, both ground-based and space-based observations are needed. We can establish national observation networks on TLEs and electromagnetic field measurements capable of locating lightning occurrence, guaranteeing a basic long-term monitoring. For several key and representative observation areas such as the Tibetan Plateau, South China, and Northwest China, comprehensive observations can be conducted by employing ground-based radio frequency electromagnetic field detectors to observe comprehensive parameters in multi-band from ULF/ELF, VLF/LF to VHF and even microwave and to depict the detailed discharge routes of lightning by locating its radiation sources. High-speed optical means (commercial or self-developed), high-energy radiation detection, in-situ E-field sounding of thundercloud, and other complementary instruments could also be deployed. Intensive observation campaigns should be organized to study the complex coupling of thunderstorms and lightning in the troposphere and retrieve the underlying physical mechanisms. High-impact events or global environmental fluctuations related to atmospheric electricity will be effectively and precisely monitored.

Current observing capabilities in China include but are not limited to:

1. ground-based TLEs observation network in some regions of China;

2. low-frequency electromagnetic field monitoring network mainly covering East and South of China, with more than twenty stations;

3. local network on lightning location and multi-parameters detection around the Beijing-Tianjin-Hebei region (named BLNET), capable of monitoring and locating full-flashes (both cloud-to-ground lightning and in-cloud lightning) in three dimensions;

4. VHF lightning radiation locating system with fine time-resolution (within several "μs") and precise spatial accuracy (within several "m");

5. balloon sounding for in-situ electric field measurements in the thundercloud. An observation test has been successfully conducted. The system is also able to detect weak E-field changes inside the cloud. Modification and improvement can be designed for use in a dedicated campaign; and

6. detector for lightning high-energy radiation. For this campaign, network observation can be arranged and conducted.

3.2.8. Lithospheric Activity: Earthquakes and Volcanoes

3.2.8.1. Lessons from Previous Observations

There have been many works on ionospheric anomalies related with earthquakes around the world. Anomalies in electron, plasma density and electromagnetic field have been reported from satellite observations (Gousheva et al., 2008; Pulinets et al., 2002; Pulinets et al., 1998). In China, ionospheric anomalies were also reported to be associated with the Wenchuan and Yushu earthquakes (Liu et al., 2009; Shen et al., 2017; Zhao S. et al., 2016). Based on a comparison of the disturbances caused by a magnetic storm and the Wenchuan Earthquake, Zhao B et al., (2008) concluded that the earthquake's anomaly generally only appears near the epicenter and has effects in the magnetic conjugate area. Superimposed epoch analysis used to study the space and time distribution of earthquake anomalies showed that these anomalies have a much larger occurrence probability at the southeast of the epicenter and within seven days before the earthquake (Sun et al., 2011; Oyama et al., 2011, 2016).

Ionospheric disturbances of the ionosphere are seen to occur particularly often before large earthquakes. Analysis of satellite data during several of these large events have taught us that:

1. the disturbed area is much larger than what is found with ground-based observations. One earthquake (M=6.5) showed a disturbed area of 60 degrees in longitude both to the west and east of the epicenter, and a latitude area extending 20 degrees to the north and south from the epicenter. This suggests that observations should cover a wide area; and

2. depending on height, latitude, and local time, the disturbance shows different

faces. At the 700-800 km altitude of satellite observations like DMSP and DEMETER, the anomaly appears around the geomagnetic equator, not over the epicenter. The disturbance is identified only when the satellite altitude is below 300 km. The disturbing driver is still not identified.

Plasma drift data obtained by DE-2 satellite showed that the eastward (westward) component of the electric field is enhanced during daytime (night-time), suggesting that the ionosphere is modified by an enhanced dynamo electric field. This could explain the behavior of the ionosphere before the earthquake on March 11, 2011, observed by DE-2, if the dynamo electric field originally produced by neutral winds is modified by Internal Gravity Waves (IGW) due to the ground motion.

.

3.2.8.2. Contributions and promises of dedicated satellite missions

The first scientific satellite dedicated to the study of the ionosphere disturbances induced by seismic and volcanic activity was the DEMETER (Detection of Electro-Magnetic Emissions Transmitted from Earthquake Regions) micro-satellite of CNES, launched on June 29, 2004, which operated until 2010. Demeter, from an altitude which varied from 710 km to 660 km and covered ±65° latitude, observed an increase of ULF wave emissions during the month preceding the Haiti 2010 earthquake, and ionospheric anomalies occurring during the 2010 eruption of Mount Merapi. A superposed-epoch analysis of its data as a function of earthquake time showed in the average a consistent but weak increase of the ionospheric electric field intensity a few hours before the occurrence of earthquakes (Nemec et al., 2008). Examples of perturbations of ionospheric parameters in relation with earthquakes in DEMETER data were published by Parrot et al. (2006), Bhattacharya et al. (2007a, b), Pulinets (2007) and Sarkar et al. (2007). Changes of signal intensity emitted by the ground-based VLF transmitters and received on board DEMETER were also observed (Molchanov et al., 2006; Rozhnoi et al., 2007; Muto et al., 2008). A summary of DEMETER scientific results can be found in the CNES archive: https://demeter.cnes.fr/en/DEMETER/lien1_res_scie.htm.

Following DEMETER, the first China Seismo-Electromagnetic Satellite (also called Zhangheng-01 or ZH-01), launched on February 2, 2018 (Shen X., 2018), can detect the geomagnetic field, electromagnetic field, ionosphere in-situ plasma parameters, ionosphere profile structure, and energetic particles. Global geomagnetic field and ionosphere models are currently designed based on its data. On August 25, 2018, CSES observed Natural and Artificial EM Events including earthquake, magnetic storm, and VLF transmitter heating phenomena. Zhangheng-02, the subsequent satellite of

the CSES series, is scheduled to be launched in March 2022. Its observation range will be extended from 65 degrees north and south latitudes of ZH-01 to the North and south poles to provide fully global observations. The interval between two traces of the sub-satellite point will be 2.5 degrees, and its re-visit time two-three days. ZH-02 will carry six scientific instruments identical to ZH-01, two optimized ones and one new instrument, thus improving the quality of scientific observations.

For the more distant future, satellite constellations will be instrumental to achieve further progress, based for instance on a combination of one small satellite and at least six CubeSat of 6U class. These small satellites will be required to measure basic ionospheric plasma parameters such as electron density and temperature, ion composition including O^+ and molecular ions (NO^+), plasma drifts, and neutral winds. Monitoring the altitude profile of electron density which might be modified by E field, possibly by topside sounding, will be useful. Each CubeSat will need to be altitude-controlled.

3.2.8.3. Requirements on a Global Observing System of Ionospheric Anomalies Associated to Earthquakes

Based on the current observational evidence and on theoretical studies of LAIC mechanisms, one can formulate two main requirements on an observing system of the ionospheric anomalies associated to Earthquakes:

A. to provide a "steric" capacity that can observe the whole broad column of atmosphere over a seismogenic zone, from the ground to the IMUA and up to its magnetic conjugate zone.

A steric Observation System of earthquake precursors and effects on the IMUA, illustrated in Figure 23, should ideally include:

1. ground equipments measuring crustal deformations, subsurface fluids, seismic waves, etc.;
2. satellite platforms carrying Infrared, Hyper Spectral and D-InSAR and electromagnetic satellites;
3. ionosphere detection by ground-based vertical and oblique sounding and GNSS stations; and
4. measurements of altitude profiles of neutral temperature and wind from the earth surface to 100 km, which are needed to study the possible contribution of AGWs.

Detecting ground motions in relation to satellite and atmospheric observations — a major objective for future observations — can be done with such a steric observing system.

Satellite observations are particularly important, as they provide a global coverage, thus greatly increasing the number of opportunities of observing earthquake effects and improving the science base for possible future earthquake prediction. They can monitor the sea areas, borders and natural disasters in harsh conditions, thus filling the blanks of ground-based observations, in China and elsewhere.

B. To cover the most active seismic zones of the planet, particularly the Pacific fire belt (see Figure 11).

A Steric Observation System deployed along the priority observation zones of the IMCP will provide a 4D Geophysical field information to build global geomagnetic field, gravity field, and ionosphere models, and comprehensively cover the physical coupling between the seismogenic zone and the upper atmosphere, serving national security as well as global geoscience and space science research.

Another major asset of the IMCP, i.e. its international dimension, will be used to encourage and promote international collaboration among earthquake prone countries.

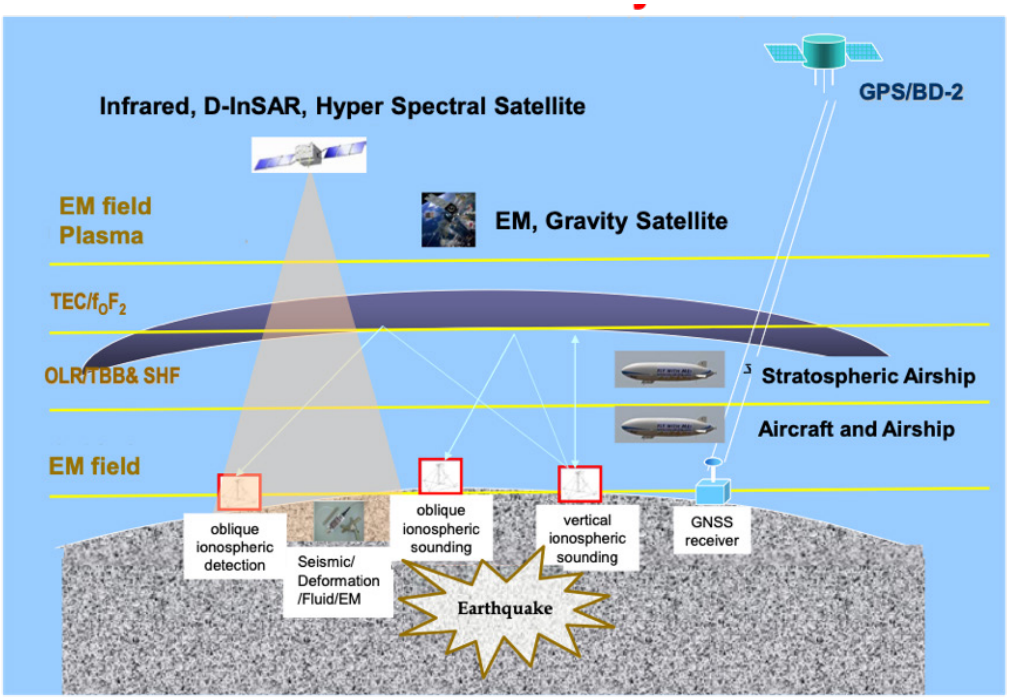

Figure 23: *Sensors for the study of atmospheric effects of seismic activity. Several presentations at the forum reviewed the occurrence of earthquake and their observed effects on Earth's upper atmosphere and discussed the needs for an intensified steric, global observation system that would allow for major progress in the understanding of coupling mechanisms between the seismogenic areas and the IMUA, possibly opening the way to a predictive capability*

3.3. Implementing the Asia-Australia-Americas Meridian Chain

3.3.1. Meridian Chain of Fabry-Perrot Interferometers in Americas

The International Meridian Chain Project (IMCP) will be an extension of the highly successful Chinese Meridian Project (see 3.1 above), which provides extensive latitudinal coverage of geospace environment in the Asian sector. Since Space weather is a global phenomenon, expanding the Meridian project to other regions of the world is a logical next step in its study.

To study solar geomagnetic storm effects on the ionosphere thermospheric winds are a key parameter. Geomagnetic storms start in the polar region, where ion convection in the polar cap is greatly enhanced in response to the southward turning of the IMF Bz component (see section 2.3). Consequently, we see an increase of Joule heating in the polar region with expanding polar cap. Joule heating leads to upwelling in the thermosphere. The resulting uplift of O_2 and N_2 heavy molecules changes the chemical balance of the ionosphere. The increase of ion recombination induced by increased O_2 and N_2 densities results in ion density decreases. Joule heating also changes the pressure gradient and enhances equatorward meridional winds, in turn pushing the depleted ionosphere from high to middle and low latitudes. These changes in the ionosphere can affect communication and navigation systems. A key objective of space weather research is to understand how fast and how far can ionosphere depletion extend to middle and low latitudes. A meridian chain of instruments measuring thermospheric winds will make it possible to determine how far ionospheric disturbances travel to low latitudes. Hence, we see the need for a meridian chain of thermospheric wind monitoring instruments, such as Fabry-Perot interferometers (FPI), which measure thermospheric winds by recording the induced Doppler shift in the O 630 nm nightglow emission.

The North-American sector has a long history of FPI observations of thermospheric winds from the Arctic to Antarctic regions. The IMCP can not only revitalize these existing instruments, but also fill some critical coverage gaps and form a truly functional meridian chain. Figure 24 shows the locations of existing instruments and some new FPI deployment sites proposed as a collaborative project to expand the existing FPI network in the American sector. This proposed expansion has many overlaps with the goal of the IMCP. One of the major expenses of deploying instruments on field sites is to build infrastructures (housing, electricity, network connection, etc.). If the IMCP can lay the foundation by providing the necessary infrastructure, it will be then possible to deploy some existing in-house instruments at the selected sites quickly. Such a fully equipped IMCP network can finally track geomagnetic

storm effects from pole to pole and fulfill the need of ionosphere and thermosphere model development by providing critical data sources for validation and assimilation.

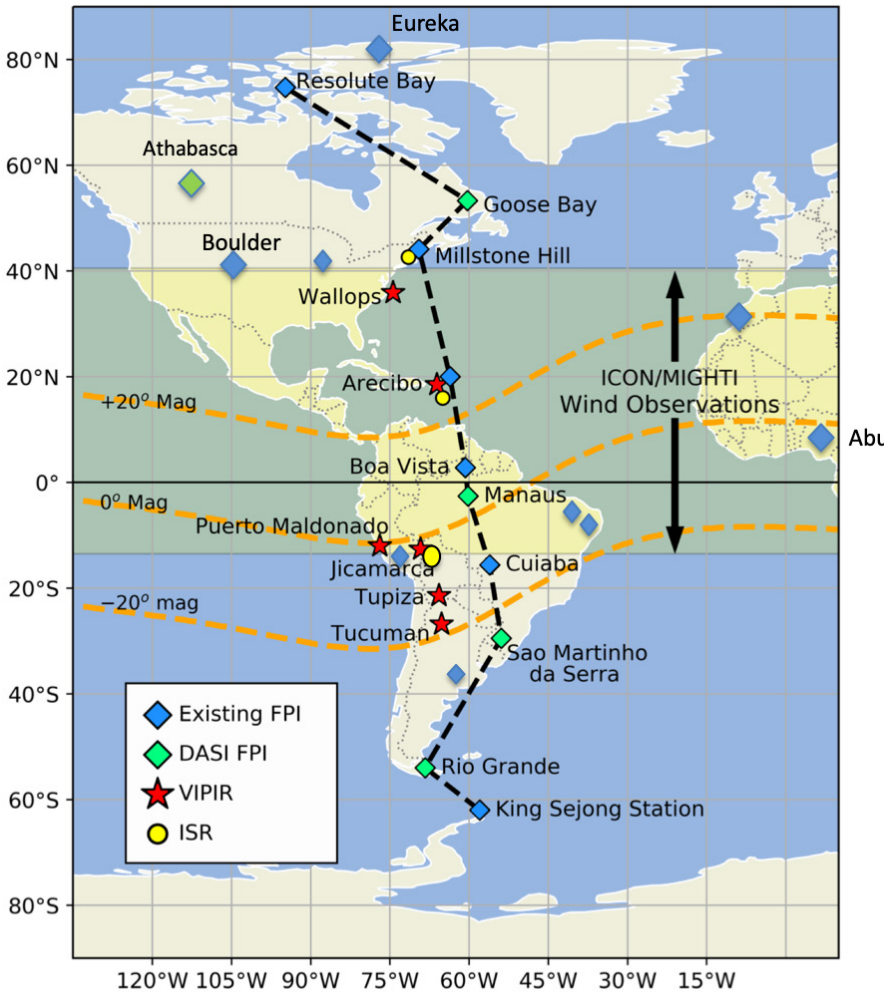

Figure 24: *A proposed expansion plan for the Fabry-Perot Interferometer network in the American sector called Distributed Array of Small Instruments (DASI). If IMCP can provide infrastructure at locations like Goose Bay, Rio Grande, and others, we will have a complete chain. The geographical coverage of the ICON/MIGHTI wind observations is also indicated.*

3.3.2. East-Siberian Chain

East Siberia is the territory extending from the tundra shore of the North Ocean to the Mongolian steppes between 80 and 140 meridians. The territory is very important for geophysical research, especially in the framework of the IMCP, but it features taiga forests and a lack of infrastructure. Nevertheless, there are two research institutes studying solar-terrestrial coupling and the aeronomy of the high-latitude upper atmosphere there: the Siberian Institute of Solar-Terrestrial Physics and the Shaffer Institute of Cosmo-Physical Research and Aeronomy, both belonging to the Siberian Branch of the Russian Academy of Sciences. The institutes have a 60-year long history. Some of their subdivisions have observed the atmosphere, ionosphere, and geomagnetic field for much longer than that — up to 130 years. Both institutions operate a set of observatories organized as regular observational points including special observatories for unique instruments and facilities. As the IMCP intends to study the Earth's atmosphere in the context of space weather, we need to identify which of these facilities (shown in Figure 25) are the most important to address its goals. The Baikal vacuum telescope studies the fine optical spectral structure of the Sun, the telescopes of Sayan Solar Observatory observe the solar corona and conduct infrared observations of solar system and deep space objects, the Siberian radioheliograph produces radio images of the Sun, the Irkutsk incoherent scatter radar observes the upper atmosphere

Figure 25: *Map of the geographical distribution of the main observation facilities that will contribute to the IMCP observation system in East Siberia.*

studies. A geophysical rocket launch pad is placed at a 70-degree latitude. Deployed instruments also include the Siberian segment of the SuperDARN radars, networks of chirp and digital ionosondes, ULF radio signal recording, optical spectrographs, and all-sky cameras (for upper atmosphere airglow studies), and neutron monitors for cosmic ray variability observations. This comprehensive set of instruments is ready for a successful participation in the IMCP as an important part of the meridional chain of instruments.

As some of these observation instruments are aging, there is a renovation program for the instruments — a megaproject proposing to build new or update old instruments. A new 3-m mirror telescope coronagraph for observation of the solar atmosphere with high spectral and temporal resolution will be constructed. The existing radio-heliograph will be renovated to extend its frequency range and upgrade its data recording systems. A new incoherent scatter radar will be able to work in the 10-1000 km altitude range and observe modifications of the upper atmosphere induced by a new HF heater facility, which will work in the 2.6-6 MHz range with an effective power of about 200 MW near lake Baikal. A new stratosphere-mesosphere-thermosphere multi-wavelength LIDAR, working in the common volume of the two radiophysical instruments mentioned earlier, will study the interaction between the charged and neutral components of the upper atmosphere. In addition to its existing optical devices and ionosondes, the geophysical observatory placed under the crossing fields of view of the instruments mentioned above will be equipped with new all-sky cameras, Fabry-Perot interferometers, and grating spectrographs.

Russian participation to the IMCP will capitalize on the previous very successful 25-year long experience of collaborative works in the framework of the Russian-Chinese space weather research center. This entire ground-based scientific infrastructure is needed to support successful space weather research. It will fill the information gap concerning the propagation of solar wind effects in the Sun-Earth space, which is very important for space weather predictions and for studies of the properties of space weather events. In return, information about near-earth space and an improved understanding of Earth's atmosphere response to space weather events are essential to make progress towards a satisfactory understanding of Solar-Terrestrial coupling and of its effects on humankind and human societies.

3.3.3. Implementing the Europe-Africa-Pacific Meridian Chain

3.3.3.1. FPI Observations of Middle/Upper Atmosphere in Morocco

The main focus of space weather research is the understanding of the whole chain of interactions taking place in the geospace system and in the Earth atmosphere in response to the variety of phenomena consecutive to both impulsive and quiet events driven by solar activity. The thermosphere/ionosphere system is one of the most complex and important layers to be understood in order to properly forecast space weather. In this regard, Fabry-Perot interferometers (FPI) play a crucial role by measuring thermospheric winds and temperature through the Doppler shift and broadening of the naturally-occurring atomic oxygen airglow emissions (see also 3.3 above). These measurements are important for space weather, especially when combined with other similar and/or complementary data from over the globe. They allow us to improve our knowledge of the large-scale structure, dynamics, and electrodynamics of the thermosphere and ionosphere, and the mechanisms driving energy transfer from the magnetosphere to the thermosphere and then from high to low latitudes. A network of interferometers can reveal the latitudinal and longitudinal dependence of the thermospheric response to geomagnetic storms, consequently leading to very valuable information on the coupling between ions and neutrals.

A Fabry–Pérot interferometer (FPI) (Makela et al., 2011, Harding et al, 2014) has been deployed at Oukaimeden observatory (31.2°N, 7.8°W, 22.8°N magnetic) in Morocco since 2014, in the framework of the International space weather initiative (ISWI). To observe the thermosphere at an altitude of 250 km this FPI performs a sequence of five measurements: north, south, east, west, and zenith. The south- and north-looking measurements are separated by 500 km and so are the east- and west-looking measurements. The climatology of the thermospheric winds and temperature has been established as well as the Midnight Temperature Maximum (MTM) phenomenon occurrences (Kaab et al 2017, Fisher et al. 2015, Kaab et al 2019 to be submitted). In regard to the wind climatology, meridional winds are equatorward for the entire night, reaching a maximum speed of 75 ms−1 in the summer time. A poleward component is present in winter, in the early evening hours. Zonal winds are eastward during the entire night, with typical speeds around 50 m.s−1 during the early evening hours, 75 to 100 m.s−1 around 21:00 UT and almost zero before dawn in wintertime. A westward reversal is present shortly before dawn in local summer.

Using the data produced by the FPI, the dependence of the thermospheric winds and temperature on seasons and solar cycle over

our region has been established by Bounhir et al (2017). Comparisons with empirical and physics-based models (HDWM07, HDWM14, MSIS, DWM07, TIE-GCM and GITM) have been achieved (Kaab et al 2017 and El Fakhiri et al 2019 forthcoming paper). From the day-to-day variations of the very quiet time wind pattern, other type of waves superposed to the main diurnal tides are exhibited and can be identified precisely. Figure 26, illustrating the components of the wind on a very quiet night, shows what could be a signature of an

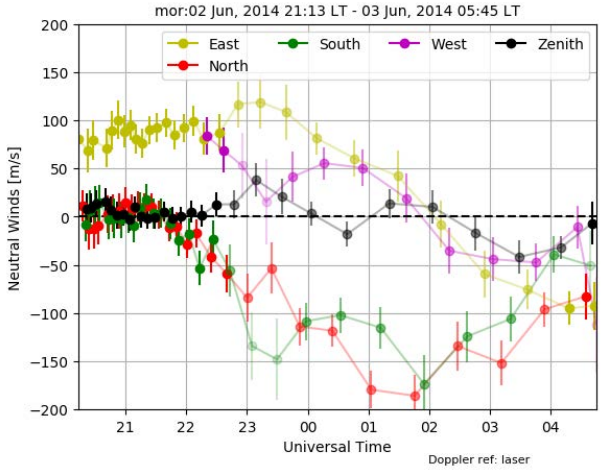

Figure 26: *Wind components of the FPI look measurements; north, south, east, west and zenith during 02 June 2014*

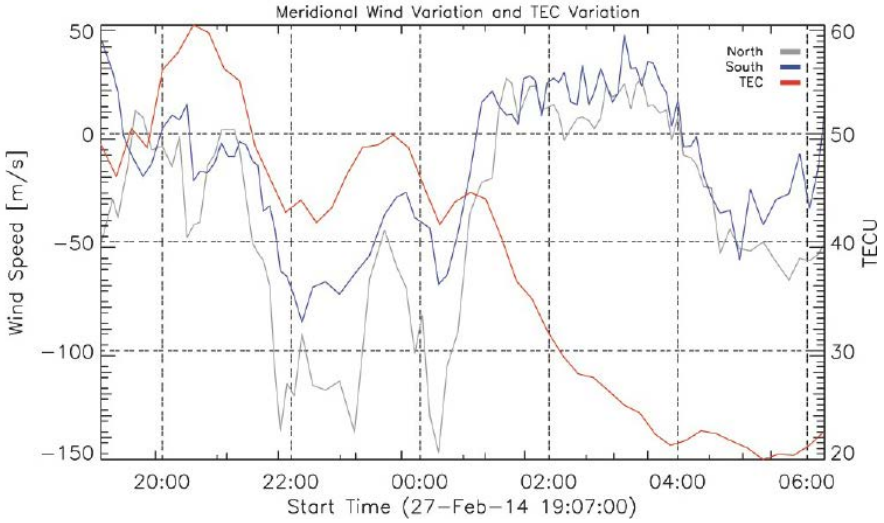

Figure 27: *Total electron content (TEC) measured over Rabat (33.998°N, 6.854°W) and thermospheric meridional wind north- and south facing components, measured by the Fabry-Perotinterferometer (FPI) over Oukaïmeden Observatory (31.206°N, 7.866°W; 22.84°N magnetic).*

upward-propagating tide or a breaking gravity wave added to the main flow. The vertical component of the wind is far from negligible, reaching values of 50 m/s, and the meridional component of the wind has reached values as large as 200 m.s-1 during geomagnetic storms.

The storm case of February 27-28, 2014, by means of multi-data analysis illustrates the importance of FPI measurements to capture the storm-time behavior of the thermosphere (Malki et al 2018). The ionospheric response of the storm was also analyzed using the VTEC data and a wide-angle imaging camera. During this storm, the winds experienced a storm-induced traveling atmospheric disturbance (TAD) behavior, the first one coming from the north and the second one being trans-equatorial and coming from the south, as illustrated in Figure 27. The propagation speed of the TAD was estimated to be 550 m.s−1, which was consistent with bibliographic results. A westward flow was observed from 22:00 to 03:00 LT. Through comparison with the DWM07 (Disturbance Wind Model) prediction model, we found that the model deviates largely inside the TADs. The effects on the ionosphere were also evident through the change observed in the background electrodynamics from the reversal in the drift direction in an observed equatorial plasma bubble (EPB). Total electron content (TEC) measurements of a GPS station installed in Morocco at Rabat (33.998°N, 6.853°W) revealed a positive storm. TADs, when propagating from polar to equatorial regions, cause an uplift in the F-peak height (HmF2), which in turn has a subsequent effect on the increase of the F-peak density (NmF2). Evidence of TIDs was noticeable from the TEC pattern, and this correlates with the meridional components of the wind until 01:00 UT on February, 28 (Figure 26). A negative correlation between HmF2 and NmF2 during the passage of the TAD was observed. A reversal in the drift direction of a plasma bubble was observed, indicating a reversal of the background electric field direction due to the neutral wind disturbance dynamo. The time of the reversal of the plasma drift corresponds to the time when the zonal wind starts reversing westward. The drift velocity matched the zonal wind magnitude, indicating a fully activated storm.

3.3.4. Meridian Chain in West Africa

The region of West Africa is located west of a North-South axis lying close to 10° East longitude. The Atlantic Ocean forms the Western as well as the Southern borders of the West African region. The Northern border is the Sahara Desert and the Eastern border lies between the Benue Trough, and a line running from Mount Cameroon to Lake Chad. It is important to note that the colonial boundaries are still reflected in the modern boundaries between contemporary West African states, cutting across ethnic and cultural lines, often dividing single ethnic groups between two or more states. The West African region concerns

fifteen countries that have both cultural and geopolitical ties and shared common economic interest through the regional organization, the ECOWAS. It is important to note that this region is crossed by the magnetic equator and thus under the direct influence of the equatorial electrojet and its subsequent effects.

3.3.4.1. History of Space Research in West Africa

In West Africa, space science research — specially in geophysics — started with the works of Prof. Onwumechilli (Nigeria) and colleagues on the Equatorial Electrojet (EEJ), as highlighted in the seminal Onwumechili and Ogbuehi (1967) article. In French speaking countries, space research began with the studies of the French scientists Faynot, Vila, and Vassal (Faynot and Vila, 1979; Vassal, 1982).

It is during the program of the International Year of EEJ for Africa that French speaking countries in West Africa have started being involved in space sciences thanks to the works of the pioneers Ephrem Sambou (Senegal) and Arsène T. Kobéa (Ivory Coast). Their studies were followed by the researches of several colleagues, e.g. Vafi Doumbia from Ivory Coast and Etienne Houngninou from Bénin. The contributions of these colleagues were produced under the supervision and the coaching of French researchers, principally Christine Amory Mazaudier, Fambitakoye (former Niger citizen), Elizabeth Blanc, Michel Menvielle, Ives Cohen, and Rolland Fleury. The next generations involved in this field are represented by Frédéric Ouattara and Pétronille Kafando (Burkina Faso), Olivier Obrou and Jean Pierre Adohi (Ivory Coast). Right now, several young scientists from West African countries are mentored by them. Under the leadership of Mazaudier, a research group has been created (Groupe international de Recherche Géophysique Europe Afrique: GIRGEA. www.girgea.org) and it is currently extended to the Americas and Asia. The contributions of this group to space sciences include more than 60 PhDs and 100 publications and many collaborations with famous scientists from all continents.

3.3.4.2. Instrument Deployment in West Africa

In French speaking countries of West Africa, space science began with the study of the ionosphere, using ionosonde stations provided by France and installed in 1966 in Ouagadougou, Burkina Faso, and in 1975 in Dakar, Senegal, by the observatory of Mbour. During the International Year of Equatorial Electrojet (1993), several magnetometers were

installed in Ivory Coast (four stations) and in Mali (six stations). There are three observatories (Mbour, Senegal; Bangui, Center Africa and Tanmarasset, Algeria). Five GPS stations have been installed through West Africa countries in Benin, Burkina Faso, Ivory Coast, Senegal, and Nigeria.

In order to better understand the variability of the African ionosphere due to scintillation, several GPS stations were installed along the magnetic equator. These stations constitute the SCINDA (Scintillation Network Decision Aid) network. The data format is not RINEX and data are not freely accessible.

The main difficulties faced:

- to maintain stations due to the obsolescence of the GPS receivers;
- to operate the station continuously despite frequent power outages;
- to train students for sustainable knowledge and space science development;
- to popularize and reinvest on research results; and
- to inform (scientific publications, exchanges with journalists and citizens, workshops) about the main results.

The main challenges:

- to finance researches in Africa;
- to develop better cooperation, both North - South and South-South;
- to train students with the help of different mentors in each field of research;
- to carry out a better global model that can reproduce the data variabilities for the African sector; and
- to implement several instruments for better future investigations.

3.3.4.3. Space Weather Studies in Africa

The fact that the magnetic equator passes through Africa makes it more vulnerable to complex ionospheric processes such as Equatorial Ionospheric Anomaly, equatorial plasma bubbles, spread F, and other such phenomena which are capable of disrupting HF communications in various forms and endanger human lives. The magnetic equator passes over the African continent in a broad range, such that the width of Equatorial Ionospheric Anomaly can be studied in its full spectrum.

The participation of African countries in the United Nations endorsed International Heliophysical Year (IHY) and International Space Weather Initiative (ISWI) programs has

changed the landscape of space weather-related research in the region. Prof. Rabiu's contribution presented some of the benefits accrued to the African continent and its researchers in the course of the twin programs.

development during the years 2007-2019 in terms of capacity building seminars, workshops, and conferences held in Africa. A number of capacity building schools were organized, courtesy of IHY/ISWI programs in Africa. The

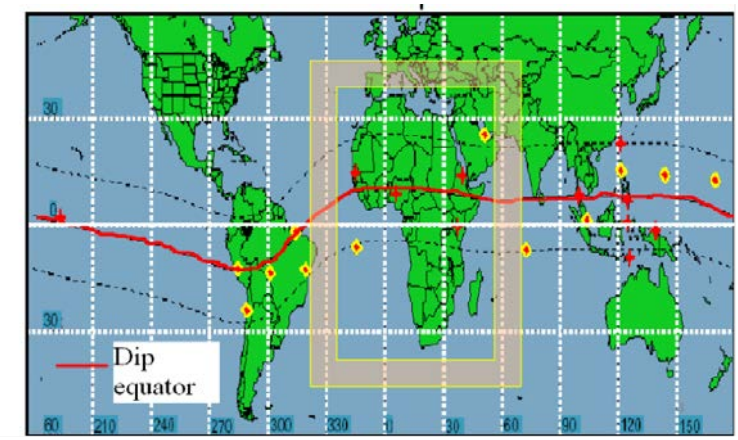

Figure 28: *Observations in the African continent are very important for the full understanding of the significant space weather effects associated with ionospheric scintillations at equatorial latitudes. The orientation of the magnetic equator is at nearly constant geographic latitude across the African continent (low declination angle) in contrast to the high declination angle of the magnetic equator in the American sector.*

Several instruments capable of monitoring space weather were deployed to a number of countries: more than one-third of Africa's 54 nations actively participated in the twin programs. Today, space weather data streams from multiple equipment installed on African soil during the IHY/ISWI programs. This list includes magnetometers (MAGDAS, AMBER), GNSS receivers (SCINDA and others), Fabry Perot Interferometers, all-sky optical imager, digisonde, SID, CALLISTO, among others. Prof. Rabiu showed the statistics of regional

impacts of the joint annual workshops on GNSS and space weather being co-organized by Boston College, USA, and Abdus Salam International Center for Theoretical Physics since 2009 were discussed.

National participation in space weather research and capacity building has been activated in some African Countries. Nigeria, South Africa, Ethiopia, Egypt, Kenya, and Ivory Coast are examples of countries with current programs in space weather research. The

model of National Schools on Space Weather in Nigeria was presented. Nigeria has hosted a number of International Schools since 2008 and recently held the International Colloquium on Equatorial and Low Latitude Ionosphere, Lagos, Nigeria, in September 2019.

The activities of the Nigerian Center for Atmospheric Research include deployment and management of space weather monitoring facilities such as four GPS stations for Space Weather monitoring, one all-sky Optical Imager, four magnetometers (one AMBER, three MAGDAS), eight locally developed magnetometers (SWONON), one scintillation monitor, one Fabry Perot Interferometer, one SOFIE, and one HF Transceiver. The Centre runs a network of space observatories that has grown to five laboratories already and has become a regional hub for space weather research in Africa. Specifically, the Center started making daily and monthly forecast of Total Electron Content TEC available to public via its webpage (www.carnasda.com) since January 2018. A regional TEC model known as AfriTEC, developed at the Center, is freely available at the Center's webpage, www.carnasda.com.

Figure 29: *The coherent scatter Blue Nile Radar (BNR) was installed in 2014 in Ethiopia to observe the E and F region irregularities associated with the equatorial ionization anomaly (EIA) in the African sector.*

3.4. Conclusions and Perspectives

The fundamental goal of the IMCP ground-based observing system is to deploy and operate networks and arrays of complementary instruments which will produce on a regular basis multi-instrument data sets characterizing the average state and disturbances of the IMUA responding to the science requirements identified in section 2. These IMCP-related data sets will need to be readily accessible, common format, real-time data with good spatial and temporal resolution along the chosen configuration of great meridian circles. There are numbers of existing or planned networks of individual or complementary instruments that could contribute to the observational capabilities needed to help realize IMCP scientific goals. Indeed, taken together the desired IMCP instrument suite shall:

- make it possible to characterize the average state and disturbances affecting the IMUA;
- provide a continuous monitoring of the sources of these disturbance acting from above, from below, and from within: solar and interplanetary space disturbances; disturbances coming from Solid Earth (like seismogenic zones and volcanoes) or from Fluid Earth (weather systems, thunderstorms, sources of greenhouse gases, etc.); and
- monitoring of the processes tranferring disturbances to the IMUA level (electrostatic disturbances, electromagnetic emissions, atmospheric-gravity and larger-scale atmospheric waves, etc.).

The forum made it possible to establish a preliminary list of networks and instruments that are excellent potential candidates to contribute to the IMCP. This preliminary list, though far from complete, is summarized in Table 1.

The forum also identified some of the key characteristics that shall be met by candidate IMCP instruments and networks of instruments:

- significance of observations for addressing the science goals and spatial coverage requirements identified for the IMCP observation system (section 2);
- existence of a source of continuing financial support;
- availability and involvement of local personnel;
- ability to produce data in a common format and to make them available to users via a developed database capability and real-time WWW access;
- agreement to provide open access to data; and
- accessibility of the facility site and ability to host visiting instruments.

Observed phenomena and observation technique(s)	Instrument or network geographical coverage				
	Global	Polar regions	120°E-60°W meridian	30°E-150°W meridian	Observations from space
Solar and interplanetary disturbances	Solar observatories around the world Neutron monitors and NMDB		Solar and interplanetary subsystem of CMP Phase II BBSO		Solar and heliospheric missions
Geomagnetic field variations	INTERMAGNET		CMP	MAGSWEDAN (ESA)	SWARM
IMUA parameters: optical, UV, X-Ray observations		Airglow and auroral imagers and spectrographs	CMP East Siberian chain FPI chain in Americas	Moroccan FPI	SMILE UV and X-ray imaging
IMUA parameters: radio observations	Worldwide ionosondes and digisondes network GNSS	EISCAT SuperDARN	CMP SuperDARN ISR chain	EISCAT Space weather and ionospheric instruments in Africa SuperDARN	Radio occultations of ionosphere
Lower atmosphere weather	Worldwide meteorological network				
Atmospheric electricity	Observations of emissions related to lightning In-situ thundercloud observations by balloon and aircraft				TARANIS
Seismogenic zones	Worldwide seismic network		"Steric" monitoring of seismogenic zones along Pacific firebelt		CSES satellites

Table 1: *The instruments and networks reviewed during the forum are listed here as a function of the type of phenomenon observed and technique used (vertical axis) and of their geographical distribution. The right-hand side column shows some of the space missions that can/will contribute to the IMCP.*

From the forum discussions a "string of pearls" arrangement for the instruments and facilities was suggested, incorporating a smaller number of large-scale high-fidelity instruments ("diamonds"), such as the large incoherent scatter radars (e.g.) PCO, Resolute Bay (RISR), EISCAT, etc. Meso-scale facilities (the "pearls"), such as MERIDIAN, MIRACLE, TREX-plus,

would provide good-fidelity regional coverage of specific parameters in selected regions and these would be supplemented by broad-scale and global observing systems such as (e.g.) SuperDARN, SuperMAG, GNSS, and selected space-based observations.

4. MODELING AND DATA ANALYSIS/ ASSIMILATION

4.1. Introduction

Achieving the objectives of the IMCP as a global monitor of signatures of major risks projected on the IMUA screen will require to be able to disentangle and separately identify the signatures of the different categories of hazards (A to E) affecting the IMUA described in section 2.1. A major challenge for the IMCP project is to design a high-efficiency pattern recognition strategy. Given the emergence of advanced pattern recognition tools related to Artificial Intelligence and Machine Learning, and the major progress accomplished in the power of numerical modeling of the different sources of hazards and of the corresponding energy transfer processes through geospace, this strategy must build upon an ambitious segment of the IMCP project dedicated to modelling, data assimilation, and pattern recognition.

This section reports on the different contributions made during the forum to this important component of the IMCP project. Though not yet comprehensive, the set of models and tools presented below provides a first solid base to design and develop further IMCP capacities in this domain.

4.2. Numerical Simulations of Galactic Cosmic Rays near Earth

Galactic cosmic rays (GCRs) originate from the outside region of the solar system. Their fluxes, detected by neutron monitors on the ground (see 3.2), are strongly modulated by the interplanetary solar wind near earth. The short-term variations (~days) of GCRs and their physical mechanisms are not understood well because particles may respond to changes in the solar wind speed (affecting the GCR convection and energy changes), magnetic irregularities (diffusive effects), and the interplanetary magnetic field magnitude

(variations of drifts and diffusion). By means of numerical simulations that combined global MHD, small-scale turbulence, and stochastic transport models, the group of Xiaocheng Guo at the State Key Laboratory of Space Weather, NSSC, CAS, was able to reproduce the recurrent short-term intensity variations of cosmic rays. They compared the simulation results, including variations of the solar wind plasma properties and GCR intensities at 1 au, with observations during the solar minimum between 2007 and 2009. The simulated variations of 2 GV protons roughly agree with the results from the neutron monitors on the ground. The depressions in the GCR intensity are directly caused by the longitudinal and radial decreases in diffusion coefficients from slow to fast solar wind, which is associated with the passages of stream interfaces. The HCS does not order the GCR variation significantly in this work, however. In summary, stream interfaces in the solar wind always trigger depressions in the GCR intensity, and diffusion has a more important role in modulating cosmic rays over a solar rotation than drifts during the past solar minimum.

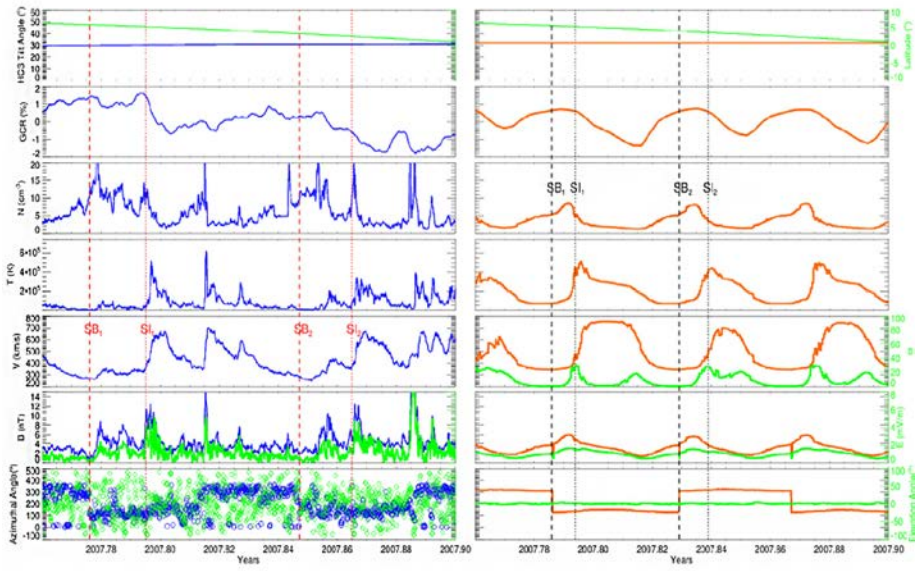

Figure 30: *The 27-day periodic variations of 2 GV proton intensity and solar wind plasma properties (left: observations, right: simulations).*

4.3. Magnetosphere-Ionosphere-Thermosphere (MIT) Coupling

The solar wind interaction with the Earth's intrinsic magnetic field creates the magnetospheric and ionospheric convections, beautiful aurora, and field-aligned currents flowing between the magnetosphere and ionosphere. During quiet or weakly disturbed conditions, the high and low latitude ionosphere-thermosphere systems are nearly separated. Small scale geomagnetic disturbances, such as sudden commencement due to the solar wind pressure increase, or substorms at nightside auroral latitudes, perturb the high-latitude system. Their energy input occasionally becomes large enough to generate traveling atmospheric disturbances (TAD) and traveling ionospheric disturbances (TID) which propagate equatorward and interact with the low-latitude system. Geomagnetic storm, the largest geomagnetic disturbance, can be triggered when the Sun sends the Earth excessive energies contained in the interplanetary coronal mass ejection (CME) or corotating interaction region (CIR) (see section 2.2). The high and low latitude ionosphere-

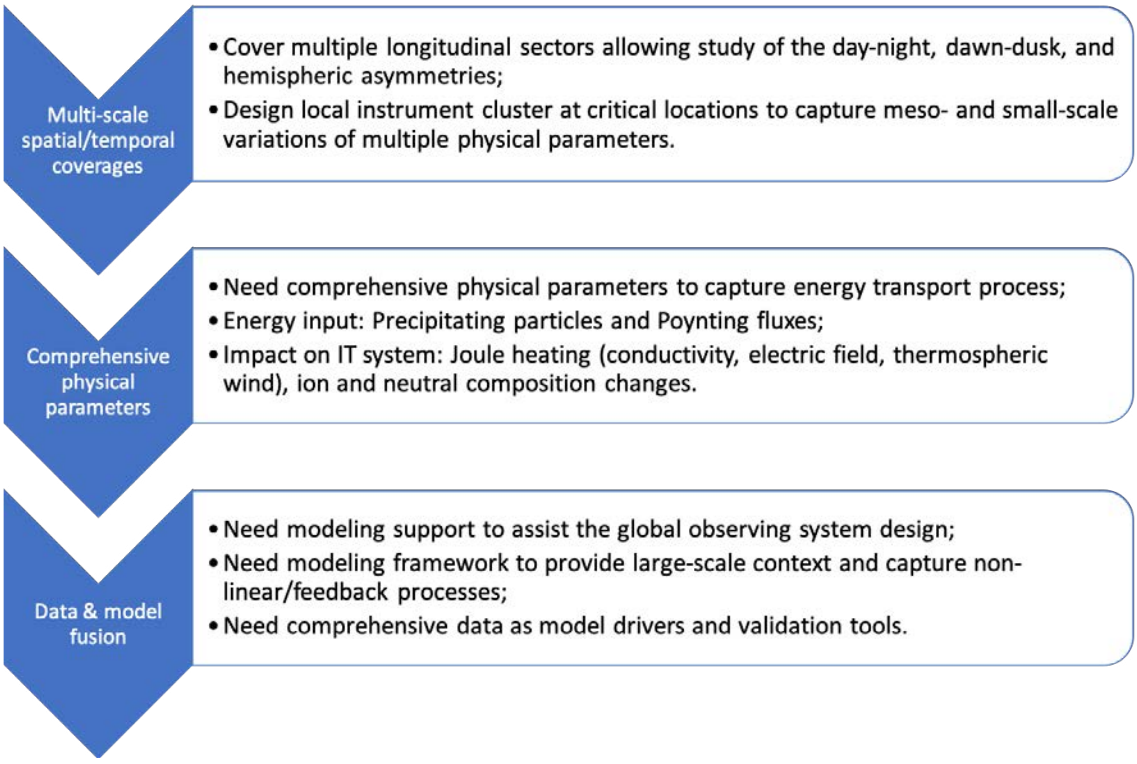

Figure 31: *Suggested considerations for global observational system design and data-model fusion*

thermosphere systems then expand and start to interact with each other. In summary, MIT coupling processes occur over multiple spatial and temporal scales and are highly driven by ever changing solar wind and interplanetary magnetic field conditions. In the middle of the chain, the ionosphere is electromagnetically coupled to the magnetosphere and collisionally coupled to the thermosphere.

Figure 31 illustrates some suggestions for the global observational system design and data and model fusion in order to fulfill the goal of the IMCP. In order to understand the energy flow in the coupled MIT system, we need to better quantify energy inputs, including both the kinetic energy of precipitating particles and Poynting fluxes, and to better characterize energy dissipation processes and their consequences, such as joule heating in the auroral zone and thermosphere composition changes. Therefore, a number of key observational measurements will need to be made over multiple longitudes and latitudes simultaneously to provide sufficient spatial coverage (see section 3). Instrument clusters, which can provide comprehensive multiple physical parameters measurements, such as incoherent scatter radars, should be planned at carefully designed locations. This will not only extend the spatial dimensions from the two-dimensional horizontal plane to the vertical direction, but also increase the complexity of the parameter space.

With the rapid development of supercomputer resources, complex numerical models, such as physics-based first principle models, have been widely used in simulating magnetosphere-ionosphere-thermosphere coupling processes and are continuously evolving. Modeling frameworks, such as the University of Michigan Space Weather Modeling Framework (SWMF) (Tóth et al., 2005 and 2012), have been created to provide the platform for users to couple various models with each other in an efficient manner. These individual models can use different numerical methods to characterize drastically different plasma regimes. Recent developments include two-way coupling between particle-in-cell model and global magnetohydrodynamics (MHD) model (Chen et al., 2019; Zhou et al., 2019) to allow a more realistic representation of the physical processes. These sophisticated modeling frameworks could be used to provide guidance on the selection of desired locations for instrument clusters, put localized observations into a global context or even map them back into the magnetosphere for source region identification (e.g., Zou et al., 2017). The comprehensive observations obtained from the network can be used for model validation or assimilation. A combination of comprehensive observations and sophisticated numerical models will enable the prediction of complex behaviors that emerge under constantly varying conditions in the solar wind and reveal how the Earth's upper atmosphere and ionosphere systems respond to space weather events.

4.4. Plasmasphere Modeling

A three-dimensional dynamic physics-based model of the plasmasphere has been developed at BIRA-IASB (Pierrard and Stegen, 2008). The simulations provide the density and temperatures inside and outside the co-rotating region of the plasmasphere, which is the extension of the ionosphere at higher altitudes (Pierrard et al., 2009). The plasmasphere contains a relatively dense plasma of low-energy (typically 1 eV) electrons and protons, with also a small amount of helium ions. The position of the plasmapause, which is the outer boundary of the plasmasphere, is highly dynamic and depends on the level of geomagnetic activity. During quiet time periods, the plasmapause is located quite far from the Earth (4-7 Re typically). During geomagnetic storms and substorms, it is eroded and a new sharp plasmapause is formed closer to the Earth (2-4 Re) in the post-midnight sector by the mechanism of interchange instability (Lemaire and Pierrard, 2008), due to the interplay between the steady co-rotation electric field and the convection electric field associated to the geomagnetic activity. The convection electric field is obtained empirically from satellite observations and different electric field models have been compared (Pierrard et al., 2008). A plume is generated a few hours after the storm in the afternoon Magnetic Local Time (MLT) sector and co-rotates with the Earth. Following the erosion associated to the storm, the ionosphere refills the plasmasphere in typically a few days, with a refilling time depending on the radial distance, up to the new plasmapause position located further from the Earth. The radial electron density profile near the plasmapause has the shape of a sharp knee just after the storm or substorm, but it can also display some finite thickness (Kotova et al., 2018). Multiple plasmaspauses can sometimes even be observed. The effect of the plasmaspheric wind can also lead to a plasmapause far from the Earth after long quiet periods.

This model is available for free run at any chosen date and in real time on the ESA website of SSA (Space Situational Awareness) at http://swe.ssa.esa.int/space-radiation (Swiff Plasmasphere Model (SPM)). It provides the time variations of the density of electrons and ions inside and outside the plasmasphere in the geomagnetic and meridian planes, the plasmapause position and the temperatures of the different particles.

The plasmasphere model has also been coupled with the international reference ionosphere model (used below 700 km) to be able to determine the density and temperature in the ionosphere and especially the ion trough position corresponding to the projection of the plasmapause in the ionosphere (Pierrard and Voiculescu, 2011). This ionospheric trough appears at lower latitudes during geomagnetic storms. Density and temperature in the ionosphere are mainly modulated by day/night solar radiation and the geomagnetic activity.

The results of the simulations have been compared with various satellite observations

(IMAGE, Cluster, CRRES, THEMIS, etc.) to statistically validate the model (Darrouzet et al., 2009, Bandic et al., 2016, Verbanac et al., 2018 and references therein). As predicted by the SPM model, the plasmapause position is mainly formed in the post-midnight sector. Observations from the meridian perspective by KAGUYA clearly show a plasmapause formation first near the equatorial region, in good agreement with the mechanism of interchange instability (Murakami et al., 2016). Different waves circulate inside and outside the plasmasphere and along the plasmapause, so that such a model of the plasmasphere is useful to determine its influence on radiation belts dynamics (Pierrard and Benck, 2012).

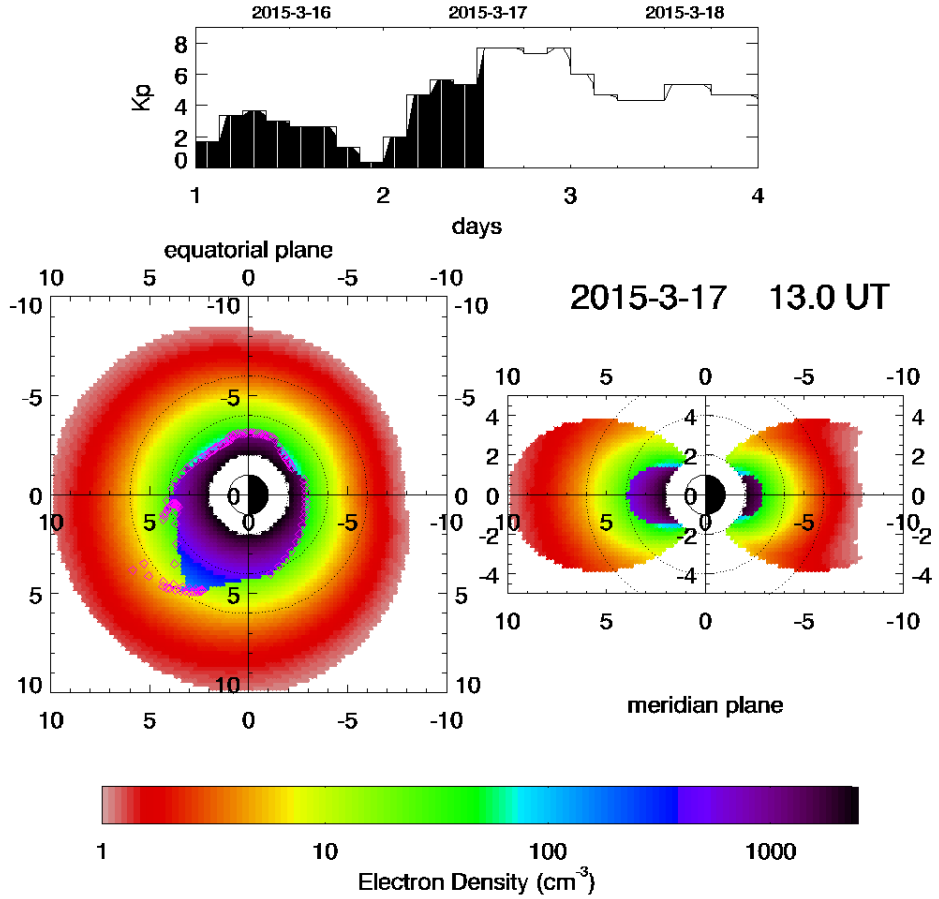

Figure 32: *Example of the plasmasphere electron density as obtained from the Swiff Plasmasphere Model (SPM) for the date of 17 March 2015 during a geomagnetic storm. The plasmasphere is eroded and a plume is formed, as clearly visible on the Figure in the afternoon MLT sector (Sun is on the left). The upper panel shows the planetary geomagnetic activity index of Bartels Kp increasing during the storm.*

4.5. Ionosphere-Thermosphere-Mesosphere (ITM) Coupling

It is well known that the ionosphere is formed mainly from the photoionization of the atmosphere by solar X-rays and EUV radiations. Since the neutral gas in the upper atmosphere is the background of the ionosphere, the upper thermosphere has a strong impact on the behavior of the ion and electron distribution in the ionosphere. Neutral temperature, composition, and neutral winds of the upper atmosphere all strongly modulate the ionosphere. The neutral temperature can affect collisions and reactions between neutral gas and plasma, and thus influence the energy exchanges between the ionosphere and the thermosphere. The major ion in the ionosphere is O^+, which is formed through photoionization of O and lost mainly through dissociative recombination with N_2 and O_2, predominantly with N_2. Therefore the magnitude of the ionospheric density in the F_2 layer depends on the O/N_2 and O/O_2 ratios, mainly on O/N_2. A horizontal wind blowing towards the magnetic equator tends to drive F region plasma (ions and electrons). This upward drift raises the ionospheric peak to altitudes of reduced chemical loss. Additionally, when the neutral gas moves the ionospheric plasma across the geomagnetic field it induces ionospheric

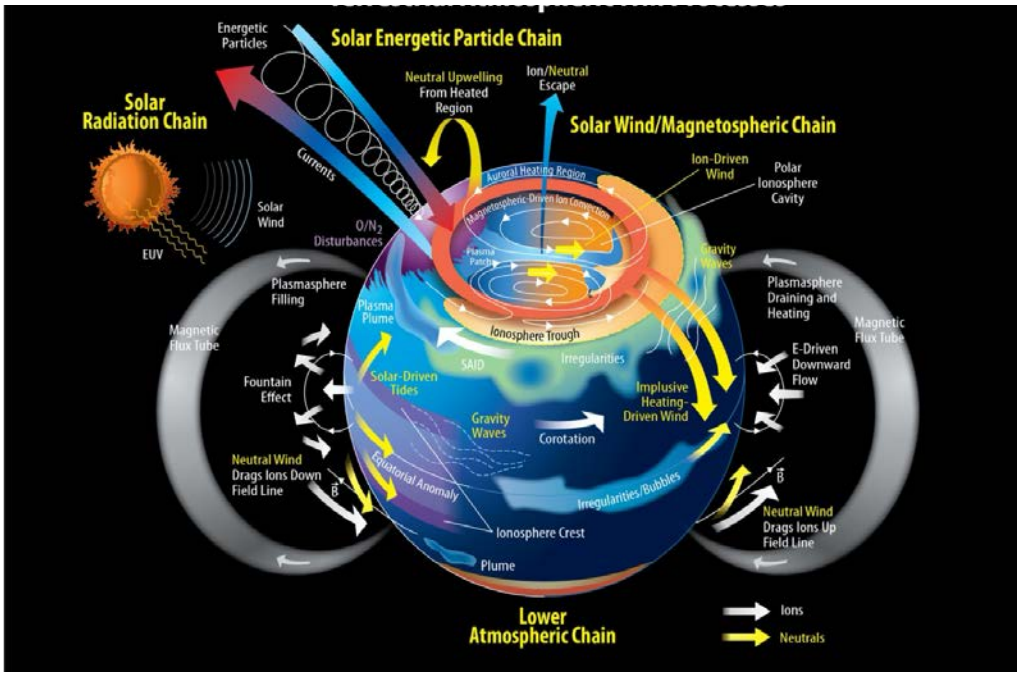

Figure 33: *Cartoon illustrating the main processes that take place and are modeled in the coupled ionosphere-thermosphere-atmosphere system. Credits: NASA's Scientific Visualization Studio https://svs.gsfc.nasa.gov/4641.*

currents and electric fields. This is called the neutral wind dynamo process. When the associated electric field is eastward (and the plasma drifts upward) it also tends to move the ionosphere to higher altitudes where chemical loss rate is lower and so increases the peak electron density as the direct transport of neutral winds does.

At the same time, the ionosphere exerts some feedback on the variations of the thermosphere, albeit the plasma density in the ionosphere is much lower (by a few orders of magnitude) than the background neutral species. At high latitudes, the pressure gradient of the neutral gas produced by solar EUV heating is generally balanced by the ion-neutral collision forcing in addition to Coriolis and centrifugal forcings. The ion-neutral collision forcing is very significant because of strong horizontal convection of the ionospheric plasma over high latitudes. This convection results from mapping of the electric field from the solar wind and magnetosphere system along the field lines. The typical two-cell convection pattern has an anti-sunward flow from the magnetic local time midday to midnight, westward return flows on the dusk side and eastward return flows on the dawn side. Its large convection speeds can influence thermospheric winds not only in the F2 layer but also in the lower thermosphere. The effect can be observed in neutral composition and temperature as well (e.g. Thayer et al., 1987). In addition, especially during storm times, the thermosphere is greatly disturbed by changes of ionospheric convection and associated conductivities, through the effects of Joule or frictional heating processes.

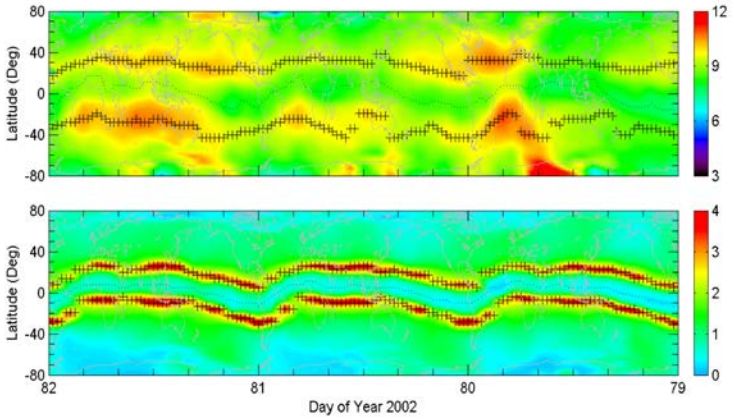

Figure 34: *The simultaneous neutral mass density (top, 10^{12} kg/m^3) and electron density (bottom, 10^{12} / m^3) from the CHAMP satellite at around 19 LT in Equinox (day 79-81 in 2002). The UT day runs from right to left. This plot demonstrates the coupling and decoupling features between the ionosphere and the thermosphere at low and middle latitudes and the modulation association with the lower atmospheric forcing (modified from Lei et al., 2010)*

The ionospheric feedback on the thermosphere is seen not only in the polar regions but also in the low and equatorial regions. The well-known phenomenon in the equatorial ionosphere is the equatorial ionization anomaly (EIA), with two crests at around ±15° in magnetic latitude and a trough at the magnetic equator (Lei et al, 2010) — see also section 2.4 and Figure 6. A phenomenon similar to the EIA, called the equatorial thermosphere anomaly (ETA), was identified in the equatorial thermosphere density (bottom panel). Additionally, the zonal wind anomaly at dusk, corresponding to the fast zonal wind, which is associated with ion drag and viscosity, was observed by the DE2 and CHAMP satellites. These are good examples of the coupling of the thermosphere and the ionosphere in the equatorial region.

The two-way coupling between thermosphere and ionosphere prevails throughout almost all solar-geophysical conditions and is significantly modulated by the momentum and energy inputs from above and below. Besides the forcing from solar flux changes and solar wind-magnetospheric energy deposition, lower atmosphere forcing on the thermosphere and ionosphere system, including gravity waves, tides, and planetary waves, attracted a lot of attention from the ionosphere-thermosphere community.

From the observational point of view, thermospheric measurements including electric fields, neutral winds, and composition in different altitudinal range and also different longitudinal sectors are sparse so that they are extremely needed to improve our current understanding of thermosphere-ionosphere-mesosphere coupling. Therefore, it is expected that the observation system of the International Meridian Circle could provide continuous monitoring of the whole atmosphere and of coupling processes in different regions.

State-of-the-art theoretical models, such as the Thermosphere-Ionosphere-Mesosphere-Electrodynamics General Circulation Model (TIME-GCM, Roble et al., 1994), the Whole Atmosphere Community Climate Model with the thermosphere and ionosphere extension (WCCAM-X, Liu et al., 2018), Whole Atmosphere Model (WAM, Akmaev, 2011), and Ground-to-topside model of Atmosphere-ionosphere for Aeronomy (GAIA, Jin et al., 2011), become available for the study of mesosphere-thermosphere-ionosphere coupling.

4.6. Models of Ionospheric Anomalies Produced by Lithosphere-Atmosphere-Ionosphere Coupling (LAIC)

Two Seismic-Lithosphere-Atmosphere-Ionosphere (SLAI) Coupling models developed to explain earthquake-related ionospheric anomalies were presented at the forum: an Electric field coupling model and an electromagnetic wave propagation model.

4.6.1. Electric Field Coupling Model

The formation of LAIC electric field is mainly based on the p-hole mechanism of rock physics. It is believed that the increase of rock stress before the earthquake will ionize the atmosphere near the surface and generate a large number of additional ions. Ions gather at the bottom of the atmosphere and generate an abnormal atmospheric electric field. This atmospheric electric field maps up to the ionosphere and produces extra E×B drifts, causing an anomaly in the conjugate area as well. Based on this mechanism, Zhou et al. (2017) constructed a 3D ionospheric electric field model which has been applied to explain the anomalies of electron density before the Nepal earthquake, as shown in Figure 35.

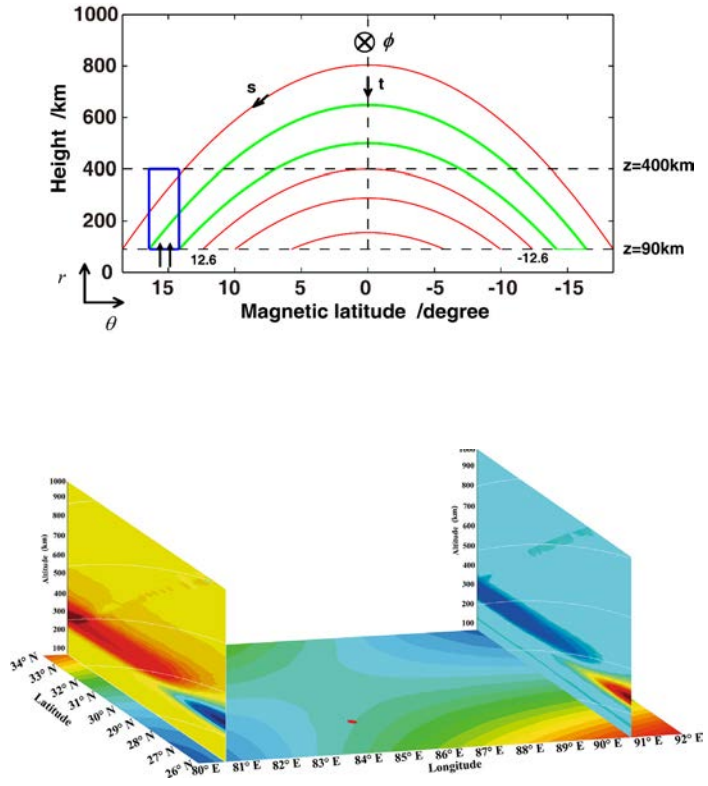

Figure 35: *The electric field coupling model of Zhou et al. (2017) and its simulated result of electron density before the Nepal earthquake. From Kong et al. (2018)*

4.6.2. Electromagnetic Wave Propagation Model

There are many VLF transmitters around the world with constant radiation frequencies and powers. The waves from these transmitters do not only propagate in the ground-ionosphere waveguide over long distances. They can also penetrate into the ionosphere. As a propagation media of VLF waves, disturbances of the ionospheric plasma possibly produced by earthquakes will cause a change in VLF signals observed on the ground and on-board satellites. An electromagnetic wave propagation model was developed (Zhao et al., 2017; Zhao et al., 2019) to explain the electric field anomalies observed on satellite and ground receivers. For the Yushu Earthquake in China, the field intensity observed by the ground-based receiver was reduced before the earthquake (Shen et al., 2017) as well as the SNR of the electric field observed by DEMETER. The results from the electromagnetic wave propagation model confirm and quantify the effects of electron density variations caused by the earthquake in the lower ionosphere on the electric fields observed on the ground and on low-earth-orbit (LEO), as shown in Figure 36.

4.7. Data assimilation

Progress in data assimilation in the ionosphere in the past decades was reviewed during the forum. The purpose of data assimilation, the most commonly used methods in numerical weather prediction (NWP) and the basic requirements for data assimilation of ionospheric radio wave propagation data were described. The differences of data assimilation approaches between NWP and ionosphere were emphasized. A very brief history and status of ionospheric data assimilation in the past decades was also given. Then, taking the research achievements of Chinese scholars as an example, the application of Kalman filter in ionospheric data assimilation was introduced and the applications of data assimilation in the study of ionospheric storm-time characteristics were described (Yue et al., 2016a, 2016b) including a reanalysis of historical data (Yue et al., 2012). Finally, the role of ensemble Kalman filter in improving the ionospheric short-term prediction due to the relatively short memory of ionized plasma was illustrated (He et al., 2019). Requirements on the IMCP program from the perspective of data assimilation were formulated. Figure 37 shows the global ionospheric electron density and corresponding peak density and total electron content (TEC) map through multi-sources Kalman filter data assimilation.

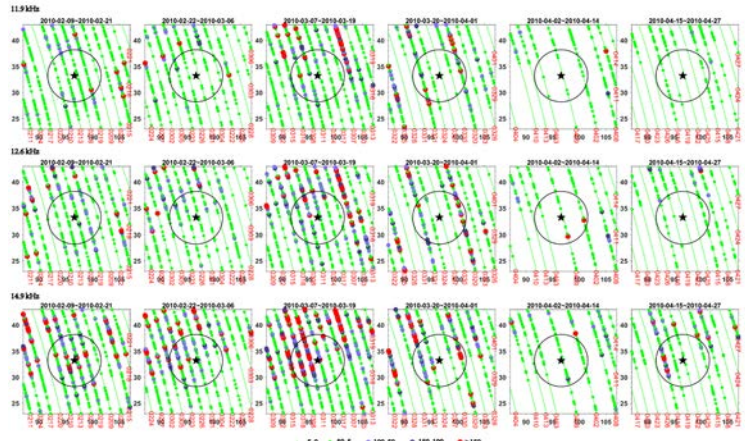

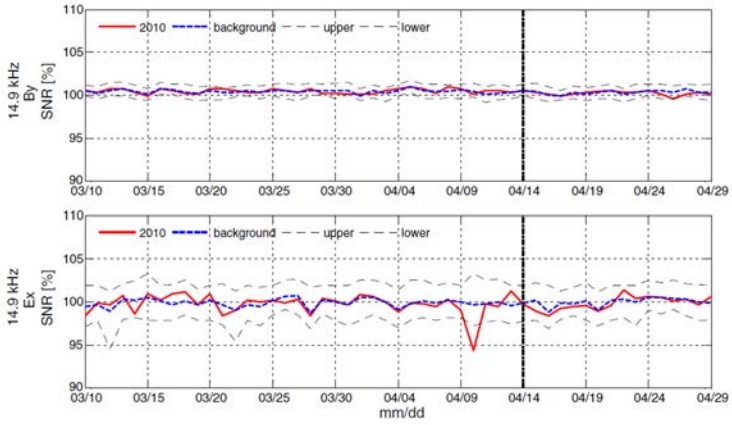

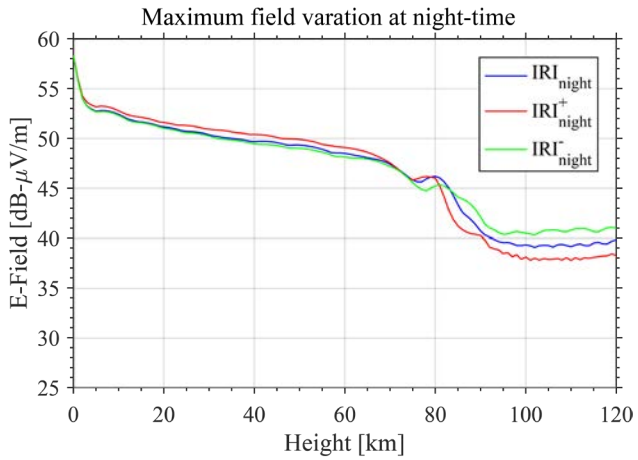

Figure 36: *Abnormal electric field observed on the satellite and on the ground, compared with the simulated electric field calculated by propagating VLF waves into the ionosphere using an International Reference Ionosphere (IRI) model. From Shen et al., 2017.*

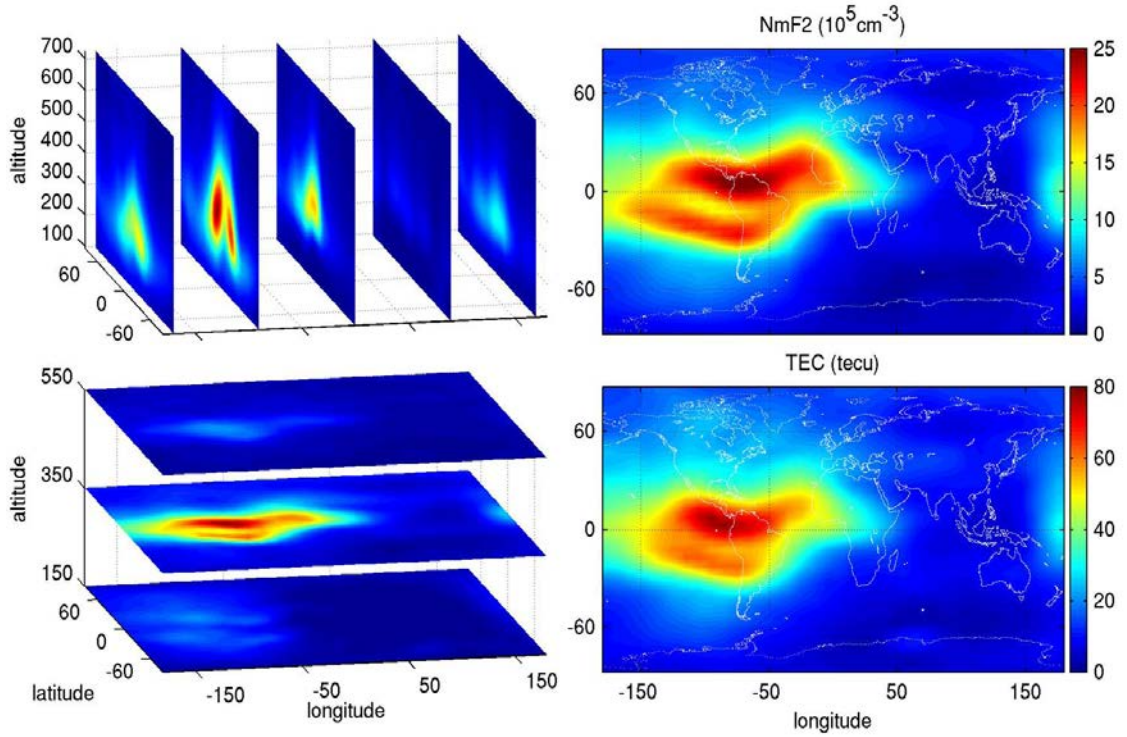

Figure 37: *An example of global Ionospheric electron density and corresponding peak density and TEC maps reproduced through data assimilation (from Yue et al., 2012).*

4.8. Preliminary Conclusions on Modeling

This section reviewed a significant fraction of the modelling and data assimilation tools that will need to be developed and made available to users in order to meet the requirements of the IMCP: numerical simulations of galactic cosmic ray modulation during their transport through the heliosphere and Earth's environment; MIT and ITM coupling: plasmasphere dynamics; LAI coupling mechanisms and related ionospheric disturbances; ionospheric data assimilation.

This first set of models will need to be extended to cover the whole chain of energy transfer processes that leave their imprint on the IMUA. Global predictive models of the propagation of solar and heliospheric disturbances through interplanetary space and of their effects on the magnetosphere as well as global to regional models of the propagation of disturbances within the IMUA itself will be particularly important additions.

5. CONCLUSIONS AND PERSPECTIVES

Our Earth's geospace is coupled to its space environment via a critical layer through which a broad diversity of energy transfer processes takes place at time scales from a fraction of a second to millenia: its Ionosphere, Upper, and Middle Atmosphere (IMUA). As the presentations and discussions at this forum showed, understanding how these processes affect the IMUA from above, from below, and from within is a major scientific challenge for the XXIst century with important social implications.

Indeed, by using the IMUA as a "screen", we will be able to better detect, understand, mitigate, and sometimes predict the diversity of natural and anthropogenic hazards (solar activity, changes in the geomagnetic field, earthquakes, atmospheric, and climatic disturbances, etc.) threatening ecosystems and human activities. We will also better assess their impacts on our space environment itself, with increasingly important implications on the safety of ground infrastructures, space systems, and space flight. Reaching this objective requires the deployment and coordinated operation of a global ground-based network of instruments to continuously and globally monitor key parameters of the IMUA.

The forum exchanges laid the foundations of the science case driving the design of this observing system. An integration of the diverse measurement requirements produced by this science case showed that the "ideal" geometry for the observing system is a set of two great meridian circles: the 120°E-60°W great circle, running over Eastern Asia, Australia, and the Americas, complemented by a second great circle along the 30°E-150°W meridians and covering Europe, Africa, and central Pacific. Deploying a chain of scientific instruments observing the IMUA along these two great circles will uniquely allow to cover its variations in geographic and geomagnetic latitudes, to monitor the most active regions of seismic and thunderstorm activity, and to capture the contrasts between lands and oceans. Deploying and operating this chain of instruments along these two great circles is the objective of the International Meridian Circle Project (IMCP), a "big science" international project currently candidate for funding in China.

To field a globe-circulating array of instruments along these two great circles, the IMCP will integrate existing or planned instruments operated by many countries over the world into a coherent observation system. Low-cost, uniform instrument clusters, and arrays will be supplemented by larger, facility-class instruments such as lidars and ionospheric radars. China's Meridian Project, whose Phase II is currently under deployment, will provide a template for the global IMCP network. The international team of experts attending the forum concluded that the strong scientific potential and high motivation needed to assemble the type of network required for the IMCP exist. Networking of the existing instruments will have to be complemented by a limited set of new instruments along the two

circles. Establishment of a strong international coordination to operate the IMCP network and jointly analyze its data will be a key element of success.

The most advanced models, data assimilation, and Artificial Intelligence tools will have to be mobilized to recognize the characteristic imprints of the different sources of hazards on the IMUA in the huge volume of data produced by the IMCP. The preliminary review of these tools accomplished during the forum showed that a very strong interplay between production and analysis of observational data, use of advanced numerical models, and data assimilation techniques will be required to take the best possible advantage of the outstanding research and monitoring tool which the IMCP will offer to the international scientific community. This synergistic use of data, models, and pattern recognition tools will have to be built from the very beginning in the global design of the IMCP scientific strategy.

Complementing the ground-based observing system of the IMCP by a specifically designed space-based component will substantially improve the coverage of IMUA key parameters. Such a space segment will make it possible to fully disentangle spatial and temporal variations and to give access to critical regions of the IMUA which are not easily accessible by ground-based measurements, such as the mesosphere/lower thermosphere transition region. Discussion of this space segment should be the subject of a dedicated forum, which the participants proposed to be organized by the International Space Science Institute in Bern, Switzerland.

More that sixty years ago, the International Geophysical Year accomplished a comprehensive investigation of our planet as a set of superposed layers. Since then, much progress has been accomplished towards a better understanding of each layer, but to address today's most important scientific questions we need to understand the Earth as a global whole, thus integrating coupling between layers. Some of the most complex and most poorly known of these coupling mechanisms occur within the IMUA, which, however, remains poorly explored. The participants to the forum unanimously concluded that deploying and operating the IMCP observation system will provide a major contribution to this perspective, as well as to a far better understanding and monitoring of the impacts of space weather on human activities of all kinds. They enthusiastically agreed to work together across the five continents to achieve this great and exciting goal.

6. ACKNOWLEDGEMENTS

Part of the findings on ionospheric anomalies associated to large earthquakes reported here were obtained by the following scientists under the grant of Mitsubishis Foundation (Mitsubishi Foundation (ID.26113) for the research support in 2015-2016: Bankov, L. (Bulgarian Geophysical Institute, Bulgaria); Devi, M. (Gauhati University, India); Ryu K. (KAIST, Korea); Liu, H. (Kyushu University, Japan); Liu, J.Y. (National Central University, Taiwan); Chen, C.H. (National Cheng Kung University, Taiwan); Kakinami, Y. (Hokkaido Information Technology University, Japan).

Mioara Mandea would like to thank VR2Planets and especially the founder of this start-up company, Francois Civet, for preparing the animation from which Figure 12 is obtained.

Walter Gonzalez would like to express his gratitude to the State Key Laboratory of Space Weather, NSSC/CAS, and the National Space Research Institute of Brazil, INPE.

Viviane Pierrard would like to thank the Solar Terrestrial enter of Excellence and the Royal Belgian Institute for Space Aeronomy for their support in the development of the plasmasphere model.

Xinan Yue acknowledges the support by the National Natural Science Foundation of China (41427901) and the Meridian Project.

Incoherent scatter radar observations at Millstone Hill, global GNSS TEC data processing, data access through the Madrigal distributed data system (http://www.openmadrigal.org), as well as related research and analysis activities are conducted at MIT Haystack Observatory under the support from the U.S. National Science Foundation (NSF) Grant AGS-1762141. We also acknowledge support from the US AFOSR MURI Project FA9559-16-1-0364.

The work of Natchimuthuk Gopalswamy was supported by NASA's Living With a Star program.

Hermann Opgenoorth would like to acknowledge the travel support received from the Swedish National Space Agency (SNSA).

7. REFERENCES

[1] Akmaev, R. A. (2011). Whole atmosphere modeling: Connecting terrestrial and space weather. *Reviews of Geophysics*, 49, RG4004. doi:10.1029/2011RG000364.

[2] Aubert, J., Finlay, C. (2019) Geomagnetic jerks and rapid hydromagnetic waves focusing at earth's core surface. *Nature Geoscience*. doi:10.1038/s41561-019-0355-1.

[3] Bandic, M., Verbanac, G., Moldwin, M., Pierrard, V., Piredda G. (2016). MLT dependence in the relationship between plasmapause, solar wind and geomagnetic activity based on CRRES: 1990-1991, *J. Geophys. Res.*, 121, 4397-4408. doi: 10.1002/2015JA022278.

[4] Blanc, E., F; Lefeuvre, R. Roussel-Dupré, J.-A. Sauvaud (2007). TARANIS: a microsatellite project dedicated to the study of impulsive transfers of energy between the Earth atmosphere, the ionosphere, and the magnetosphere. *Adv. Space Res.*, 40, 1268-1275.

[5] Blanc, E. (2010). Space observations of Transient Luminous Events and associated emissions in the upper atmosphere above thunderstorm areas. *C R Geosci,* 342, 312–322.

[6] Blanc, E., Le Pichon, A., Ceranna, L., Farges, T., Marty, J., Herry, P. (2010). Global scale monitoring of acoustic and gravity waves for the study of the atmospheric dynamics. In A. Le Pichon, E. Blanc, A. Hauchecorne (Eds.), *Infrasound monitoring for atmospheric studies* (647-664), Berlin: Springer.

[7] Blanc, E., Farges, T., Le Pichon, A., Heinrich, P. (2014). Ten-year observations of gravity waves from thunderstorms in western Africa. *J Geophys Res,* 119(11), 6409–6418. doi: 10.1002/2013JD020499.

[8] Blanc, E., Charlton-Perez, A., Keckhut, P., Evers, L., Heinrich, P., Le Pichon, A., Hauchecorne, A. (2015). The ARISE project: dynamics of the atmosphere and climate. Our common future under climate change. *International scientific conference*. Paris, France, July 2015, 1108-01. https://hal-insu.archives- ouvertes.fr/insu-01183228/

[9] Blanc, E. et al. (2018). Toward an Improved Representation of Middle Atmospheric Dynamics Thanks to the ARISE Project, *Surv Geophys*, 39, 171–225. doi: 10.1007/s10712-017-9444-0

[10] Blanc, M., Amayenc, P., Bauer, P., Taieb, C. (1977). Electric field induced drifts from the French incoherent scatter facility. *Journal of Geophysical Research,* 82, 87-97.

[11] Blanc, M., Amayenc, P. (1979). Seasonal variations of the ionospheric E x B drifts above Saint-Santin on quiet days. *Journal of Geophysical Research,* 84, 2691-2704.

[12] Bounhir, A., Benkhaldoun, Z., Makela, J., Kaab, M., Harding, B., Fisher, D., . . . Daassou, A. (2017). Thermospheric Dynamics in Quiet and Disturbed Conditions. *Proceedings of the International Astronomical Union*, 13(S335), 151-158. doi:10.1017/S174392131700919X.

[13] Bütikofer R., 2018, Ground-based measurements of energetic particles by neutron monitors, in O.E. Malandraki, N.B. Crosby (Eds.), *Solar Particle Radiation Storms Forecasting and Analysis* (pp. 95-112), Springer, Astrophysics and Space Science Library, 444. doi: 10.1007/978-3-319-60051-2_6.

[14] Carlson, H. C. (1994). The dark polar ionosphere: Progress and future challenges. *Radio Science*, 29(1), 157–165.

[15] Carlson, H. C. (2012). Sharpening our thinking about polar cap ionospheric patch morphology, research, and mitigation techniques. *Radio Science*, 47(4). doi:10.1029/2011RS004946.

[16] Chen, Y., Toth, G., Jia, X., Slavin,J. A., Sun, W., Markidis, S., Gombosi, T. I., and Raines, J. (2019). Studying dawn-dusk asymmetries of Mercury's magnetotail using MHD-EPIC simulations. *Journal of Geophysical Research – Space Physics*, 124(11), 8954-8973. doi:10.1029/2019JA026840.

[17] Christian, H.J., Blakeslee, R.J., Boccipio, D.J., et al. (2003). Global frequency and distribution of lightning as observed from space by the optical transient detector. *J. Geophys. Res.*, 108(D1), 4005.

[18] Cnossen, I., Liu, H., Lu, H. (2016). The whole atmosphere response to changes in the Earth's magnetic field from 1900 to 2000: An example of "top-down" vertical coupling. *J. Geophys. Res. Atmos.*, 121, 7781-7800. doi:10.1002/2016JD/024890.

[19] Crowley, G. (1996), Critical review of ionospheric patches and blobs. in W. R. Stone (Ed.), *Review of Radio Science 1992-1996 (*pp. 619-648), Oxford University Press: Oxford, U. K.

[20] Darrouzet, F., De Keyser, J., Pierrard, V. (2009). *The Earth's plasmasphere: Cluster and IMAGE – A modern perspective*, Springer: New York, 296.

[21] Emmert, J.T. (2015). Altitude and solar activity dependence of 1967-2005 thermospheric density trends derived from orbital drag. *J. Geophys. Res. Space Phys.*, 120, 2940-2950. doi: 10.102/2015JA021047.

[22] Fear, R. C., S. E. Milan, R. Maggiolo, A. N. Fazakerley, I. Dandouras, and S. B. Mende (2014). Direct observation of closed magnetic flux trapped in the high-latitude magnetosphere. *Science*, 346, 1506–1510. doi:10.1126/science.1257377.

[23] Fisher, D. J., Makela, J. J., Meriwether, J. W., Buriti, R. A., Benkhaldoun, Z., Kaab, M., and Lagheryeb, A. (2015). Climatologies of nighttime thermospheric winds and temperatures from Fabry-Perot interferometer measurements: From solar minimum to solar maximum. *J. Geophys. Res.-Space*, 120, 6679–6693. doi:10.1002/2015JA021170.

[24] Frank, L. A., Craven, J. D., Burch, J. L., and Winningham, J. D. (1982). Polar views of the Earth's aurora with dynamics explorer. *Geophys. Res. Lett.*, 9, 1001–1004. doi:10.1029/GL009i009p01001.

[25] Foster, J. C., et al. (2005). Multiradar observations of the polar tongue of ionization, *J. Geophys. Res.*, 110(A9). doi:10.1029/2004JA010928.

[26] Foster, J. C., et al. (2007). On the relationship of SAPS to storm-enhanced density. *J. Atmos. Terr. Phys.*, 69, 303-313. doi:10.1016/j.jastp.2006.07.021.

[27] Freund, F. (2011). Pre-earthquake signals: Underlying physical processes. *Journal of Asian Earth Sciences*, 41(4-5), 383-400.

[28] Freund, F., Kulahci, I. G., Cyr, G., Ling, J., Winnick, M., Tregloan-Reed, J., & Freund, M. M. (2009). Air ionization at rock surfaces and pre-earthquake signals. *Journal Of Atmospheric And Solar-Terrestrial Physics*, 71(17-18), 1824-1834.

[29] Freund, F., Takeuchi, A., Lau, B. W., Post, R., Keefner, J. W., Mellon, J., & Almanaseer, A. (2004). Stress-Induced Changes in the Electrical Conductivity of Igneous Rocks and the Generation of Ground Currents. *Terrestrial Atmospheric and Oceanic Sciences*, 15(3), 437-467.

[30] Freund, F., Takeuchi, A., & Lau, B. W. S. (2006). Electric currents streaming out of stressed igneous rocks - A step towards understanding pre-earthquake low frequency EM emissions. *Physics And Chemistry Of the Earth*, 31(4-9), 389-396.

[31] Fritts, D. C., Alexander, M.J. (2003). Gravity wave dynamics and effects in the middle atmosphere. *Rev Geophys,* 41(1),1003. doi: 10.1029/2001RG000106.

[32] Gao, Y. X., Harris, J. M., Wen, J., Huang, Y. H., Twardzik, C., Chen, X. F., & Hu, H. S. (2016). Modeling of the coseismic electromagnetic fields observed during the 2004 M-w 6.0 Parkfield earthquake. *Geophysical Research Letters*, 43(2), 620-627.

[33] Hao, Y. Q., Xiao, Z., & Zhang, D. H. (2012). Multi-instrument observation on co-seismic ionospheric effects after great Tohoku earthquake. *Journal Of Geophysical Research-Space Physics*, 117.

[34] Goncharenko L. P. et al. (2018). Deep Ionospheric Hole Created by Sudden Stratospheric Warming in the Nighttime Ionosphere, *Journal of Geophysical Research: Space Physics,* 123(9), 7621-7633. doi: 10.1029/2018JA025541.

[35] Gopalswamy, N., The CME link to geomagnetic storms. In *Solar and Stellar Variability: Impact on Earth and Planets*, Brazil, 3–7 August 2009, (Eds.) Kosovichev, A.G., Andrei, A.H., Roelot, J.-P., vol. 264 of IAU Symposia, pp. 326–335, Cambridge University Press, Cambridge; New York. 326-335.

[36] Gousheva, M., Glavcheva, R., Danov, D., Hristov, P., Kirov, B. B., and Georgieva, K. (2008). Electric field and ion density anomalies in the mid latitude ionosphere: Possible connection with earthquakes?. *Advances in Space Research*, 42(1), 206-212.

[37] Harding, B. J., Gehrels, T. W., and Makela, J. J. (2014). Nonlinear regression method for estimating neutral wind and temperature from Fabry–Perot interferometer data, *Appl. Opt.*, 53, 666–673.

[38] Hauchecorne, A., Keckhut, P., Chanin M.L. (2010). Dynamics and transport in the middle atmosphere using remote sensing techniques from ground and space. In A. Le Pichon, E. Blanc, and A. Hauchecorne (Eds.), *Infrasound Monitoring for Atmospheric Studies* (pp. 665-683), Springer: Dordrecht.

[39] Hauchecorne, A., Khaykin, S., Keckhut, P., Mze, N., Angot, G., and Claud, C. (2019). Recent dynamic studies on the middle atmosphere at mid- and low-latitudes using Rayleigh Lidar and other technologies, In A. Le Pichon, E. Blanc, and A. Hauchecorne (Eds.), *Infrasound Monitoring for Atmospheric Studies* (pp. 665-683), Springer: Dordrecht, 1167.

[40] Hayakawa, M., Itoh, T., Hattori, K., & Yumoto, K. (2000). ULF electromagnetic precursors for an earthquake at Biak, Indonesia on February 17, 1996. Geophysical Research Letters, 27(10), 1531-1534.

[41] Hayakawa, M., Kasahara, Y., Nakamura, T., Muto, F., Horie, T., Maekawa, S., et al. (2010). A statistical study on the correlation between lower ionospheric perturbations as seen by subionospheric VLF/LF propagation and earthquakes. *Journal of Geophysical Research: Space Physics*, 115(A9). doi:10.1029/2009JA015143.

[42] He, J., Yue, X., Wang, W., & Wan, W. (2019). EnKF ionosphere and thermosphere data assimilation algorithm through a sparse matrix method. *Journal of Geophysical Research: Space Physics*, 124, 7356– 7365. Doi: 10.1029/2019JA026554.

[43] Holton, J.R. (1983). The influence of gravity wave breaking on the general circulation of the middle atmosphere. *J Atmos Sci,* 40, 2497–2507.

[44] Hulot, G., N. Olsen, T. Sabaka, A. Fournier, The present and future geomagnetic field. Schubert G (ed)Treatise on Geophysics (Second Edition), 33–78 (2015). doi: 10.1016/B978-0-444-53802-4.00096-8

[45] Jackson, A., Jonkers, A.R.T., Walker, M.R. (2000). Four centuries of geomagnetic secular variation from historical records. *Philos. Trans. R. Soc. Lond.*, 358(1768), 957-990.

[46] Korte, M., Mandea, M. (2019). Geomagnetism: From Alexander von Humboldt to current challenges. *Geochemistry, Geophysics, Geosystems,* 20(8), 3801-3820. doi: 10.1029/2019GC008324

[47] Jin, H., Miyoshi, Y., Fujiwara, H., Shinagawa, H., Terada, K., Terada, N., Ishii, M., Otsuka, Y., and Saito, A. (2011). Vertical connection from the tropospheric activities to the ionospheric longitudinal structure simulated by a new Earth's whole atmosphere-ionosphere coupled model. *J. Geophys. Res.*, 116(A01), 316. doi:10.1029/2010JA015925.

[48] Kaab, M., Benkhaldoun, Z., Fisher, D. J., Harding, B., Bounhir, A., Makela, J. J., Laghriyeb, A., Malki, K., Daassou, A., and Lazrek, M. (2017). Climatology of thermospheric neutral winds over Ouka¨ımeden Observatory in Morocco. *Annales Geophysicae*, 35(1), 161–170. doi: 10.5194/angeo-35-161-2017.

[49] Keckhut P, Gelman ME, Wild JD, Tissot F, Miller AJ, Hauchecorne A, Taylor, F. W. (1996). Semidiurnal and diurnal temperature tides (30–55 km): Climatology and effect on UARS-LIDAR data comparisons. *J Geophys Res.*, 101(D6), 10299-10310.

[50] Malki, K., Bounhir, A., Benkhaldoun, Z., Makela, J., Vilmer, N., Fisher, D.J., Kaab, M., El bouyahyaoui, K., Harding, B.J., Laghriyeb, A., Daassou, A., and Lazrek, M. (2018). Ionospheric and thermospheric response to the 27–28 February 2014 geomagnetic storm over north Africa. *Ann. Geophys.*, 36, 1-12.

[51] Kishore, P., Namboothiri, S.P., Igarashi, K., Murayama, Y., Watkins, B.J. (2002). MF radar observations of mean winds and tides over Poker Flat, Alaska (65.1 N, 147.5 W). *Ann. Geophys.*, 20(5), 679-690.

[52] Kong, J., Yao, Y., Zhou, C., Liu, Y., Zhai, C., Wang, Z., & Liu, L. (2018). Tridimensional reconstruction of the Co-Seismic Ionospheric Disturbance around the time of 2015 Nepal earthquake. *Journal of Geodesy*, 92(11), 1255-1266. doi:10.1007/s00190-018-1117-3.

[53] Korte, M., M.C. Brown, S. Panovska, I. Wardinski (2019). Robust characteristics of the laschamp and mono lake geomagnetic excursions: Results from global field models. *Frontiers in Earth Science,* 7, 86. doi:10.3389/feart.2019.00086

[54] Kotova, G., Verigin, M., Lemaire, J., Pierrard, V., Bezrukikh, V., Smilauer, J. (2018). Experimental study of the plasmasphere boundary layer using MAGION 5 data, *J. Geophys. Res: Space Physics*,123, 1251-1259. doi: 10.1002/2017JA024590.

[55] Kuo, C. L., Huba, J. D., Joyce, G., & Lee, L. C. (2011). Ionosphere plasma bubbles and density variations induced by pre-earthquake rock currents and associated surface charges. *Journal Of Geophysical Research-Space Physics*, 116.

[56] Kuo, C. L., Lee, L. C., & Huba, J. D. (2014). An improved coupling model for the lithosphere-atmosphere-ionosphere system. *Journal Of Geophysical Research-Space Physics*, 119(4), 3189-3205.

[57] Kuo, C.L., Ho, Y.Y., Lee, L.C. (2018). Electrical Coupling Between the Ionosphere and Surface Charges in the Earthquake Fault Zone. In D. Ouzounov, S. Pulinets, K. Hattori (Eds), *Pre-Earthquake Processes: A Multidisciplinary Approach to Earthquake Prediction Studies*, Geophysical Monograph Series. doi: 10.1002/9781119156949.ch7.

[58] Laštovička, J. (2017). A review of recent progress in trends in the upper atmosphere. *J. Atmos. Sol.-Terr. Phys.*,163, 2-13. doi:10.1016/j.jastp.2017.03.009.

[59] Laštovička, J., Akmaev, R.A., Beig, G., Bremer, J., Emmert, J.T., Jacobi, C., Jarvis, M.J., Nedoluha, G., Portnyagin, Y.I., Ulich, T. (2008). Emerging pattern of global change in the upper atmosphere and ionosphere. *Ann. Geophys.*, 26(5), 1255–1268. doi: 10.5194/angeo-26-1255-2008.

[60] Leger, J., Bertrand, F., Jager, T., Le Prado, M., Fratter, I., Lalaurie, J. (2009). Swarm absolute scalar and vector magnetometer based on helium 4 optical pumping. *Proceedings of the Eurosensors XXIII conference*, 634-637. doi:10.1016/j.proche.2009.07.158

[61] Lei, J., J. P. Thayer, and J. M. Forbes (2010), Longitudinal and geomagnetic activity modulation of the equatorial thermosphere anomaly, J. Geophys. Res., 115(A8). doi:10.1029/2009JA015177.

[62] Lemaire, J., Pierrard, V. (2008). Comparison between two theoretical mechanisms for the formation of the plasmapause and relevant observations. *Geomagnetism and Aeronomy*, 48(5), 553-570. doi: 10.1134/S0016793208050010.

[63] Le Pichon, A., Blanc, E., Drob, D. (2005). Probing high-altitude winds using infrasound. *Journal of Geophysical Research*. 110(D20), 104. doi: 10.1029/2005JD006020.

[64] Lindzen, R.S. (1981). Turbulence and stress owing to gravity wave and tidal breakdown. *J Geophys Res,* 86, 9707–9714.

[65] Liu, H.L., Bardeen, C.G., Foster, B.T., Lauritzen, P., Liu, J., Lu, G., Wang, W. (2018). Development and validation of the Whole Atmosphere Community Climate Model with thermosphere and ionosphere extension (WACCM-X 2.0). *Journal of Advances in Modeling Earth Systems*, 10(2). doi: 10.1002/2017MS001232.

[66] Liu, R.Y., et al. (2005). The Chinese ground-based instrumentation in support of the combined Cluster/Double Star satellite measurements. *Ann. Geophys.*, 23, 2943-2951.

[67] Lockwood, M., Carlson, H. C. (1992). Production of polar cap electron density patches by transient magnetopause reconnection. *Geophys. Res. Lett.*, 19(17), 1731-1734.

[68] Liu, J. Y., Chen, Y. I., Pulinets, S. A., Tsai, Y. B., & Chuo, Y. J. (2000). Seismo-ionospheric signatures prior to M >= 6.0 Taiwan earthquakes. *Geophysical Research Letters*, 27(19), 3113-3116.

[69] Liu, J. Y., Tsai, Y. B., Chen, S. W., Lee, C. P., Chen, Y. C., Yen, H. Y., et al. (2006). Giant ionospheric disturbances excited by the M9.3 Sumatra earthquake of 26 December 2004. *Geophysical Research Letters*, 33(2).

[70] Liu, J. Y., Chen, Y. I., Chen, C. H., Liu, C. Y., Chen, C. Y., Nishihashi, M., et al. (2009). Seismoionospheric GPS total electron content anomalies observed before the 12 May 2008 Mw7.9 Wenchuan earthquake. *Journal of Geophysical Research: Space Physics*, 114(A4). doi: 10.1029/2008JA013698.

[71] Livermore, P., Finlay, C., Hollerbach, R. (2016). An accelerating high-latitude jet in earth's core. *Nature Geoscience*, 2016, 10(1), 62-68.

[72] Lübken, F.J., Berger, U., Baumgartner, G. (2013). Temperature trends in the midlatitude summer mesosphere. *J. Geophys. Res. Atmos.*, 118, 13347-13360. doi:10.1002/2013JD020576.

[73] Makela, J. J., Meriwether, J. W., Huang, Y., and Sherwood, P. J. (2011). Simulation and analysis of a multi-order imaging Fabry–Perot interferometer for the study of the thermospheric winds and temperatures. *Appl. Opt.*, 50, 4403–4416.

[74] Mandea, M., Dormy, E. (2003). Asymmetric behaviour of magnetic dip poles. *Earth, Planets, and Space*, 55, 153-157.

[75] Mandea, M., Holme, R. , Pais, A., Pinheiro, K., Jackson, A., Verbanac, G. (2010). Geomagnetic jerks: Rapid core field variations and core dynamics. *Space Sci. Rev.*, 155, 147-75. doi:10.1007/s11214- 010-9675-6.

[76] Mandea, M., Purucker, M. (2018). The varying core magnetic field from a space weather perspective. *Space Sci Review*, 214, 11. doi: 10.1007/s11214-017-0443-8.

[77] Mandea, M., Petrovský, E. (2019). IAGA: a major role in understanding our magnetic planet, Hist. Geo Space. Sci., 10, 163–172. doi: 10.5194/hgss-10-163-2019.

[78] Merrill, T.T., McElhinny, M.W., McFadden, P.L. (1996). The Magnetic Field of the Earth. Academic Press: London.

[79] Mewaldt, R. A., et al. How Efficient are Coronal Mass Ejections at Accelerating Solar Energetic Particles? Proceedings of the Solar Wind 11 / SOHO 16, "Connecting Sun and Heliosphere" Conference (ESA SP-592). 12-17 June 2005 Whistler, Canada. Editors: B. Fleck, T.H. Zurbuchen, H. Lacoste, p. 67.

[80] Moen, J., Oksavik, K., Alfonsi, L., Daabakk, Y., Romano, V., Spogli, L. (2013). Space weather challenges of the polar cap ionosphere. *J. Space Weather Space Clim.*, 3(A02). doi:10.1051/swsc/2013025.

[81] Molchanov, O. A., Hayakawa, M. (1995). Generation Of Ulf Electromagnetic Emissions by Microfracturing. *Geophysical Research Letters*, 22(22), 3091-3094.

[82] Murakami, G., Yoshioka, K., Yamazaki, A., Nishimura, Y., Yoshikawa, I., Fujimoto, M. (2016). The plasmapause formation seen from meridian perspective by KAGUYA, *J. Geophys. Res: Space Physics*, 121(12), 973–11,984. doi:10.1002/2016JA023377.

[83] Nemec, F., Santolik, O., Parrot, M., Berthelier, J. J. (2008). Spacecraft observations of electromagnetic perturbations connected with seismic activity. *Geophysical Research Letters*, 35(5). doi: 10.1029/2007GL032517

[84] Newitt, L. R., Mandea, M., McKee, L.A., Orgeval, J.J. (2002). Recent acceleration of the North Magnetic Pole linked to magnetic jerks. *EOS, Transactions American Geophysical Union*, 83(35), 381–389.

[85] Olsen, N., Mandea, M. (2007). Will the Magnetic North Pole wind up in Siberia? EOS, Transactions American Geophysical Union, 88(29), 293-300.

[86] Ouzounov, D., Pulinets, S., Katsumi Hattori, and Taylor, P. ed., Pre-earthquake processes – a Multidisciplinary Approach to Earthquake prediction studies, AGU Monograph, John Wiley and sons, 2018.

[87] Oyama, K. I., Kakinami, Y., Liu, J. Y., Abdu, M. A., Cheng, C. Z. (2011). Latitudinal distribution of anomalous ion density as a precursor of a large earthquake. *J. Geophys. Res.*, 116, A04319. doi:10.1029/2010JA015948.

[88] Oyama, K. I., Devi, M., Ryu, K., Chen, C. H., Liu, J. Y., Liu, H., Bankov, L., Kodama, T. (2016). Modifications of the ionosphere prior to large earthquakes: report from the Ionosphere Precursor Study Group. *Geosci. Lett.*, 3, 6. doi: 10.1186/s40562-016-0038-3

[89] Pierrard V., Benck, S. (2012). The Dynamics of the Terrestrial Radiation Belts and its Links to the Plasmasphere, in Space weather: the space environment, AIP Conf. Proc., 1500, 216. doi: 10.1063/1.4768769.

[90] Pierrard, V., Khazanov, G., Cabrera, J., Lemaire, J. (2008). Influence of the convection electric field models on predicted plasmapause positions during the magnetic storms. *J. Geophys. Res.*, 113, A08212, 1-21. doi: 10.1029/2007JA012612.

[91] Pierrard V., and K. Stegen (2008), A three dimensional dynamic kinetic model of the plasmasphere, *Journal Geophys. Res.*, 113, A10209. doi: 10.1029/2008ja013060.

[92] Pierrard, V., Goldstein, J., André, N., Jordanova, V. K., Kotova, G. A., Lemaire, J. F., Liemohn, M. W., Matsui, H. (2009). Recent progress in physics-based models of the plasmasphere, Space Sci. Rev., 145, 193-229, doi: 10.1007/s11214-008-9480-7.

[93] Pierrard, V., Voiculescu, M. (2011). The 3D model of the plasmasphere coupled to the ionosphere. Geophys. Res. Lett., 38, L12104. doi:10.1029/2011GL047767.

[94] Pulinets, S. A., Khegai, V. V., Boyarchuk, K. A., Lomonosov, A. M. (1998). Atmospheric electric field as a source of ionospheric variability. Uspekhi Fizicheskikh Nauk, 168(5), 582-589.

[95] Pulinets, S. A., Boyarchuk, K. A., Lomonosov, A. M., Khegai, V. V., Lyu, I. Y. (2002). Ionospheric precursors to earthquakes: A preliminary analysis of the foF2 critical frequencies at Chung-Li ground-based station for vertical sounding of the ionosphere (Taiwan Island). *Geomagnetism And Aeronomy*, 42(4), 508-513.

[96] Pulinets, S., Davidenko, D., Ionospheric precursors of earthquakes and Global Electric Circuit. *Advances in Space Research* (2014). doi: http://dx.doi.org/10.1016/j.asr.2013.12.035

[97] Pulinets, S., Ouzounov, D. (2018) The possibility of earthquake forecasting – learning from Nature, IOP Publishing: Bristol, UK.

[98] Purucker, M., Whaler, K. (2015). Crustal magnetism. Schubert G (Eds.)Treatise on Geophysics (Second Edition), 185-218.

[99] Rezac, L., Yue, J., Yongxiao, J., Russell III, J. M., Garcia, R., López-Puertas, M., Mlynczak, M. G. (2018). On long-term SABER CO2trends and effects due to nonuniform space and time sampling. *J. Geophys. Res. Space Phys.*, 123(9), 7958-7967. doi: 10.1029/2018JA025892.

[100] Richmond, A.D., et al. (1980). An empirical model of quiet-day ionospheric electric fields at middle and low latitudes. *Journal of Geophysical Research,* 85, 4658-4664. doi: 10.1029/JA085iA09p04658.

[101] Roble, R. G., Ridley, E. C. (1994), A thermosphere-ionosphere-mesosphere-electrodynamics general circulation model (TIME-GCM): Equinox solar cycle minimum simulations (30–500 km). *Geophys. Res. Lett.*, 21(6), 417–420. doi:10.1029/93GL03391.

[102] Rycroft, M.J., Israelsson, S., Price, C. (2000). The global atmospheric circuit, solar activity and climate change, *Journal of Atmospheric and Solar-Terrestrial Physics*, 62, 1563–1576. doi: 10.1016/S1364-6826(00)00112-7.

[103] Sagnotti, L., Scardia, G., Giaccio, B., Liddicoat, J.C., Nomade, S., Renne, P.R., Sprain, C.J. (2014). Ex- tremely rapid directional change during matuyama-brunhes geomagnetic polarity reversal. *Geophysical Journal International,* 199(2), 1110–1124. doi:10.1093/gji/ggu287.

[104] Salby, ML.. (1984). Survey of planetary-scale traveling waves: The state of theory and observations. *Rev Geophys*, 22(2), 209-236.

[105] Sarris, T. et al. (2019). Geosci. Instrum. Method. Data Syst. Discuss., Manuscript under review for journal Geosci. Instrum. *Method. Data Syst.* doi: 10.5194/gi-2019-3.

[106] Shen, X., Zhima, Z., Zhao, S., Qian, G., Ye, Q., & Ruzhin, Y. (2017). VLF radio wave anomalies associated with the 2010 Ms 7.1 Yushu earthquake. *Advances in Space Research*, 59(10), 2636-2644.

[107] Shen, X., et al., (2018). The state-of-the-art of the China Seismo-Electromagnetic Satellite mission. *Science China Technological Sciences*, 61, 634-642.

[108] Shepherd, T.G. (2000). The middle atmosphere. *J. Atmos. Sol.-Terr. Phys.*, 62, 1587-1601.

[109] Simpson, J. J., Taflove, A. (2005). Electrokinetic effect of the Loma Prieta earthquake calculated by an entire-Earth FDTD solution of Maxwell's equations. *Geophysical Research Letters*, 32(9).

[110] Sorokin, V. M., Chmyrev, V. M., Yaschenko, A. K. (2001). Electrodynamic model of the lower atmosphere and the ionosphere coupling. *Journal Of Atmospheric And Solar-Terrestrial Physics*, 63(16), 1681-1691.

[111] Sun Y. Y., Oyama, K.I., Liu, J. Y., Jhuang, H. K., Cheng, C. Z. (2011). The neutral temperature in the ionospheric dynamo region and the ionospheric F region density during Wenchuan and Pingtung Doublet earthquakes. *Nat. Hazards Earth Syst. Sci.*, 11, 1759–1768.

[112] Thayer, J. P., Killeen, T. L., McCormac, F. G., Tschan, C. R., Ponthieu, J.-J., Spencer, N. W. (1987). Thermospheric neutral wind signatures dependent on the east–west component of the interplanetary magnetic field for northern and southern hemispheres as measured from Dynamics Explorer-2. *Ann. Geophys.*, 5A, 363–368.

[113] Thebault, E., Finlay, C.C., Beggan, C.D., Alken, P., Aubert, J., Barrois, O., Bertrand, F., Bondar, T., Boness, A., Brocco, L., Canet, E., Chambodut, A., Chulliat, A., Coısson, P., Civet, F., Du, A., Fournier, A., Fratter, I., Gillet, N., Hamilton, B., Hamoudi, M., Hulot, G., Jager, T., Korte, M., Kuang, W., Lalanne, X., Langlais, B., Leger, J.M., Lesur, V., Lowes, F.J., Macmillan, S., Mandea, M., Manoj, C., Maus, S., Olsen, N., Petrov, V., Ridley, V., Rother, M., Sabaka, T.J., Saturnino, D., Schachtschneider, R., Sirol, O., Tangborn, A., Thomson, A.,Tøner-Clausen, L., Vigneron, P., Wardinski, I., Zvereva, T. (2015). International geomagnetic reference field: the 12th generation. *Earth, Planets and Space,* 67(79), 1-19. doi: 10.1186/s40623-015-0228-9.

[114] Tóth, G., Sokolov, I. V., Gombosi, T. I., Chesney, D. R., Clauer, C. R., De Zeeuw, D. L., Hansen, K. C., Kane, K. J., Manchester, W. B., Oehmke, R. C., Powell, K. G, Ridley, A. J., I. Roussev, I., Stout, Q. F., Volberg, O., Wolf, R. A., Sazykin, S., Chan, A., Yu, B., Kota, J. (2005). Space Weather Modeling Framework: A new tool for the space science community. *J. Geophys. Res.*, 110(A12), 226. doi:10.1029/2005JA011126.

[115] Tóth, G., van der Holst, B., Sokolov, I. V., De Zeeuw, D. L., Gombosi, T. I., Fang, F., Manchester, W. B., Meng, X., Najib, D., Powell, K. G., Stout, Q. F., Glocer, A., Ma, Y.J., Opher, M. (2012). Adaptive Numerical Algorithms in Space Weather Modeling. *J. Comput. Phys.*, doi:10.1016/j.jcp.2011.02.006.

[116] Valet, J.P. (2003). Time variations in geomagnetic intensity. *Rev. Geophys.*, 41. doi:10.1029/2001/RG000104

[117] Valet, J.P., Fournier, A., Courtillot, V., Herrero-Bervera, E. (2012). Dynamical similarity of geomagnetic field reversals. *Nature*, 490 (7418), 89-93.

[118] Verbanac, G., Bandic, M., Pierrard, V. (2018). MLT plasmapause characteristics: comparison between THEMIS observations and numerical simulations. *J. Geophys. Res: Space Physics*,123, 2000-2017. doi: 10.1002/2017JA024573.

[119] Wang, Y., et al., (2016). A comparison between large-scale irregularities and scintillations in the polar ionosphere. *Geophys. Res. Lett.*, 43(10), 4790-4798. doi: 10.1002/2016GL069230.

[120] Yue, X., et al. (2012), Global 3-D ionospheric electron density reanalysis based on multisource data assimilation. *J. Geophys. Res.*, 117(A9). doi:10.1029/2012JA017968.

[121] Yue, X., Wang, W., Lei, J., Burns, A., Zhang, Y., Wan, W., Liu, L., Hu, L., Zhao, B., and Schreiner, W. S. (2016a), Long-lasting negative ionospheric storm effects in low and middle latitudes during the recovery phase of the 17 March 2013 geomagnetic storm. *J. Geophys. Res. Space Physics*, 121(9), 9234-9249. doi:10.1002/2016JA022984.

[122] Yue, X., Wan, W., Liu, L., Liu, J., Zhang, S., Schreiner, W. S., Zhao, B., Hu, L. (2016b), Mapping the conjugate and corotating storm-enhanced density during 17 March 2013 storm through data assimilation. *J. Geophys. Res. Space Physics*, 121(12), 202-12,210. doi:10.1002/2016JA023038.

[123] Zhang, Q.H., et al. (2013). Direct Observations of the Evolution of Polar Cap Ionization Patches. *Science*, 339, 1597-1600. doi:10.1126/science.1231487.

[124] Zhang, Q.-H., et al. (2015). Direct observations of the full Dungey convection cycle in the polar ionosphere for southward interplanetary magnetic field conditions. *J. Geophys. Res.*, 120, 4519-4530. doi:10.1002/2015JA021172.

[125] Zhang, Q.H., et al. (2016). Earth's ion upflow associated with polar cap patches: Global and in situ observations. *Geophys. Res. Lett.*, 43, in press. doi:10.1002/2016GL067897

[126] Zhang, S.R., Erickson, P. J., Coster, A. J., Rideout, W., Vierinen, J., Jonah, O., & Goncharenko, L. P. (2019). Subauroral and polar traveling ionospheric disturbances during the 7-9 September 2017 storms. *Space Weather*, 17(12), 1748-1764. doi: 10.1029/2019SW002325

[127] Zhao, B. Q., Wang, M., Yu, T., Wan, W. X., Lei, J. H., Liu, L. B., Ning, B. Q. (2008). Is an unusual large enhancement of ionospheric electron density linked with the 2008 great Wenchuan earthquake?. *Journal of Geophysical Research-Space Physics*, 113(A11).

[128] Zhao, S., Liao, L., Zhang, X. (2017). Trans-ionospheric VLF wave power absorption of terrestrial VLF signal. *Chinese Journal of Geophysics* (in Chinese), 60(8), 3004-3014. doi: 10.6038/cjg20170809.

[129] Zhao, S., Zhang, X., Liao, L., Qian, G. (2016). Amplitude anomalies of Alpha signals before Yushu earthquake. *Earthquake*, 36(4), 153-162.

[130] Zhao, S., Zhang, X., Zhao, Z., Shen, X. (2014). The numerical simulation on ionospheric perturbations in electric field before large earthquakes. *Annales Geophysicae*, 32(12), 1487-1493.

[131] Zhao, S., Zhou, C., Shen, X., Zhima, Z. (2019). Investigation of VLF transmitter signals in the ionosphere by ZH-1 observations and full-wave simulation. *Journal of Geophysical Research: Space Physics*, 124, 4697-4709. doi: 10.1029/2019JA026593.

[132] Zhou, C., Liu, Y., Zhao, S., Liu, J., Zhang, X., Huang, J., et al. (2017). An electric field penetration model for seismo-ionospheric research. *Advances in Space Research*, 60(10), 2217-2232. doi: 10.1016/j.asr.2017.08.007.

[133] Zhou, H., Toth, G., Jia, X., Chen, Y., Markidis, S. (2019). Embedded kinetic simulation of Ganymede's magnetosphere: Improvements and inferences. *Journal of Geophysical Research: Space Physics*, 124(7), 5441-5460. doi: 10.1029/2019JA026643.

[134] Zou, S., Ridley, A., Jia, X., Boyd, E., Nicolls, M., Coster, A., Thomas, E., Ruohoniemi, J. M. (2017a). Multi-instrument observations of intense ion upflow fluxes associated with SED observed during the June 1, 2013 geomagnetic storm. *J. Geophys. Res.*, 122(2). doi:10.1002/2016JA023697.

[135] Zou, S. , Ozturk, D., Varney, R., Reimer, A. (2017b). Effects of Sudden Commencement on the Ionosphere: PFISR Observations and Global MHD Simulation. *Geophys. Res. Lett.*, 44(7), 3047-3058. doi:10.1002/2017GL072678.

太空 | TAIKONG

LIST OF PARTICIPANTS AND CONTRIBUTORS

Michel Blanc	Research Institute in Astrophysics and Planetology, France
Aziza Bounhir	University of Marrakech and Oukaimeden Observatory, Morocco
Eric Donovan	University of Calgary, Canada
Maurizio Falanga	National Space Science Center, CAS, China
John Foster	MIT Haystack Observatory, US
Fu Suiyan	Peking University, China
Alvaro Giménez	CSIC, Spain
Walter Gonzalez	INPE, Brazil
Natchimuthuk Gopalswamy	NASA Goddard Space Flight Center, United States
Guo Xiaocheng	National Space Science Center, CAS, China
Ludwig Klein	LESIA, Observatoire de Paris, France
Lei Jiuhou	University of Science and Technology of China, China
Mark Lester	University of Leicester, UK
William Liu	National Space Science Center, CAS, China
Lu Daren	Institute of Atmospheric Physics, CAS, China
Hermann Opgenoorth	University of Umeå, Sweden University of Leicester, UK/ ESF/ESSC
Frédéric Ouattara	University Norbert Zongo, Koudougou, Burkina Faso
Koh-Ichiro Oyama	Kyushu University, Japan
Viviane Pierrard	Belgian Institute for Space Aeronomy, Brussels, Belgium
Qie Xiushu	The Institute of Atmospheric Physics, CAS, China
Babatunde Rabiu	Centre for Atmospheric Research National Space Research and Development Agency, Nigeria
Rao Haiyan	National Space Science Center, CAS, China
Ren Liwen	National Space Science Center, CAS, China
Shen Xuhui	Institute of Earthquake Forecasting, China
Roman Vasilyev	Irkutsk Institute of Solar-Terrestrial Physics, Russia
Wu Qian	High Altitude Observatory, National Center for Atmospheric Research, Boulder, Colorado, United States
Xu Jiyao	National Space Science Center, CAS, China
Yan Yihua	National Astronomical Observatories, CAS, China
Yang Fang	National Space Science Center, CAS, China
Yue Xinan	Institute of Geology and Geophysics, CAS, China
Zhang Beichen	Polar Research Institute of China
Zhang Qinghe	Shandong University, China
Zhang Shunrong	MIT Haystack Observatory, United States
Zou Shasha	University of Michigan, United States

INTERNATIONAL SPACE SCIENCE INSTITUTE - BEIJING